Title
ATOMIC BEAM RESEARCH ON THE SPINS HYPERFINE STRUCTURES, AND MOMENTS OF K43, Y90, La140 AND Lu177

Author
Petersen, Fred Russell.

Publication Date
1960-11-21

UCRL 9480

UNIVERSITY OF
CALIFORNIA

Ernest O. Lawrence

Radiation Laboratory

ATOMIC BEAM RESEARCH ON THE SPINS, HYPERFINE STRUCTURES, AND MOMENTS OF K^{43}, Y^{90}, La^{140}, AND Lu^{177}

DISCLAIMER

UCRL-9480
UC-34 Physics
TID-4500 (16th Ed.)

UNIVERSITY OF CALIFORNIA
Lawrence Radiation Laboratory
Berkeley, California

Contract No. W-7405-eng-48

ATOMIC BEAM RESEARCH ON THE SPINS, HYPERFINE STRUCTURES, AND MOMENTS OF K^{43}, Y^{90}, La^{140}, AND Lu^{177}

Fred Russell Petersen

(Ph.D. Thesis)

November 21, 1960

Printed in USA. Price $2.75. Available from the
Office of Technical Services
U. S. Department of Commerce
Washington 25, D.C.

TABLE OF CONTENTS

Table of Contents (continued)

ABSTRACT

The atomic beam magnetic resonance method has been used to investigate the hyperfine-structure separations of radioactive isotopes K^{43}, Y^{90}, La^{140}, and Lu^{177}. Excepting K^{43}, which was produced by the reaction $A^{40}(\alpha,p)K^{43}$ with the Crocker 60-Inch cyclotron at Berkeley, all isotopes were reactor-produced by (n,γ) reactions.

Potassium-43 was investigated in the $^2S_{1/2}$ electronic ground state with the following results:

$I = 3/2$, $\Delta\nu = 192.64(5)$ Mc/sec, $|\mu_I| = 0.163(2)$ nm;

$|\mu_I|$ was obtained with the aid of the Fermi-Segrè formula from the zero-field hyperfine-structure separation, $\Delta\nu$, and the known constants of K^{39} or K^{41}.

The remaining isotopes were investigated in both the $^2D_{3/2}$ and the $^2D_{5/2}$ electronic states. These measurements yielded the following spins and hyperfine-structure interaction constants:

$^2D_{3/2}$ electronic state

Y^{90}	Lu^{177}
$I = 2$	$I = 7/2$
$a = -169.749(7)$ Mc/sec	$a = 194.84(2)$ Mc/sec
$b = -21.602(27)$ Mc/sec	$b = 1466.71(12)$ Mc/sec

$^2D_{5/2}$ electronic state

Y^{90}	Lu^{177}
$I = 2$	$I = 7/2$
$a = -85.258(6)$ Mc/sec	$a = 147.17(1)$ Mc/sec
$b = -29.716(38)$ Mc/sec	$b = 1805.93(14)$ Mc/sec

The spin I = 3 was measured in both electronic states for La^{140}.

The uncorrected nuclear magnetic moment of Y^{90} calculated from the hyperfine structure by use of the magnetic moment and interaction constants of Y^{89} was

$$\mu_I = -1.623(8) \text{ nm.}$$

The sign of the moment was determined from the g_I-dependent $\Delta F = \pm 1$ transitions for which the magnetic field dependence of the frequency was zero at high fields. The uncorrected nuclear electric quadrupole moment of Y^{90} calculated from the interaction constants for both electronic states was

$$Q = -0.155(3) \text{ barns.}$$

The uncorrected nuclear magnetic moment of Lu^{177} calculated from the hyperfine structure with the aid of the magnetic moment and interaction constants of Lu^{175} was

$$\mu_I = +2.0(2) \text{ nm.}$$

The sign of the moment was determined by the method previously indicated. Uncertainty in this measurement will be considerably reduced when improved values of the magnetic moment of Lu^{175} become available. The uncorrected nuclear electric quadrupole moment of Lu^{177} calculated from the interaction constants for both electronic states was

$$Q = +5.0(6) \text{ barns.}$$

Because of the large quadrupole moment in Lu^{177}, the zero-field level ordering was inverted, in order of decreasing energy:

$^2D_{3/2}$ state: F = 5, 2, 4, and 3

$^2D_{5/2}$ state: F = 6, 5, 1, 4, 2, and 3.

Resonance detection was accomplished by collecting radioactive atoms on sulfur-coated surfaces, which were subsequently counted in continuous-flow methane beta counters.

I. Introduction

Yttrium ore, discovered in 1794 at Ytterby, Sweden, was not obtained in pure form until 1843 when C. G. Mosander showed that yttria could be resolved into the three oxides yttria, erbia, and terbia. The free element was finally obtained by Wöhler by reduction of the chloride with potassium.

Yttrium is a common ingredient of the minerals gadolinite, xenotime, and euxenite. In the preliminary separation process, yttrium is the principal metal of the "yttrium group," which also includes the rare earths lutetium, ytterbium, thulium, erbium, and holmium. Probably because of its remarkably similar chemical properties and low abundance, the rare earth lutetium was not discovered until 1906 by G. Urbain, who named it after Lutecia, the Roman name for the city of Paris. It was also independently discovered at about the same time by Auer von Welsbach, who named the element cassiopium. Although this term persisted in most of the German literature during the first half of the twentieth century, lutetium is now the commonly accepted name.

Lanthanum was discovered in 1839 by C. G. Mosander, who named the element after the Greek word "lanthanein" meaning "to be hidden or concealed." Lanthanum is a member of the "cerium group" of rare earths, whose principal ores are cerite and monazite. The most abundant element in this group is cerium; others, in addition to lanthanum, are praseodymium, neodymium, promethium, and samarium.

Because of their similar chemical properties, high-purity production of these metals has not be possible until recent years. A universal

method for production at present is by calcium reduction of the anhydrous fluorides. The metal is prepared by mixing the fluoride with a 10 to 15% excess of calcium metal powder in a tantalum crucible. The temperature is raised above the melting point of all constituents in an inert atmosphere. After the reduction reaction, the CaF_2 slag is mechanically removed and small calcium impurities are diminished by vacuum remelting. Various refinements to this general process have been made for each individual element. The original literature should be consulted for exact details. These elements are now commercially available with a 99.9% purity designation.

Discovery of the radioactive isotopes Y^{90}, La^{140}, and Lu^{177} occurred over a shorter period of time than for their stable predecessors. Marsh and Sugden (MAR 35) in 1935 reported discovery of a 1.9(2)-day activity from the neutron bombardment of stable lanthanum which they ascribed to La^{140}. They also reported a 4.0(1)-hour activity from neutron bombardment of stable lutetium. Since only the most abundant stable isotope of lutetium was known at the time, the activity was ascribed to Lu^{176}. In 1936, Hevesy and Levi (HEV 36) observed a 4-hr and also a 6- to 7-d activity, both of which could be attributed to a neutron bombardment of stable lutetium. They concluded that a second stable isotope in small abundance but with a large cross section must be present. This isotope is now known as 2.60%-abundant Lu^{176}, which has a thermal neutron absorption cross section of about 3800 barns. The 6- to 7-d activity was correctly identified as Lu^{177} and the 4-hr activity is now known to be Lu^{176m}.

In the same paper, Hevesy and Levi also reported production of a

70-hr activity from a neutron bombardment of stable yttrium. The new isotope β^- decayed into Zr^{90}. Their identification of the activity as Y^{90} has been verified by a number of investigators (STR 58).

With the advent of several competing nuclear structure theories, the importance of the nuclear properties of these isotopes has increased. A critical test of any nuclear model is its ability to predict the nuclear angular momentum, magnetic dipole moment, and electric quadrupole moment of any isotope. In order to test nuclear structure theory, therefore, experimental measurements of these properties must be available.

An interesting way to study nuclear structure is to study the nuclear spin and moment properties of a given element as neutrons are added or subtracted from the neutron configuration of the stable isotope. Since these properties have been or are being measured for stable isotopes of yttrium, lanthanum, and lutetium by other laboratories, it was desirable to attempt measurements of a similar kind on the radioactive isotopes.

Special significance was attached to Y^{90}, since the quadrupole moment of this isotope would be the first yttrium quadrupole moment to be measured ($I = 1/2$ for Y^{89}). The very large expected quadrupole moment for Lu^{177} made this isotope especially interesting.

One of the better methods for measuring nuclear spins and moments of radioactive isotopes is to study the hyperfine-structure interaction by the atomic beam magnetic resonance method. Since isotope production is a principal problem, and since a successful atomic beam experiment can be performed with as few as 10^{10} atoms, its great advantage is immediately seen.

II. THEORY

A. The Hyperfine-Structure Interaction

The method of atomic beams for the study of nuclear properties is extremely useful because of the simplicity of the Hamiltonian that represents the interaction of the nucleus with the orbital electrons. Because of relatively large distances between atoms in the beam, each atom is essentially isolated from all the others and the interatomic interaction is negligible.

In treating the noncentral interaction between electrons and nuclear particles or the hyperfine interaction, it is convenient to expand nuclear and orbital electronic potentials in terms of their multipole moments. Then, in terms of these multipole moments of order 2^{ℓ}, the following theoretical restrictions have been shown to exist:

(a) From parity considerations, if all nuclear electrical effects arise from electrical charges, and if the nuclear Hamiltonian is unaltered by an inversion of the coordinates, then no even (ℓ even) nuclear magnetic multipole moment or odd (ℓ odd) nuclear electrical multipole moment can exist.

(b) In an atom with a nuclear spin $\vec{I}$ and a total electronic angular momentum $\vec{J}$, it is impossible to observe a nuclear multipole moment greater than 2^{ℓ}, where $\ell = 2I$ or $2J$, whichever is smaller.

1. Magnetic Interaction Between the Atomic Nucleus and Its Orbital Electrons

From the above considerations, the smallest magnetic moment one could expect to observe would be the magnetic dipole moment. The term in the

Hamiltonian representing this interaction is

$$\mathcal{H}_D = -\vec{\mu}_I \cdot \vec{H}_J \,, \tag{II-1}$$

where $\vec{\mu}_I$ is the nuclear magnetic moment and $\vec{H}_J$ is the magnetic field at the nucleus arising from the rest of the atom having angular momentum $\vec{J}\hbar$. The magnetic moment can be taken as proportional to its spin angular momentum $\vec{I}$ and written as

$$\vec{\mu}_I = (\mu_I/I)\vec{I} = g_I \vec{I}\mu_0 \,, \tag{II-2}$$

where g_I is the nuclear g factor and μ_0 is the absolute value of the Bohr magneton. Thus,

$$\mathcal{H}_D = -g_I\mu_0 \vec{I} \cdot \vec{H}_J \,. \tag{II-3}$$

$\vec{H}_J$ can be taken as proportional to $\vec{J}$ for matrix elements diagonal in $\vec{J}$, so that the above equation becomes

$$\mathcal{H}_D = ha\vec{I} \cdot \vec{J}, \tag{II-4}$$

with

$$ha = \frac{-g_I\mu_0 H_J}{\vec{J}} = -g_I\mu_0 \frac{\vec{H}_J \cdot \vec{J}}{\vec{J} \cdot \vec{J}} \,, \tag{II-5}$$

where a is the magnetic dipole interaction constant.

The matrix element of $\vec{I} \cdot \vec{J}$ can be obtained in the following way. Let the angular momentum which is the vector sum of $\vec{I}$ and $\vec{J}$ be $\vec{F} = \vec{I} + \vec{J}$ with quantum number F. Then,

$$\vec{F}^2 = (\vec{I} + \vec{J})^2 = \vec{I}^2 + \vec{J}^2 + 2\vec{I} \cdot \vec{J},$$

or

$$\vec{I} \cdot \vec{J} = \frac{1}{2}(\vec{F}^2 - \vec{I}^2 - \vec{J}^2).$$

In the limit of small quantum numbers,

$$\vec{I} \cdot \vec{J} = \tfrac{1}{2}[F(F+1) - I(I+1) - J(J+1)] \equiv C/2. \qquad \text{(II-6)}$$

Thus, the interaction energy $W_D(F)$ for the state specified by the quantum number F becomes, in the F,m representation,

$$W_D(F) = (F,m|\mathcal{H}_D|F,m) = haC/2. \qquad \text{(II-7)}$$

In order to calculate g_I from the interaction constant a, one must obtain an estimate of $\vec{H}_J$, the effective magnetic field at the nucleus due to the rest of the atom. This calculation has been made by a number of authors, and the results are summarized by Kopfermann (KOP 58).

(a) For an s electron:

$$a \text{ (in Mc/sec)} = -\frac{8}{3}\frac{g_I g_J \mu_0^2 Z Z_0^2}{h n_0^3 a_0^3 10^6}\left(1 - \frac{d\sigma}{dn}\right) F_r(J,Z)(1-\delta)(1-\epsilon), \qquad \text{(II-8)}$$

where g_J = the electronic g factor for the element,

a_0 = the first Bohr radius,

Z = the atomic number of the atom,

Z_0 = the effective atomic charge as seen by the electron when outside all electron shells,

$n_0 = n - \sigma$ is the effective principal quantum number of the electron,

$(1 - \frac{d\sigma}{dn})$ is the so-called Fermi-Segrè factor and can be obtained from spectroscopic data. $F_r(J,Z)$ is a relativistic correction factor (≈ 1) given by Casimer (CAS 36) and tabulated as a function of J and Z by Kopfermann (KOP 58, p. 445); $(1 - \delta)$ is the

Breit-Rosenthal correction which arises because the nucleus is not a point charge as was assumed in the derivation of the basic expression for a (ROS 32, CRA 49, ION 60). The factor $(1 - \epsilon)$ is the Bohr-Weisskopf correction, necessary because nuclear magnetism is not concentrated in a point dipole but is distributed throughout the nuclear volume (BOH 50; and BOH 51).

(b) For p,d electrons:

$$a \text{ (in Mc/sec)} = \frac{2\mu_0^2 g_I}{10^6 h} \frac{L(L+1)}{J(J+1)} \overline{\langle r^{-3} \rangle} F_r(J,Z_i)(1-\delta)(1-\epsilon). \qquad \text{(II-9)}$$

The factor $\overline{\langle r^{-3} \rangle}$ can best be evaluated from the fine-structure splitting δ (cm^{-1}) between the $(L + 1/2)$ and $(L - 1/2)$ electronic states,

$$\overline{\langle r^{-3} \rangle} = \frac{hc\delta}{2\mu_0^2 (L+1/2) Z_i H_r(L,Z_i)}, \qquad \text{(II-10)}$$

where Z_i is the effective atomic charge as seen by the electron when inside the atomic core, and $H_r(L,Z_i)$ is another relativistic correction factor (CAS 36; KOP 58, p. 446). Thus,

$$a \text{ (in Mc/sec)} = \frac{g_I c\delta}{10^6 Z_i} \frac{L(L+1)}{(L+1/2)J(J+1)} \frac{F_r(J,Z_i)}{H_r(L,Z_i)} (1-\delta)(1-\epsilon). \qquad \text{(II-9a)}$$

A more accurate method for obtaining g_I from a exists, however, if accurate measurements of g_I and a for another isotope of the same element are available. Since the factors involving the electronic coordinates

are the same, we have the relationship

$$\frac{a_1}{a_2} = \frac{g_{I_1}}{g_{I_2}}, \qquad \text{(II-11)}$$

if we neglect the Breit-Rosenthal and Bohr-Weisskopf corrections. Experimental deviation from this theoretical relation results in the hfs anomaly. Of the two corrections for this anomaly, the Bohr-Weisskopf correction is the more important and is appreciable only for 2^{ℓ}-pole magnetic interactions with an electron in a state $J = \ell/2$. For various orders the effect varies as $1/(\ell + 1)$. Since the accuracy of measurement for K^{43} was not sufficient to determine an anomaly, and since the other measurements were made in electronic states corresponding to $J = 3/2$ and $J = 5/2$, the hfs anomaly is not an important factor in analysis of the experimental data.

2. Electrostatic Interaction Between the Atomic Nucleus and Its Orbital Electrons

Since the smallest electric moment ($\ell = 1$) that could give rise to hyperfine structure should theoretically be--and has indeed experimentally been found to be--zero, we shall consider now the nuclear electric quadrupole interaction ($\ell = 2$). Furthermore, we shall limit discussion to only the quadrupole moment, since higher-ordered electric moments have been too small to be observed and are not necessary to explain the experimental results in this dissertation.

Ramsey (RAM 53), for example, has shown that the quadrupole interaction energy can be represented by

$$\mathcal{H}_Q = hb\left[\frac{3(\vec{I}\cdot\vec{J})^2 + \frac{3}{2}(\vec{I}\cdot\vec{J}) - I(I+1)J(J+1)}{2I(2I-1)J(2J-1)}\right], \qquad \text{(II-12)}$$

where $hb = e^2 q_J Q$. Q is a scalar quantity with the dimension of square centimeters which is conventionally called the nuclear quadrupole moment and is defined by

$$Q \equiv \frac{1}{e}\int \rho_n(\vec{r}_n)_{m_I=I}(3z_n^2 - r_n^2)d\tau_n, \qquad \text{(II-13)}$$

where the subscript indicates that the integral is carried out for the nuclear state whose magnetic quantum number m_I is I. Likewise, q_J is defined by the integral

$$q_J \equiv \frac{1}{e}\int \rho_e(\vec{r}_e)_{m_J=J}\frac{(3\cos^2\theta - 1)d\tau_e}{r_e^3}, \qquad \text{(II-14)}$$

where the subscript indicates that the integral is carried out for the electronic state whose magnetic quantum number m_J is J. Here θ is the angle between $\vec{r}_e$ and the z axis relative to which this state has $m_J = J$. In the quantum-mechanical treatment, the integral is the average of $(3\cos^2\theta - 1)/r^3$ over the appropriate eigenfunction for $m_J = J$, or

$$\left\langle \overline{\frac{3\cos^2\theta - 1}{r^3}} \right\rangle_{J,J} = \left\langle m_J, J \left| \frac{3\cos^2\theta - 1}{r^3} \right| m_J, J \right\rangle_{m_J=J}. \qquad \text{(II-15)}$$

If the eigenfunction of an electron can be approximated by a product of a radial and an angular part, then

$$\left\langle \overline{\frac{3\cos^2\theta - 1}{r^3}} \right\rangle = \left\langle \overline{\frac{1}{r^3}} \right\rangle \cdot \overline{(3\cos^2\theta - 1)}. \qquad \text{(II-16)}$$

Since we already have an expression for $\langle r^{-3} \rangle$, we need consider only $\overline{(3\cos^2\theta - 1)}$. Kopfermann (KOP 58) shows that

$$\overline{(3\cos^2\theta - 1)}_{JJ} = -\frac{2J - 1}{2J + 2} \qquad \text{(II-17)}$$

for $J = L \pm 1/2$. Thus,

$$b = \frac{e^2Q}{h}\frac{(2J - 1)}{(2J + 2)}\overline{(r^{-3})}R_r(L,J,Z_i), \qquad \text{(II-18)}$$

or with the help of Eq. (II.10),

$$b\ (\text{in Mc/sec}) = \frac{e^2Qc\delta(2J - 1)}{10^6\mu_0{}^2Z_i(2L + 1)(2J + 2)}\frac{R_r(L,J,Z_i)}{H_r(L,Z_i)} \qquad \text{(II-19)}$$

$R_r(L,J,Z_i)$ is another relativistic correction factor (≈ 1) given by Casimer (CAS 36; KOP 58, p. 448), and the other symbols have been previously defined.

In Eq. (II-19), Z_i is not generally well known. Therefore, a more accurate method for evaluating Q from the interaction constants is to make use of the relation

$$Q = \frac{4g_I\mu_0{}^2}{e^2}\frac{F_r(J,Z_i)}{R_r(L,J,Z_i)}\frac{L(L + 1)}{J(2J - 1)}\frac{b}{a}, \qquad \text{(II-20)}$$

which was obtained from Eqs. (II-9) and (II-18). Volume corrections have been omitted from this formula since they are negligible in $^2P_{3/2}$ states, and even more so in ^2D states.

The $\vec{I} \cdot \vec{J}$ factor in Eq. (II-12) can be evaluated in the F,m representation with the aid of Eq. (II-6). This operation yields the

quadrupole interaction energy for the state specified by the quantum number F:

$$W_Q(F) = (F,m|\mathcal{H}_Q|F,m)$$

$$= hb \frac{\frac{3}{4}C(C+1) - I(I+1)J(J+1)}{2I(2I-1)J(2J-1)} . \qquad \text{(II-21)}$$

3. Interaction With an External Magnetic Field

Each hfs level is split into $(2F + 1)$ levels when an external magnetic field $\vec{H}$ is applied. The additional term in the Hamiltonian representing the interaction between the atom and the external magnetic field is

$$\mathcal{H}_M = -\vec{\mu}_J \cdot \vec{H} - \vec{\mu}_I \cdot \vec{H}, \qquad \text{(II-22)}$$

where $\vec{\mu}_J = g_J \mu_0 \vec{J}$ and $\vec{\mu}_I = g_I \mu_0 \vec{I}$ are the electronic and nuclear magnetic moments, respectively. The two simplest cases are the weak-field and strong-field limits.

The weak-field or Zeeman effect is characterized by an external field splitting that is small compared with the natural zero-field hfs splitting. The moments of the electron and nucleus are magnetically coupled to each other strongly to form a resultant magnetic moment $\vec{\mu}_F = g_F \mu_0 \vec{F}$. Consequently $\vec{F}$, according to Larmor's theorem, precesses around the direction of the external field $\vec{H}$. $\vec{I}$ and $\vec{J}$ in turn precess together with a much greater frequency about the direction of $\vec{F}$ (Fig. 1a).

The definition of g_F can be obtained from the vector model:

$$\vec{\mu}_F = \vec{\mu}_J + \vec{\mu}_I , \qquad \text{(II-23)}$$

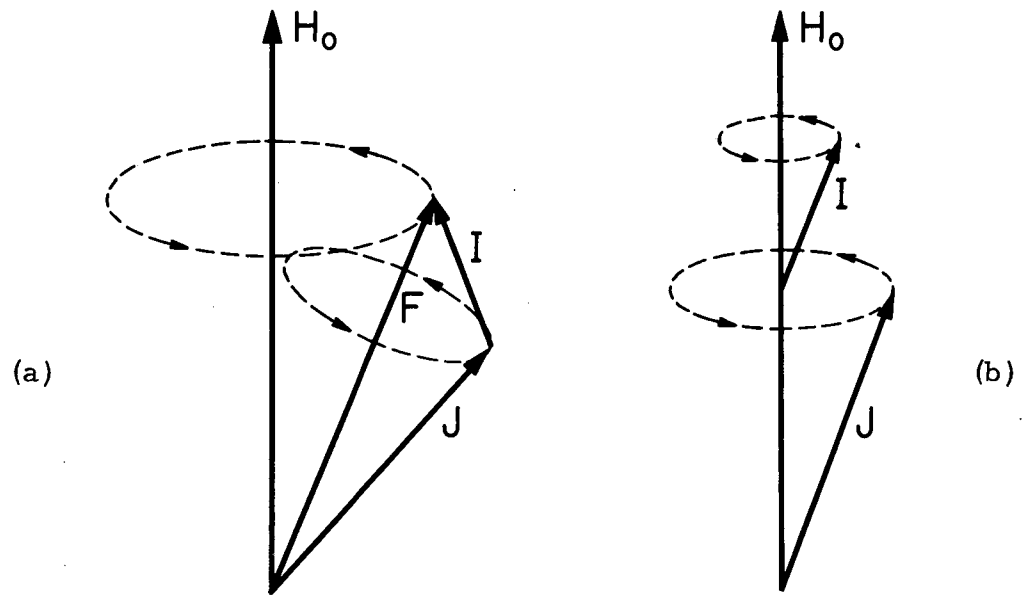

MU-13365

Fig. 1. Precession of $\vec{I}$, $\vec{J}$, and $\vec{F}$ in (a) a weak magnetic field and (b) a strong magnetic field.

$$g_F \mu_0 \vec{F} = g_J \mu_0 \vec{J} + g_I \mu_0 \vec{I}. \tag{II-24}$$

Thus,

$$g_F = \frac{g_J \vec{J} \cdot \vec{F} + g_I \vec{I} \cdot \vec{F}}{F^2}, \tag{II-25}$$

which, because of the relations

$$J^2 = F^2 + I^2 - 2\vec{I} \cdot \vec{F},$$

and

$$I^2 = F^2 + J^2 - 2\vec{J} \cdot \vec{F}, \tag{II-26}$$

is for large quantum numbers equal to

$$g_F = g_J \frac{F^2 + J^2 - I^2}{2F^2} + g_I \frac{F^2 + I^2 - J^2}{2F^2}. \tag{II-27}$$

For small quantum numbers,

$$g_F = g_J \frac{F(F+1) + J(J+1) - I(I+1)}{2F(F+1)} + g_I \frac{F(F+1) + I(I+1) - J(J+1)}{2F(F+1)}. \tag{II-28}$$

Since $g_I \approx 1/2000\, g_J$, the last term in the equation above is usually neglected in most calculations.

At low fields the good quantum numbers are F and m, where m is the magnetic quantum number. Calculation of the interaction energy of an atom in the presence of an external magnetic field for the state specified by quantum numbers F and m can be approached in the general case by use of perturbation theory. At low fields, the principal part of the

Hamiltonian is $\mathcal{H}_0 = \mathcal{H}_D + \mathcal{H}_Q$. The perturbing portion is $\mathcal{H}_M$. In an F,m representation, therefore, one can write the energy up to third order as

$$W(F,m) = W^0(F) + W^1(F,m) + W^2(F,m) + W^3(F,m), \tag{II-29}$$

where the superscripts refer to the order of the perturbation and (CON 57)

$$W^0(F) = (F,m|\mathcal{H}_0|F,m), \tag{II-30}$$

$$W^1(F,m) = (F,m|\mathcal{H}_M|F,m), \tag{II-31}$$

$$W^2(F,m) = \frac{(F,m|\mathcal{H}_M|F+1,m)^2}{W^0(F) - W^0(F+1)} + \frac{(F,m|\mathcal{H}_M|F-1,m)^2}{W^0(F) - W^0(F-1)}, \tag{II-32}$$

and

$$W^3(F,m) = \frac{(F,m|\mathcal{H}_M|F+1,m)^2[(F+1,m|\mathcal{H}_M|F+1,m) - (F,m|\mathcal{H}_M|F,m)]}{[W^0(F) - W^0(F+1)]^2}$$

$$+ \frac{(F,m|\mathcal{H}_M|F-1,m)^2[(F-1,m|\mathcal{H}_M|F-1,m) - (F,m|\mathcal{H}_M|F,m)]}{[W^0(F) - W^0(F-1)]^2}. \tag{II-33}$$

The additional matrix elements required in the above formulae are given, for example, by Ramsey (RAM 56). They are:

$$(F,m|J_z|F,m) = \frac{F(F+1) + J(J+1) - I(I+1)}{2F(F+1)}\, m, \tag{II-34}$$

$$(F,m|J_z|F+1,m) = \frac{[(F+1-I+J)(F+1+I-J)(I+J+2+F)(I+J-F)[(F+1)^2 - m^2]]^{1/2}}{4(F+1)^2(2F+1)(2F+3)}, \tag{II-35}$$

$$(F,m|J_z|F+1,m) = (F+1,m|J_z|F,m), \tag{II-36}$$

$$(F,m|J_z|F',m') = -(F,m|I_z|F',m'). \tag{II-37}$$

$W^0(F)$, which is degenerate in m, gives the zero-field hfs splittings. In the case of normal level ordering and positive magnetic moment, the highest F level corresponds to the highest energy. However, depending on the sign and the magnitude of the ratio of the interaction constants, $\xi \equiv b/a$, the level ordering can be in almost any order. Baker (BAK 60) has used the IBM 653 to obtain solutions of Eq. (II-30) for $1 \leq I \leq 8$ and $1 \leq J \leq 8$ over all possible F levels in half-integral steps in I and J. Level intersection points are calculated and the results are graphically presented over a convenient range of ξ. Figures 2, 3, 4, and 5 present the results for the four cases of interest.

If the zero-field hfs separations are assumed to be large, then the frequency separation ν_∞ of the various m levels for a given F is obtained from

$$\nu_\infty = \frac{W^1(F,m) - W^1(F,m-1)}{h} = \frac{-g_F \mu_0 H}{h} . \qquad \text{(II-38)}$$

Thus, if J and g_J are known for a given isotope, the transition frequency is proportional to a known function of the nuclear spin.

$W^2(F,m)$, $W^3(F,m)$, and the higher-ordered terms are useful for estimating the zero-field hfs separations from the higher-ordered shifts in the measured $\Delta F = 0$ transition frequencies. To second order in H, the shift is

$$\nu - \nu_\infty = \left[\frac{f_1(I,J,g_J)}{\Delta\nu_{F+1,F}} + \frac{f_2(I,J,g_J)}{\Delta\nu_{F,F-1}} \right] H^2, \qquad \text{(II-39)}$$

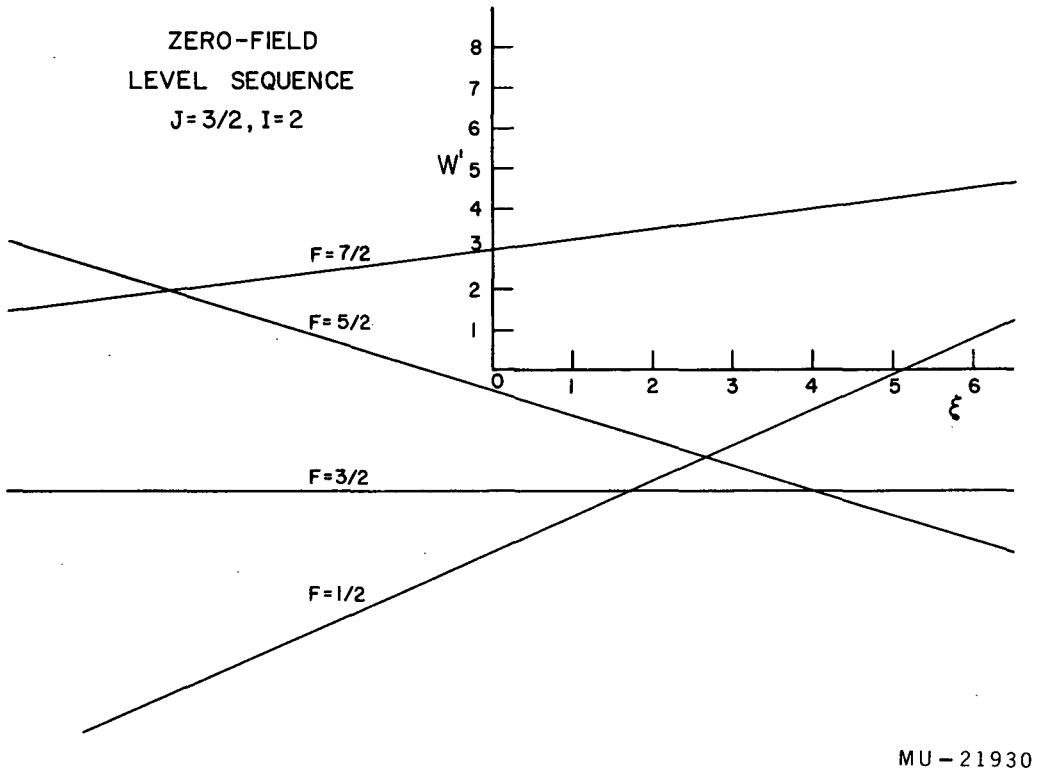

Fig. 2. Zero-field level sequence for $J = 3/2$, $I = 2$.

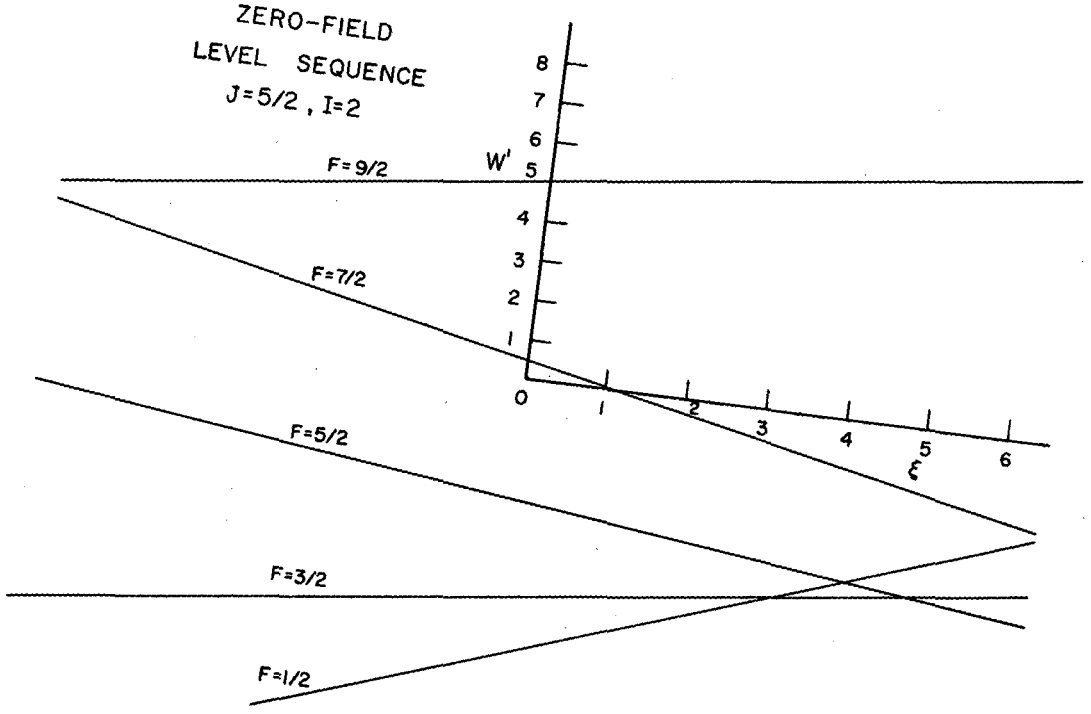

Fig. 3. Zero-field level sequence for J = 5/2, I = 2.

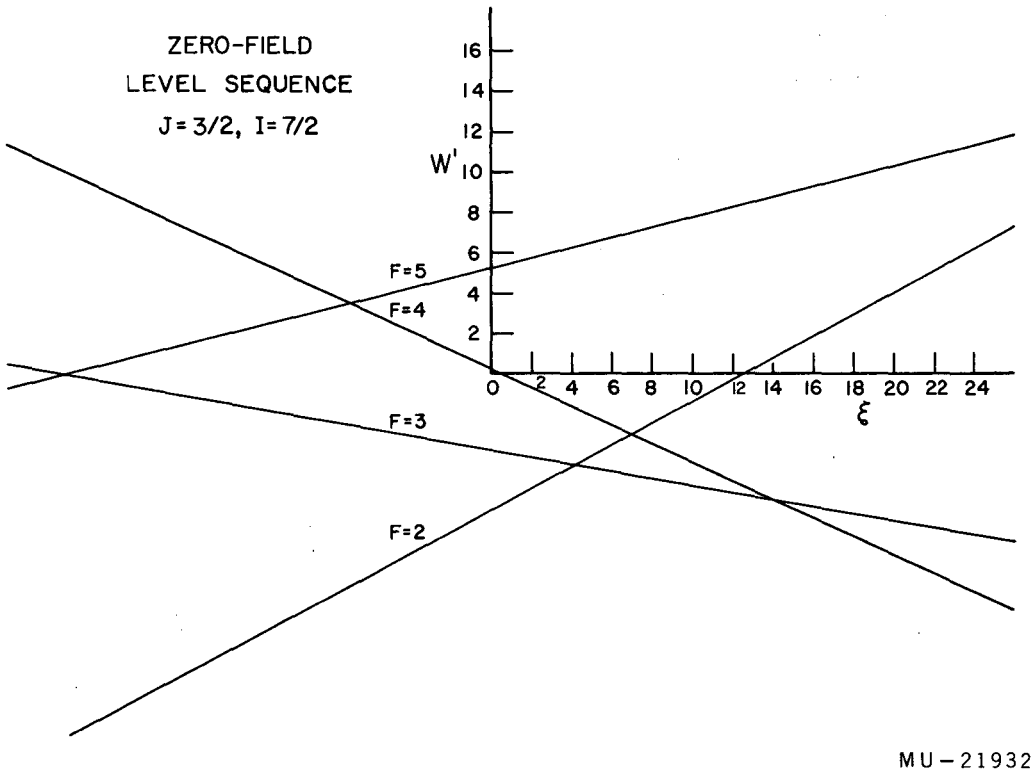

Fig. 4. Zero-field level sequence for J = 3/2, I = 7/2.

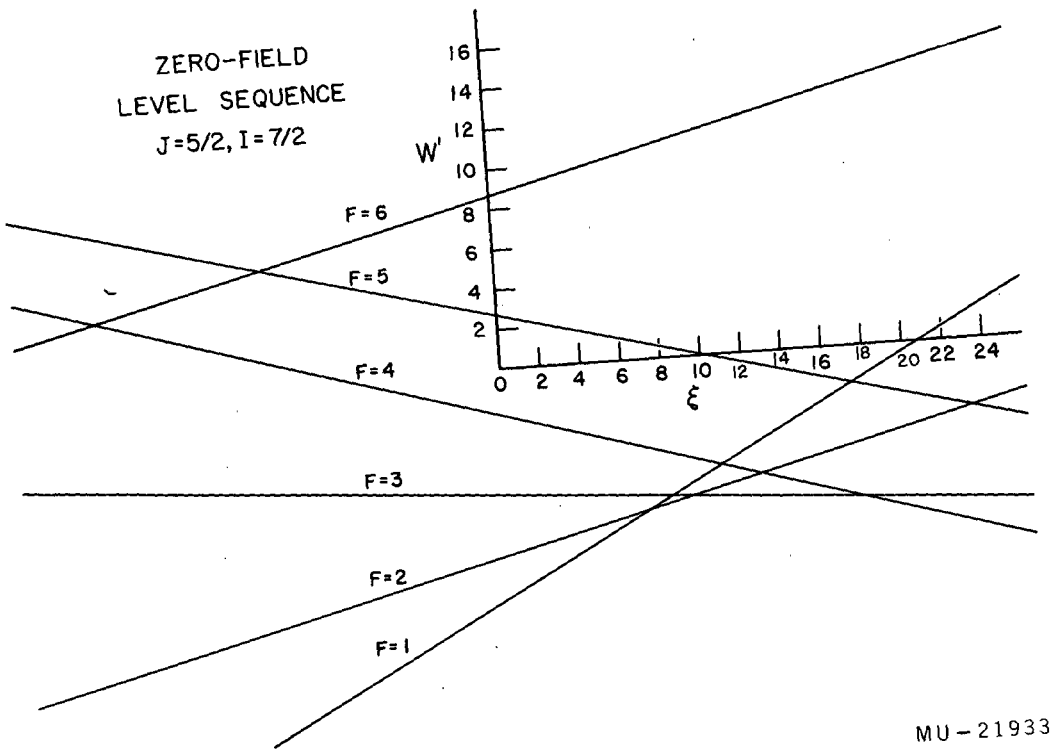

Fig. 5. Zero-field level sequence for J = 5/2, I = 7/2.

where $f_1(I,J,g_J)$ and $f_2(I,J,g_J)$ can be identified with the off-diagonal matrix elements in Eq. (II-32). The $\Delta\nu$'s in turn can be used with Eq. (II-30) to obtain estimates of the hyperfine-structure interaction constants. In principle, this procedure can be extended to higher-ordered terms. However, the calculations become very long and tedious, and consequently, a computer routine (to be described) has been devised to solve the hyperfine Hamiltonian numerically.

In the limit of a very strong magnetic field corresponding to the Paschen-Back effect, $\vec{\mu}_J$ and $\vec{\mu}_I$ are decoupled, and $\vec{I}$ and $\vec{J}$ each separately precess about $\vec{H}$ (Fig. 1b). For this case, F and m are no longer good quantum numbers; the good quantum numbers are m_I and m_J of I and J, respectively. Since the external field interactions are diagonal, and the averages of the cosine couplings are the first-order perturbations, we can write the total energy of any level approximately as

$$W(m_I,m_J) = W^0(m_I,m_J) + W^1(m_I,m_J)$$

$$= (m_I,m_J|\mathcal{H}_M|m_I,m_J) + (m_I,m_J|\mathcal{H}_D + \mathcal{H}_Q|m_I,m_J). \qquad \text{(II-40)}$$

Here, the principal part of the Hamiltonian is $\mathcal{H}_M$ and the perturbing portion is $\mathcal{H}_D + \mathcal{H}_Q$. To first order, then,

$$W(m_I,m_J) = -g_J m_J \mu_0 H - g_I m_I \mu_0 H + hAm_I m_J$$

$$+ \frac{hB[3m_I^2 - I(I+1)][3m_J^2 - J(J+1)]}{4I(2I-1)J(2J-1)}. \qquad \text{(II-41)}$$

From knowledge of the term energies in the weak- and strong-field limits, one can qualitatively represent the energy levels as a function

of the magnetic field on a "Breit-Rabi diagram." Transition from a weak to a strong field for any Zeeman level takes place in such a way that its magnetic quantum number m is preserved. This fact and the "no m cross rule," which states that levels of the same m cannot cross, enable one to qualitatively represent the energy levels in the intermediate field region.

4. Solution of the Secular Equation

For intermediate fields, the approximations used previously are no longer valid, and the secular equation of the matrix corresponding to the Hamiltonian

$$\mathcal{H} = \mathcal{H}_D + \mathcal{H}_Q + \mathcal{H}_M \qquad \text{(II-42)}$$

must be solved. In the general case, this calculation is tedious and therefore the problem has been programmed for both the IBM 653 and the IBM 704.

The original method of solution and the original computer programs were constructed by Professor W. A. Nierenberg for use on the IBM 653. The method of solution as well as other details of the routines is outlined in the program guides and in Marino's Ph.D. thesis (MAR 59).

Ehlers (EHL 60) has made several modifications to these programs, the essential feature of which consists of changing the input and output from a dimensionless to a dimensional form.

The most recent modification to the programs above has been their adaptation for use on the IBM 704 by Donald H. Zurlinden (ZUR 60). This program, Hyperfine III, uses the same procedures as the previous programs to fit observational data to a set of four parameters a, b, g_I, and g_J. Any combination (15 are possible) of these parameters can be allowed to

vary or can be held constant at the discretion of the user.

A brief outline of this program containing all the essential features of the previous programs follows.

The Hamiltonian for the hyperfine interaction in the presence of a magnetic field is written

$$\frac{\mathcal{H}}{h} = a\vec{I}\cdot\vec{J} + b\left[\frac{3(\vec{I}\cdot\vec{J})^2 + \frac{3}{2}(\vec{I}\cdot\vec{J}) - I(I+1)J(J+1)}{2I(2I-1)J(2J-1)}\right] - \frac{g_J\mu_0 HJ_z}{h} - \frac{g_I\mu_0 HI_z}{h}. \qquad \text{(II-43)}$$

It is assumed that electronic states are not mixed by the interaction. A discussion of corrections that must be applied to the interaction constants to account for this effect is given in Sec. II.5.

Equation (II-42) is rewritten

$$\frac{\mathcal{H}}{h} = a\vec{I}\cdot\vec{J} + b\left[\frac{3(\vec{I}\cdot\vec{J})^2 + \frac{3}{2}(\vec{I}\cdot\vec{J}) - I(I+1)J(J+1)}{2I(2I-1)J(2J-1)}\right] + \frac{(-g_J + g_I)\mu_0 HJ_z}{h} - \frac{g_I\mu_0 HF_z}{h}. \qquad \text{(II-44)}$$

Since $|g_I| \approx 1/2000\ |g_J|$, the term $-g_I\mu_0 HF_z/h$, where $F_z = I_z + J_z$, is temporarily neglected.

In an F,m representation, we can show the only nonvanishing matrix elements of the Hamiltonian by

$$a_p \equiv (F,m|\vec{I}\cdot\vec{J}|F,m),$$

$$b_p \equiv \left(F,m\left|\frac{3(\vec{I}\cdot\vec{J})^2+\frac{3}{2}(\vec{I}\cdot\vec{J})-I(I+1)J(J+1)}{2I(2I-1)J(2J-1)}\right|F,m\right), \quad \text{(II-45)}$$

$$c_p \equiv (F,m|J_z|F,m),$$

$$d_p \equiv (F,m|J_z|F+1,m)^2 = (F+1,m|J_z|F,m)^2.$$

These matrix elements can be evaluated with the aid of Eqs. (II-7), (II-21), (II-34), and (II-35).

There is one submatrix for each value of m. These submatrices are arranged along the diagonal of the total matrix. From Eqs. (II-44) and (II-45), each diagonal element of a given m submatrix can be written

$$A_p = a\,a_p + b\,b_p + H^* c_p , \quad \text{(II-46)}$$

where

$$H^* = \frac{(-g_J + g_I)\mu_0 H}{h} . \quad \text{(II-47)}$$

The elements one off the diagonal are

$$E_p = H^{*2} d_p ; \quad \text{(II-48)}$$

A_1 and E_1 correspond to the smallest F value and A_n and E_n correspond to the largest F value for a given m submatrix.

The term values for a given submatrix H_n are obtained by solving the determinant

$$D_n = |H_n - 1\,X|. \quad \text{(II-49)}$$

If D_n is expanded by the method of cofactors, the recursion relation that arises for D_p as $p \to n$ is

$$D_p = (A_p - X)D_{p-1} - E_{p-1}D_{p-2}. \tag{II-50}$$

The determinental equation can be constructed from this relationship if one chooses $D_0 = 1$ and $D_{-1} = 0$. This equation is solved by Newton's method for improving an approximate root of a polynomial function. If X is a trial root of D_n, then a better approximation is

$$X' = X - \delta X, \tag{II-51}$$

where

$$\delta X = \frac{D_n}{\partial D_n/\partial X}. \tag{II-52}$$

The derivative can be constructed in a manner similar to the construction of D_n from the recursion relation

$$\frac{\partial D_p}{\partial X} = (A_p - X)\frac{\partial D_{p-1}}{\partial X} - E_{p-1}\frac{\partial D_{p-2}}{\partial X} - D_{p-1}. \tag{II-53}$$

The procedure used in solving for the term values at a given magnetic field H is the following. First, D_n is solved at zero field, where all off-diagonal terms are zero and the roots are easily obtained and identified. H is then incremented by a small amount ΔH, and D_n is solved again to the desired degree of accuracy by using the previous root as the trial root and iterating with Newton's method a sufficient number of times. A new root at $H = \Delta H + \Delta H$ is obtained by using the root at $H = \Delta H$ as the trial root. The procedure is repeated until the final value of H is attained.

To determine the best fit for the parameters, we must find the minimum of a function $N(a,b,g_J,g_I)$, which is commonly called the Chi-square. Here $N(a,b,g_J,g_I)$ is defined by

$$N(a,b,g_J,g_I) = \sum_i \left[f^i_{obs} + \frac{(m_1{}^i - m_2{}^i)g_I\mu_0 H^i}{h} - X_1{}^i + X_2{}^i \right]^2 \omega^i, \quad \text{(II-54)}$$

where f^i_{obs} is the frequency of a transition defined by the quantum numbers $F_1{}^i, m_1{}^i \longleftrightarrow F_2{}^i, m_2{}^i$ observed at magnetic field H^i. The weighting factor for the ith set of observed values, ω^i, is determined by the equation

$$\omega^i = \left[(\delta f^i_{obs})^2 + \left\{ \left(\frac{\partial f}{\partial H^*} \right)^i \left(\frac{(-g_J + g_I)\mu_0}{h} \right) \delta H^i \right\}^2 \right]^{-1}, \quad \text{(II-55)}$$

where

$$\frac{\partial f}{\partial H^*} = \frac{\partial X_1}{\partial H^*} - \frac{\partial X_2}{\partial H^*} .$$

Also δf^i_{obs} and δH^i are the uncertainties in the measured frequency and magnetic field, respectively.

The procedure chosen for minimizing N is a quadratic method for minimizing a function of n variables described by Nierenberg (NIE 57). A set of linear equations is set up in terms of the variables. This system of linear equations resulting from Eq. (II-54) is the following:

$$\frac{\partial^2 N}{\partial a^2}\delta a + \frac{\partial^2 N}{\partial a \partial b}\delta b + \frac{\partial^2 N}{\partial a \partial g_J}\delta g_J + \frac{\partial^2 N}{\partial a \partial g_I}\delta g_I = \frac{\partial N}{\partial a},$$

$$\frac{\partial^2 N}{\partial a \partial b}\delta a + \frac{\partial^2 N}{\partial b^2}\delta b + \frac{\partial^2 N}{\partial b \partial g_J}\delta g_J + \frac{\partial^2 N}{\partial b \partial g_I}\delta g_I = \frac{\partial N}{\partial b},$$

$$\frac{\partial^2 N}{\partial a \partial g_J}\delta a + \frac{\partial^2 N}{\partial b \partial g_J}\delta b + \frac{\partial^2 N}{\partial g_J^2} + \frac{\partial^2 N}{\partial g_J \partial g_I}\delta g_I = \frac{\partial N}{\partial g_J},$$

$$\frac{\partial^2 N}{\partial a \partial g_I}\,\delta a + \frac{\partial^2 N}{\partial b \partial g_I}\,\delta b + \frac{\partial^2 N}{\partial g_J \partial g_I}\,\delta g_J + \frac{\partial^2 N}{\partial g_I^2}\,\delta g_I = \frac{\partial N}{\partial g_I} \,. \qquad \text{(II-56)}$$

Usually, initial values of the constants g_I and g_J are obtained from the known constants of another isotope (usually stable) of the same element. The atomic g factor, of course, is the same for the two isotopes, and g_I is calculated with the Fermi-Segrè formula. Initial values of a and b are generally determined from an analysis of high-field $\Delta F = 0$ transitions with second- and higher-ordered perturbation theory (Sec. II.A.3).

The partial derivatives are treated as constants and are evaluated for initial values of a, b, g_J, and g_I. This system of equations is solved for δa, δb, δg_J, δg_I. The new improved values of the parameters are determined by

$$\begin{aligned} a' &= a - \delta a, \\ b' &= b - \delta b, \\ g_J' &= g_J - \delta g_J, \\ g_I' &= g_I - \delta g_I. \end{aligned} \qquad \text{(II-57)}$$

By iterations of the above procedure, N may be minimized to within the desired accuracy.

Errors in the parameters are determined with the aid of Eqs. (II-56) evaluated with the parameters which minimized N, as follows:

$$\Delta a = \left[\text{minor of } \frac{\partial^2 N/\partial a^2}{\Delta}\right]^{1/2},$$

$$\Delta b = \left[\text{minor of } \frac{\partial^2 N/\partial b^2}{\Delta}\right]^{1/2},$$

$$\Delta g_J = \left[\text{minor of } \frac{\partial^2 N/\partial g_J^2}{\Delta}\right]^{1/2},$$

$$\Delta g_I = \left[\text{minor of } \frac{\partial^2 N/\partial g_I^2}{\Delta}\right]^{1/2}, \qquad \text{(II-58)}$$

where Δ is the determinant of the system of equations.

The true energies for each level are given by

$$X^*_1 = X_1 - \frac{m_1 g_I \mu_0 H}{h},$$

$$X^*_2 = X_2 - \frac{m_2 g_I \mu_0 H}{h}. \qquad \text{(II-59)}$$

The residual for each observation is calculated from the equation

$$R^i = f_{obs}{}^i - X^*{}_1{}^i + X^*{}_2{}^i = f_{obs}{}^i + \frac{(m_1 - m_2) g_I \mu_0 H^i}{h} - X_1{}^i + X_2{}^i. \qquad \text{(II-60)}$$

5. Effects of Configuration Mixing

Mixing of configurations is caused by the electrostatic interactions between electrons. The Hamiltonian for the electrons in an atom, neglecting magnetic interactions, can be written

$$\mathcal{H} = \sum_i \left(\frac{\vec{p}_i^{\,2}}{2m} - \frac{Ze^2}{r_i} \right) + \frac{1}{2} \sum_{i \neq j} \frac{e^2}{r_{ij}}, \qquad \text{(II-61)}$$

where r_{ij} represents the distance between two electrons and Z is the atomic number. Matrix elements of this Hamiltonian vanish if the states arising from the two configurations differ in either multiplicity, total orbital angular momentum L, total angular momentum J, or parity.

Schwartz (SCH 55) has considered the effect of configuration interaction on the hfs interaction constants for electronic configurations of the type $s^2\ell_j$ (or $s^2\ell^{-1}{}_j$). The case in which one of the s electrons is raised to a higher s state, s', is considered.

The wave function in LS coupling is then written

$$\Psi_J = \alpha_0(s^2(S=0)^2L_J) + \alpha_1(ss'(S=1)^2L_J) + \alpha_2(ss'(S=0)^2L_J), \qquad \text{(II-62)}$$

with normalization $\alpha_0^2 + \alpha_1^2 + \alpha_2^2 = 1$, where S is the resultant spin angular momentum of the two s electrons which then couples to the spin of the ℓ electron to give the doublet. We make the approximation $\alpha_1^2 \ll 1$. Koster (KOS 52) has evaluated these normalization constants for gallium, using numerical wave functions, and has found $\alpha_1^2 = 0.001$.

The theoretical formula for the fine-structure splitting δ is not affected by this type of configuration interaction, since s electrons do not contribute to the fine-structure separations. Also, the octupole and quadrupole matrix elements are essentially the same (to order α_1^2) as those one would get from considering only the valence ℓ electron. The dipole matrix elements, however, can be quite large, and consequently the nuclear moment, calculated from the measured interaction constant a

[Eq. (II-9a)], can be greatly in error. Schwartz outlines a method by which the interaction constant a can be corrected when measured in both the $J = L + 1/2$ and $J = L - 1/2$ electronic states.

From Schwartz, the interaction constant is

$$a = \frac{M_1}{IJ} \frac{(2J)!}{[(2J-1)!(2J+2)!]^{1/2}} (J\|T_e^{(1)}\|J), \qquad \text{(II-63)}$$

where M_1 is the nuclear magnetic moment in appropriate units and the double-barred matrix element is the reduced matrix element of the electronic dipole operator. We write the total electronic dipole operator, $T_e^{(1)}$, as the sum of an operator $T_\ell^{(1)}$ acting on the valence ℓ electrons and another, $T_s^{(1)}$, acting on the s electrons. The general reduced matrix element becomes

$$(J\|T_e^{(1)}\|J') = (J\|T_\ell^{(1)} + T_s^{(1)}\|J') = (J\|T_\ell^{(1)}\|J') + \Delta_{JJ'}, \qquad \text{(II-64)}$$

where $\Delta_{JJ'} = (J\|T_s^{(1)}\|J')$. $\Delta_{JJ'}$ is a sum of matrix elements between various terms of Eq. (II-60), all of the form

$$\Delta_{JJ'} \sim (s\tfrac{1}{2}, \tfrac{1}{2}\ell, J\|T_s^{(1)}\|s'\tfrac{1}{2}, \tfrac{1}{2}\ell, J')$$

$$= W(\tfrac{1}{2}J\tfrac{1}{2}J'; \ell 1)(2J+1)^{\frac{1}{2}}(2J'+1)^{\frac{1}{2}}(-1)^{-\ell+\frac{1}{2}+J}$$

$$\times (s\tfrac{1}{2}, \tfrac{1}{2}\|T_s^{(1)}\|s'\tfrac{1}{2}, \tfrac{1}{2}). \qquad \text{(II-65)}$$

The W is a known function called the Racah coefficient (RAH 42). Thus, without actually calculating $\Delta_{JJ'}$, we have separated out its dependence on J and J'.

Now, we can write

$$a = a_0 + \delta, \tag{II-66}$$

where

$$a_0 = \frac{M_1}{IJ} \frac{(2J)!}{[(2J-1)!(2J+2)!]^{1/2}} (J\|T_\ell^{(1)}\|(J), \tag{II-67}$$

$$\delta = \frac{M_1}{IJ} \frac{(2J)!}{[(2J-1)!(2J+2)!]^{1/2}} (J\|T_s^{(1)}\|J). \tag{II-68}$$

The theoretical relations between a_0 and δ in the $J = L + 1/2$ (primed) and $J = L - 1/2$ (double-primed) electronic states is now obtained:

$$\frac{a_0'}{a_0''} = \left[\frac{(J-1)(2J-1)}{(J+1)(2J+1)}\right]^{\frac{1}{2}} \frac{(J\|T_\ell^{(1)}\|J)}{(J-1\|T_\ell^{(1)}\|J-1)},$$

$$\frac{\delta'}{\delta''} = \left[\frac{(J-1)(2J-1)}{(J+1)(2J+1)}\right]^{\frac{1}{2}} \frac{\Delta_{JJ}}{\Delta_{J-1,J-1}}. \tag{II-69}$$

From Schwartz, we obtain the relation

$$\frac{(J\|T_\ell^{(1)}\|J)}{(J-1\|T_\ell^{(1)}\|J-1)} = \left[\frac{(J-1)(2J+1)}{(J+1)(2J-1)}\right]^{\frac{1}{2}} \frac{1}{\theta}, \tag{II-70}$$

where

$$\theta = \frac{F_r''}{F_r'} \left|\frac{C''}{C'}\right|^2 \sim 1. \tag{II-71}$$

Here F_r is relativistic correction factor (CAS 36) and C is a normalization constant which gives the density at the nucleus of the wave function of the outer valence electron. For the two different electronic states of the doublet, one has

$$\frac{C''}{C'} \approx -1. \qquad \text{(II-72)}$$

A more accurate approximation of the ratio, however, is given by Casimer (CAS 36, p. 55),

$$\left| \frac{C''}{C'} \right|^2 = 1 + \frac{3\alpha Z^2}{2L(L+1)n^*}, \qquad \text{(II-73)}$$

where n^* is the effective quantum number. This expression is fairly valid for the lighter nuclei ($Z \lesssim 50$), but should be used with caution for heavier nuclei. From Eq. (II-65), we have

$$\frac{\Delta_{JJ}}{\Delta_{J-1,J-1}} = -\left[\frac{(J+1)(2J+1)}{(J-1)(2J-1)} \right]^{\frac{1}{2}}. \qquad \text{(II-74)}$$

Thus,

$$\frac{a_0'}{a_0''} = \frac{1}{\theta} \frac{J-1}{J+1};$$

$$\delta' = -\delta''. \qquad \text{(II-75)}$$

With the aid of Eqs. (II-66) and (II-75), the measured values of a for both electronic states can be used to obtain the corrected interaction constants a_0. These are the values which must be used in Eqs. (II-9a), (II-11), and (II-20) to obtain the proper nuclear moments.

B. Nuclear Structure

1. Independent-Particle Model

Various systematic trends in experimental measurements of nuclear spins and moments led to a number of interesting conclusions in nuclear

theory.

One of the first trends to be noticed was that isotopes with odd A have half-integral spins, while isotopes with even A have integral spins. Also, isotopes with even Z and even A (even-even nuclei) have zero spin in the nuclear ground state. Since the orbital angular momentum of the nucleons can give rise only to integral values, it was concluded that the intrinsic spin of the proton or neutron was I = 1/2. This value has been verified by direct experimental measurement.

Magnetic moments of the proton in hydrogen and the free neutron have been measured and found to be

$$\mu_p = 2.793 \text{ nm},$$

$$\mu_n = -1.913 \text{ nm}. \qquad \text{(II-76)}$$

From naive arguments, one would expect $\mu_p = 1$ and $\mu_n = 0$. The anomalous values appear to be associated with π-mesonic fields surrounding the individual nucleons.

Another interesting systematic trend was demonstrated by Schmidt (SCH 37) who observed that one could, to a fair degree of approximation, represent the magnetic moments of the odd-A nuclei by the following equations:

Odd proton:

$$\mu_s = j - \tfrac{1}{2} + \mu_p, \qquad \text{for } j = \ell + \tfrac{1}{2};$$

$$\mu_s = j + \frac{1}{j+1}\left(\tfrac{1}{2} - \mu_p\right), \qquad \text{for } j = \ell - \tfrac{1}{2}; \qquad \text{(II-77)}$$

Odd neutron:

$$\mu_s = \mu_n, \qquad \text{for } j = \ell + \tfrac{1}{2};$$

$$\mu_s = -\frac{j}{j+1}\mu_n, \qquad \text{for } j = \ell - \tfrac{1}{2}. \tag{II-78}$$

In this model, the angular momentum I of the nucleus is due to the total angular momentum j of the last odd nucleon, where j consists of an orbital angular momentum ℓ coupled with the intrinsic spin of the nucleon. If μ_p and μ_n in Eqs. (II-77) and (II-78) are assigned the anomalous values given by Eq. (II-76), the "Schmidt limits" on the magnetic moments for odd-A nuclei are obtained.

If the Dirac values $\mu_p = 1$ and $\mu_n = 0$ are used in Eqs. (II-77) and (II-78), then the "Dirac limits" for the nuclear magnetic moments are obtained. Experimentally, it has been found that in almost every case the observed magnetic moments for odd-A nuclei fall between these two limits. Thus, by knowing the nuclear spin and magnetic moment, one can ascertain the parity of the nuclear ground state.

The existence of the "magic numbers" 2, 8, 20, 28, 50, 82, 126, and 184, associated with nuclei having particularly stable nucleon configurations, prompted the postulation of nuclear shell theory. This theory essentially assumes a suitable combination of a box-type potential for heavy nuclei and a parabolic potential for light nuclei. The theory introduced the magic numbers 2, 8, 20, 40, 70, and 112. Since the numbers 40, 70, and 112 have no experimental basis, and since the numbers 28, 50, 82, 120, and 184 are missing, Maria Goepert-Mayer and, indepen-

dently, Haxel, Jensen, and Suess (MAY 55) proposed to describe the occurrence of the missing stable nucleon numbers by a strong spin-orbit coupling of individual nucleons which increases with increasing ℓ. The resulting energy-level diagram, which satisfactorily accounted for all magic numbers, is shown in Fig. 6.

The theory with this modification has had spectacular success in prediction of nuclear spins of odd-A nuclei. All levels are to be filled with as many particles as allowed by the Pauli exclusion principle. The predicted nuclear spin, then, is the total angular momentum of the last odd neutron or proton.

For odd-odd nuclei, the independent-particle shell model does not predict the spins with as much precision. Nordheim (NOR 51) has formulated empirical rules for coupling the j_p of the odd proton to the j_n of the odd neutron. In detail, they are:

(N1) If both proton and neutron are in levels in which $j_p = \ell_p \pm 1/2$ and $j_n = \ell_n \pm 1/2$, then the angular momenta j_p and j_n tend to add, although not necessarily to the highest possible value $I = j_p + j_n$.

(N2) If the odd nucleons are in levels in which $j_p = \ell_p \pm 1/2$ and $j_n = \ell_n \mp 1/2$, then the total angular momentum of the ground state is the smallest possible, or $I = |j_n - j_p|$.

Brennan and Bernstein (BRE 60) have recently proposed revisions to Nordheim's rules, which essentially leave the strong rule, N2, unaffected but strengthen the weak rule, N1. For configurations in which both the odd protons and odd neutrons are particles (or holes) in their respective unfilled subshells, the revised coupling rules are:

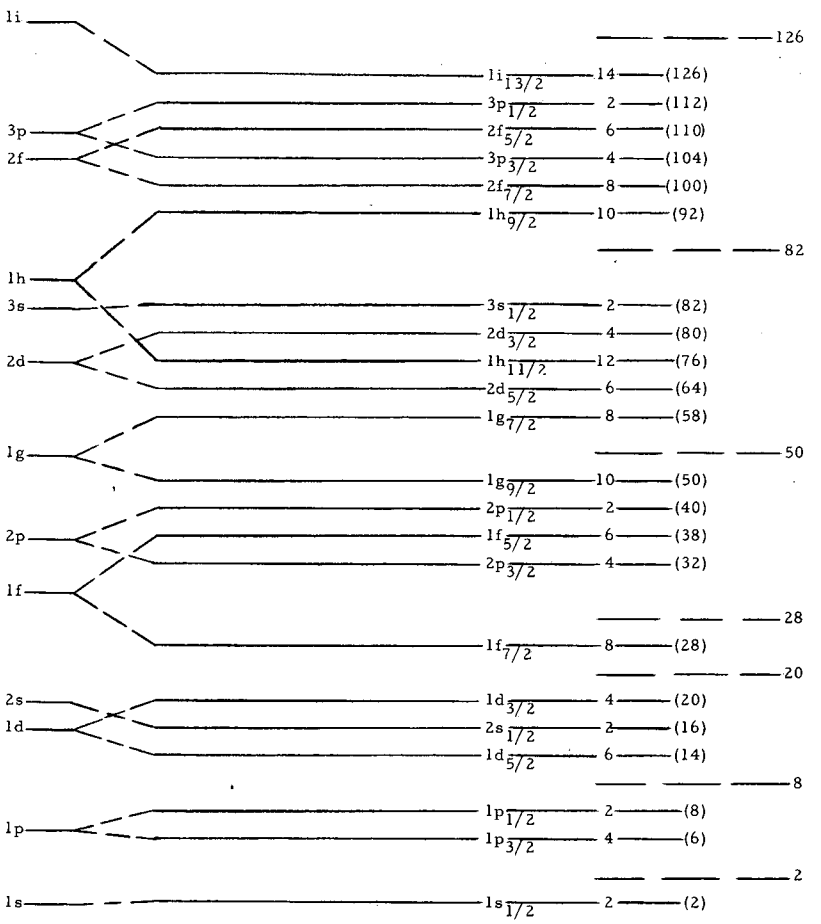

MU-17154

Fig. 6. Schematic diagram of nuclear level systems with spin-orbit coupling.

(BB1) $I = |J_p \pm J_n|$, for $j_p = \ell_p \pm 1/2$ and $j_n = \ell_n \pm 1/2$,

(BB2) $I = |J_p - J_n|$, for $j_p = \ell_p \pm 1/2$ and $j_n = \ell_n \mp 1/2$.

For the special case J_p or J_n equal to 1/2, the ambiguity in BB1 is removed and the spin $I = J_p + J_n$ is predicted. For configurations in which there is a combination of particles and holes, the prediction is much less certain, although there is a tendency for the resultant spin to be given by

$$(BB3) \quad I = J_p + J_n - 1.$$

Here, a distinction is made between the single-particle total angular momentum, j_p (or j_n), and the observed total angular momentum of adjacent odd-A nuclei, J_p (or J_n), to include cases of high seniority in which $j_p \neq J_p$ (or $j_n \neq J_n$).

The magnetic moments predicted by the independent-particle model for odd-A nuclei are given by Eqs. (II-77) and (II-78), in which μ_p and μ_n are the anomalous proton and neutron magnetic moments.

In the case of odd-odd nuclei, fair agreement between experiment and theory is attained if jj coupling is used to combine the magnet effects of the proton and neutron. The resulting expression for μ is

$$\mu = \frac{I}{2}(g_p + g_n) + (g_p - g_n)\left[\frac{j_p(j_p + 1) - j_n(j_n + 1)}{2(I + 1)}\right], \qquad (II-79)$$

where g_p and g_n are the g factors of the odd proton and neutron, respectively, given by Eqs. (II-77) and (II-78).

For a single nucleon in a given subshell, the independent-particle

model yields the following expressions for the nuclear electric quadrupole moments (BLI 57):

$$Q_j = -\frac{(2j-1)}{2(j+1)}\langle r^2\rangle, \quad \text{for an odd-proton nucleus,} \tag{II-80}$$

$$Q \approx \frac{Z}{(A-1)^2} Q_j, \quad \text{for an odd-neutron nucleus,} \tag{II-81}$$

where j is the total angular momentum of the single particle. The $\langle r^2\rangle$ is the average value of r^2 for the nucleon orbit and is usually replaced by $3R_0^2/5$, where R_0 is the nuclear radius.

For more than one nucleon in a given subshell, the quadrupole moments are given by

$$Q_{I=j} = Q_j \frac{2j+1-2\lambda}{2j-1}, \quad (\lambda \text{ odd}),$$

$$Q_{I=0} = 0, \quad (\lambda \text{even}), \tag{II-82}$$

where λ is the occupation number of the subshell. Since Q_j is negative, Q_I is negative for $\lambda < (2j+1)/2$ and positive for $\lambda > (2j+1)/2$.

For an odd-odd nucleus, the independent-particle model gives the expression

$$Q = \frac{(2I+1)!}{2j_p!}\left[\frac{(2j_p-2)!(2j_p+3)!}{(2I-2)!(2I+3)!}\right]^{1/2} W(j_p I j_p I; j_n 2)(-)^{(j_n-j_p-I)} Q_{j_p}, \tag{II-83}$$

where Q_{j_p} is the quadrupole moment of a proton in the state j_p and $W(j_p I J_p I; j_n 2)$ is a Racah coefficient.

2. Collective Model

In the region of closed shells, the equilibrium shape of the nucleus is approximately spherical and the independent-particle model can be expected to give a good description. However, in regions far removed from closed-shell configurations, the many "loose" nucleons enable the nucleus to assume an energetically more favorable nonspherical shape. Deviations of this kind can give rise to quadrupole moments 10 to 20 times the values predicted by the independent-particle model.

Various models have been proposed to account for these effects. Rainwater (RAI 51) has proposed a semiempirical static model which makes fairly accurate predictions for the quadrupole moments if the nuclear deformations are small. However, for large deformations of the nucleus, the dynamic collective model of Bohr, Mottelson, and Nilsson has had more success. A brief description of this model,as well as references to the original literature, is given by Kopfermann (KOP 58). More recently, the model has been applied to the odd-A nuclei in the interesting regions $A \approx 25$, $150 < A < 190$, and $A > 222$ by Mottelson and Nilsson (MOT 59).

An interesting feature of this model has been the reduction of the degeneracy of each of the levels in the shell model brought about by the introduction of a nuclear deformation parameter δ. Each j level is split into $\frac{1}{2}(2j + 1)$ components, characterized by the components Ω of j, in the direction of the axis of symmetry of the deformed nucleus. Each Ω state is doubly degenerate, since states with $+\Omega$ and $-\Omega$ have the same energy. The energy-level diagrams, plotted as a function of δ, are the so-called "Nilsson diagrams."

The spin of an odd-A nucleus is determined by filling levels for a given value of δ with nucleons in much the same manner as for the shell model. The nuclear spin is then the value of Ω characterizing the energy level of the last odd nucleon.

For odd-odd nuclei, Gallagher and Moszkowski (GAL 58) have proposed rules very similar to those of Nordheim for coupling the Ω_p of the odd proton to the Ω_n of the odd neutron. The rules are

$$\text{(GM1)} \quad I = \Omega_p + \Omega_n, \qquad \text{for } \Omega_p = \Lambda_p \pm \tfrac{1}{2} \text{ and } \Omega_n = \Lambda_n \pm \tfrac{1}{2} ;$$

$$\text{(GM2)} \quad I = |\Omega_p - \Omega_n|, \qquad \text{for } \Omega_p = \Lambda_p \pm \tfrac{1}{2} \text{ and } \Omega_n = \mp \tfrac{1}{2} .$$

Here Λ_p and Λ_n are asymptotic quantum numbers characterizing the orbital angular momenta of the last odd proton and neutron, respectively.

In the collective model, the magnetic moment in the limit of strong coupling of the nucleon to the surface is given by the expression

$$\mu_c = (g_\Omega \Omega + g_R) \frac{I}{I+1} , \qquad \text{(II-83)}$$

where g_Ω is the g factor of the loose nucleons having a component of angular momentum Ω in the direction of the deformed nuclear core, and g_R is the g factor for the angular momentum carried by the surface. For a uniformly charged nucleus, g_R may be estimated from the expression

$$g_R \approx Z/A. \qquad \text{(II-84)}$$

If j is still a good quantum number for odd-A nuclei, then g_Ω may be replaced by the Schmidt value for the last odd particle (g_j). For the nuclear ground state, then, Eq. (II-83) becomes

$$\mu_c = (g_j I + g_R) \frac{I}{I+1}, \qquad I = j > 3/2. \tag{II-85}$$

The principal difference between this expression and the Schmidt formula is a shift of the upper Schmidt line downward in the case of an unpaired proton, and a shift of the lower Schmidt line upward in the case of an unpaired neutron.

For odd-odd nuclei, Gallagher and Moszkowski (GAL 58) give the expression

$$g_\Omega \Omega = [\pm(\Lambda_p + 5.6\,\Sigma_p) \mp 3.8\,\Sigma_n], \tag{II-86}$$

where Σ_p and Σ_n are the asymptotic quantum numbers for the intrinsic spin of the proton and neutron deduced from the Nilsson diagrams. The signs of the two terms in the expression are determined from the signs of Ω_p and Ω_n appearing in the coupling rule, i.e., if the sign of Ω_p (or Ω_n) is positive, the upper sign is used; if the sign of Ω_p (or Ω_n) is negative, the lower sign is used. The signs of Σ_p and Σ_n are plus or minus depending on whether the particle intrinsic spins are parallel (+) or anti-parallel (-) to their respective orbital angular momenta. Equation (II-86) used in conjunction with Eqs. (II-83) and (II-84) yields theoretical magnetic moments for odd-odd nuclei useful for comparison with the moments predicted by the independent-particle model.

The intrinsic nuclear electric quadrupole moments are related to the deformation parameter by the expression

$$Q_0 = \frac{4}{5}\,\delta Z R_0^2 (1 + \frac{1}{2}\,\delta + \cdots), \tag{II-87}$$

where Z is the nuclear charge number and R_0 is the mean charge radius of the nucleus. In the dynamic model, the quadrupole moment is composed of the loose nucleon moment Q_j and the core moment Q_c,

$$Q = Q_j + Q_c . \tag{II-88}$$

For large deformation, Q_j can be neglected compared with Q_c. Since the measured Q_I involves the component of Q_0 in the direction of the nuclear spin axis about which the symmetry axis performs a precession, we have the relation

$$Q_c = Q_0 \frac{3\Omega^2 - I(I+1)}{(I+1)(2I+3)} , \tag{II-89}$$

where Ω is the component of the angular momentum in the direction of the spin axis. For the ground state of the nucleus, $I = \Omega$ and

$$Q_I \cong Q_c = \frac{I}{I+1} \frac{2I-1}{2I+3} Q_0 . \tag{II-90}$$

III. EXPERIMENT

A. Experimental Apparatus

1. Atomic Beam Machine

The atomic beam machine used in these experiments was built by previous experimenters. Details of design and construction are described in Sunderland's thesis (S 56), and consequently is not considered here.

The basic theory of operation is shown pictorially in Fig. 7. Atom 1 leaves oven O and enters the deflecting magnet A, which has a field gradient $(\nabla H)_z$ in the direction shown. The atom, having an appreciable effective magnetic moment, is deflected through the collimating slit at the end of the A magnet. Since, in this case, no transition is induced in the uniform field (H_c) and the gradient in magnet B is in the same direction as in magnet A, Atom 1 is deflected onto the pole faces of magnet B. If, however, a transition is induced in the uniform C field which changes the sign of the effective magnetic moment, Atom 2 is deflected in the opposite direction and refocused at D. The refocusing condition for this machine is that atoms must undergo transitions in the C field corresponding to the change $m_J = \pm \frac{1}{2} \longleftrightarrow \mp \frac{1}{2}$ in the high fields of the A and B magnets. The stop wire S prevents undeflected atoms in the high-velocity tail of the modified Maxwellian distribution from reaching the detector.

Figure 8a-b shows the actual atomic beam machine used in the experiments. Several external modifications are shown which resulted mainly from the work on these isotopes, and in particular on La^{140}.

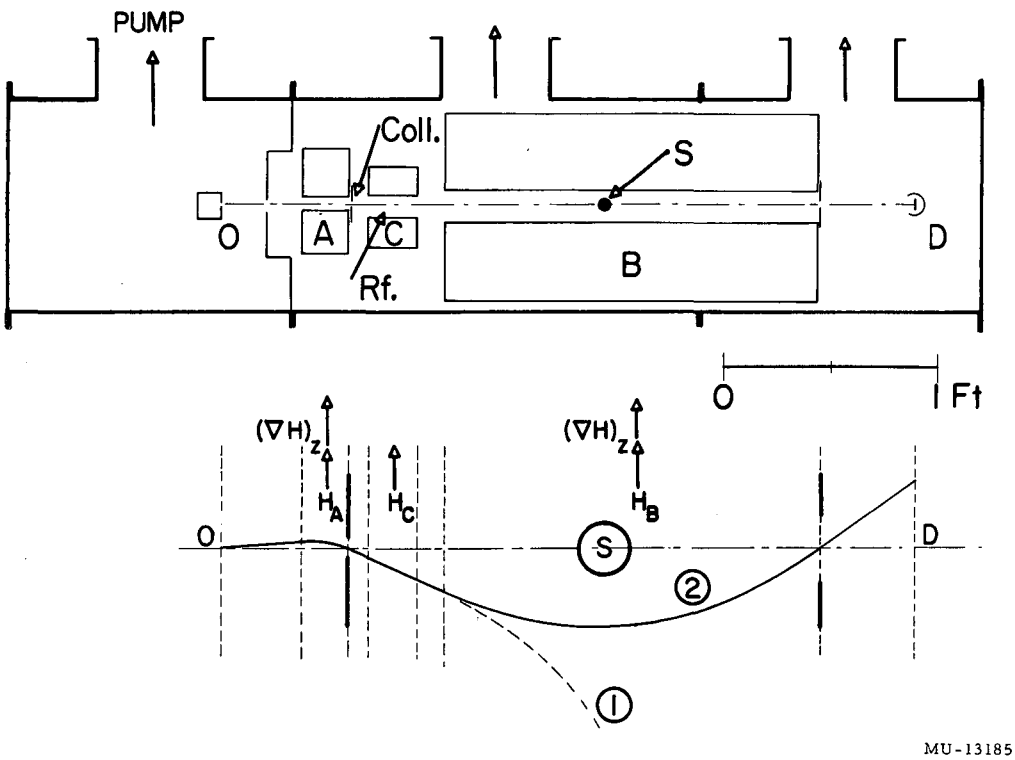

Fig. 7. Schematic component arrangement and atom trajectory in an atomic-beam magnetic-resonance (flop-in) machine.

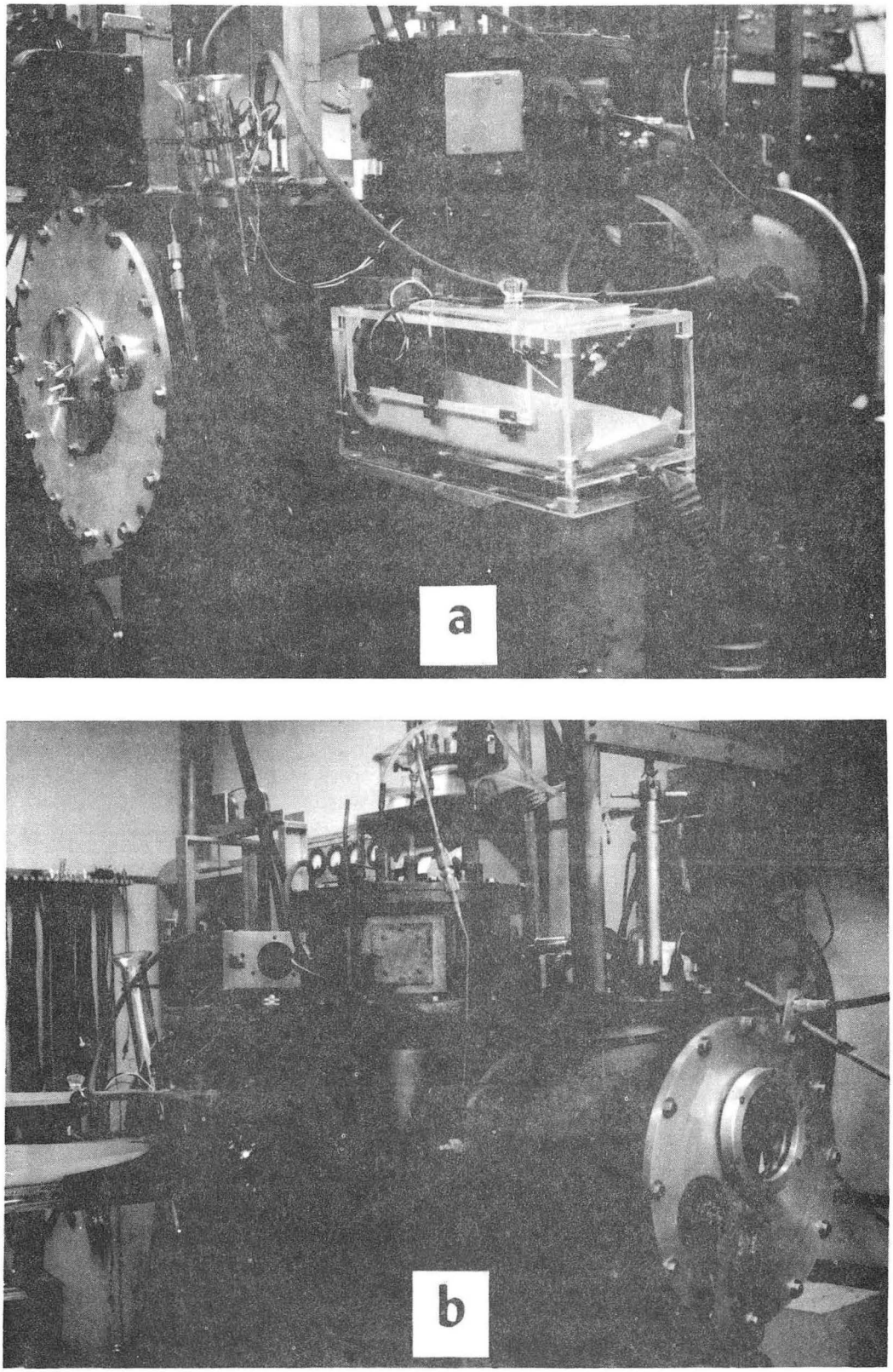

ZN-2370

Fig. 8. (a) Oven end of atomic beam machine.
(b) Detector end of atomic beam machine.

The high-energy γ rays given off by La^{140} created a serious health hazard when work on this isotope was initiated. The γ-ray activities of the ovens were sometimes as high as 70 r/hr at a distance of 4 inches. After the oven had been placed in the machine, the γ-ray activity in some of the operating areas around the machine was as high as 2.5 r/hr, so the experimenter usually received his maximum allowable monthly dosage of radiation in one or two days.

As a result, additional shielding as shown in Fig. 8c was added. The lead walls, consisting of lead bricks, are 3 in. thick and can "easily" be removed in certain strategic locations if required. In addition to the side shielding shown in the figure, shielding has also been placed on top of the machine in order to reduce the 20-mr/hr γ activity in the research room above. Chalk marks on the shielding (in units of mr/hr) in Fig. 8c indicate the effectiveness of this modification with a typical oven load of La^{140} in the machine. Access to the oven loader is afforded by the four steel-clad lead doors.

Another modification was necessary because the half lives of these isotopes are somewhat longer than the isotopes involved in previous research. Large quantities of activity accumulated on the oven loader and tended to flake off onto the floor when the loader was removed from the machine. The lucite box shown in Fig. 8a has virtually eliminated this problem. Not shown in the figure are the pump and filters which maintain a negative pressure in the box.

During the experimental investigation, thermal expansion and contraction opened a leak in a weld in the cold trap on one of the main

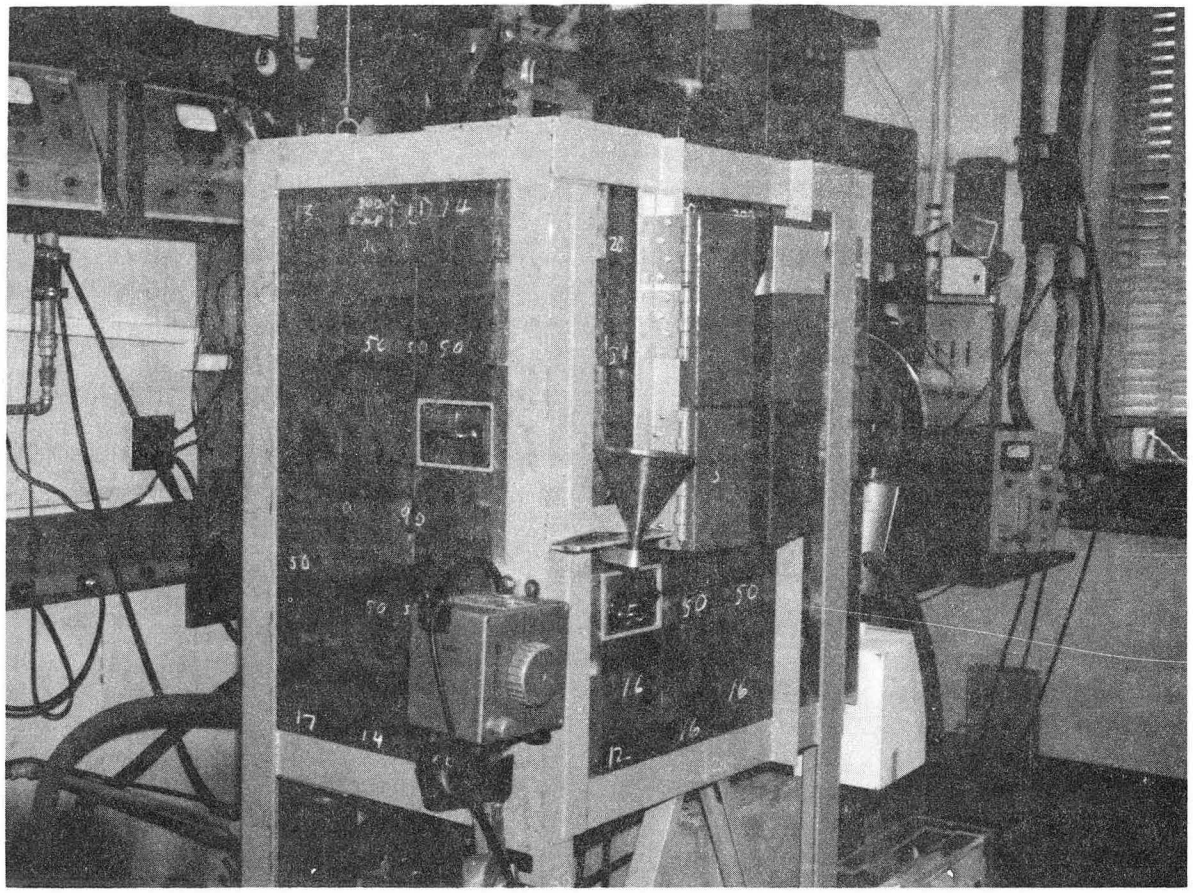

ZN-2362

Fig. 8 (c) Oven end of machine after installation of lead shielding.

diffusion pumps. After repair, it was impossible to observe a resonance. It was found that mechanical vibration had moved the hairpin into a very inhomogeneous region of the magnetic field during the course of the repair. In order to eliminate future difficulty, facilities to control positively the position of the hairpin in the C field from outside the machine were added. In this modification, rf power was fed to the hairpin through a rigid brass-walled coaxial line which extends from the hairpin through a Wilson vacuum seal in the end plate at the detector end of the machine. The hairpin was adjusted by varying the position of the end of the coaxial line. For a given setting of the A, B, and C fields, the position of the hairpin was adjusted to obtain minimum line width. As might be expected, the best average position was in the center of the C field. However, 30% reductions in line widths were realized under certain conditions by small variations from this central position.

2. Ovens

Beams of alkali atoms were produced by using resistance-heated iron ovens. The K^{43} oven, shown in Fig. 9, had the dimensions 3/4 × 7/8 × 3/4 in., with a 1/2-in.-diam chamber. Four tantalum-wire heating elements on each side of the chamber, and one in front, raised the oven to the temperature required for beam production. Good power stability made this oven very desirable where temperature limitations permitted.

Because of the high temperatures required by the other isotopes under investigation, tantalum ovens of the type shown in Fig. 10 were generally used. The sharp-edged tantalum crucible was used to prevent the molten metal from creeping out through the slits. Slit widths ranged from 3 to

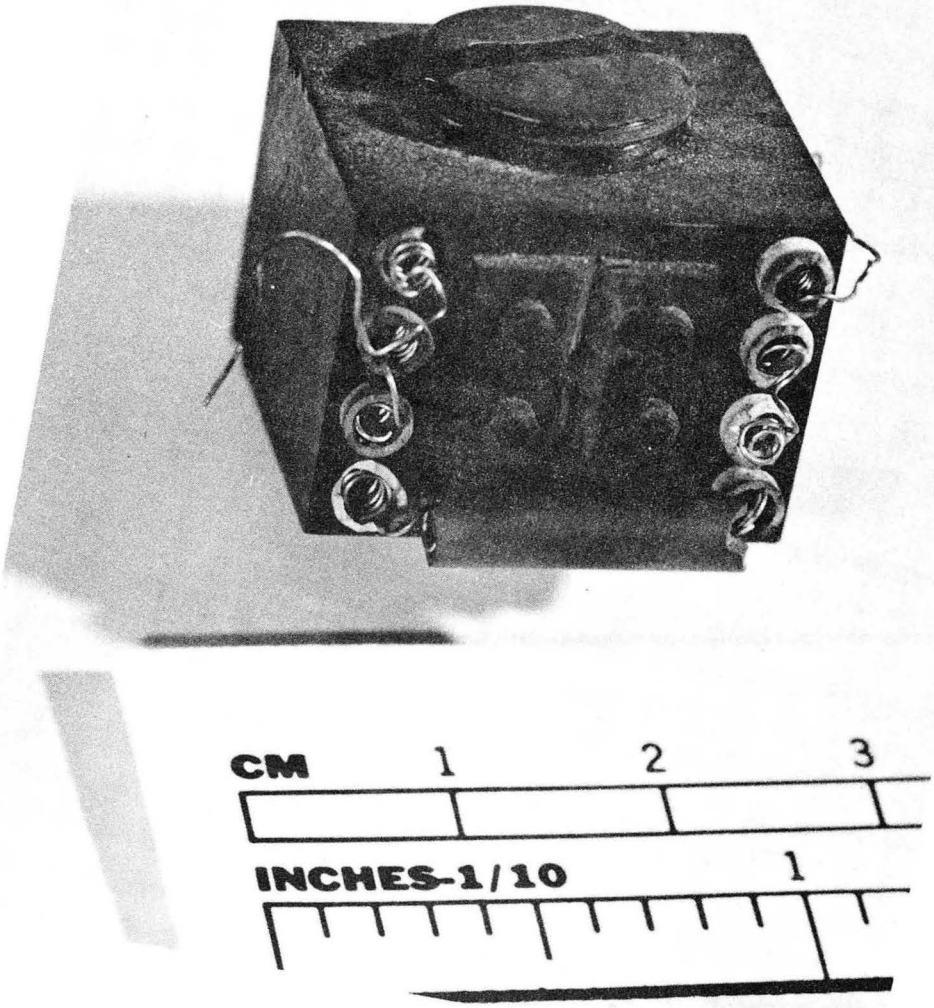

ZN-2678

Fig. 9. Resistance heated K^{43} oven.

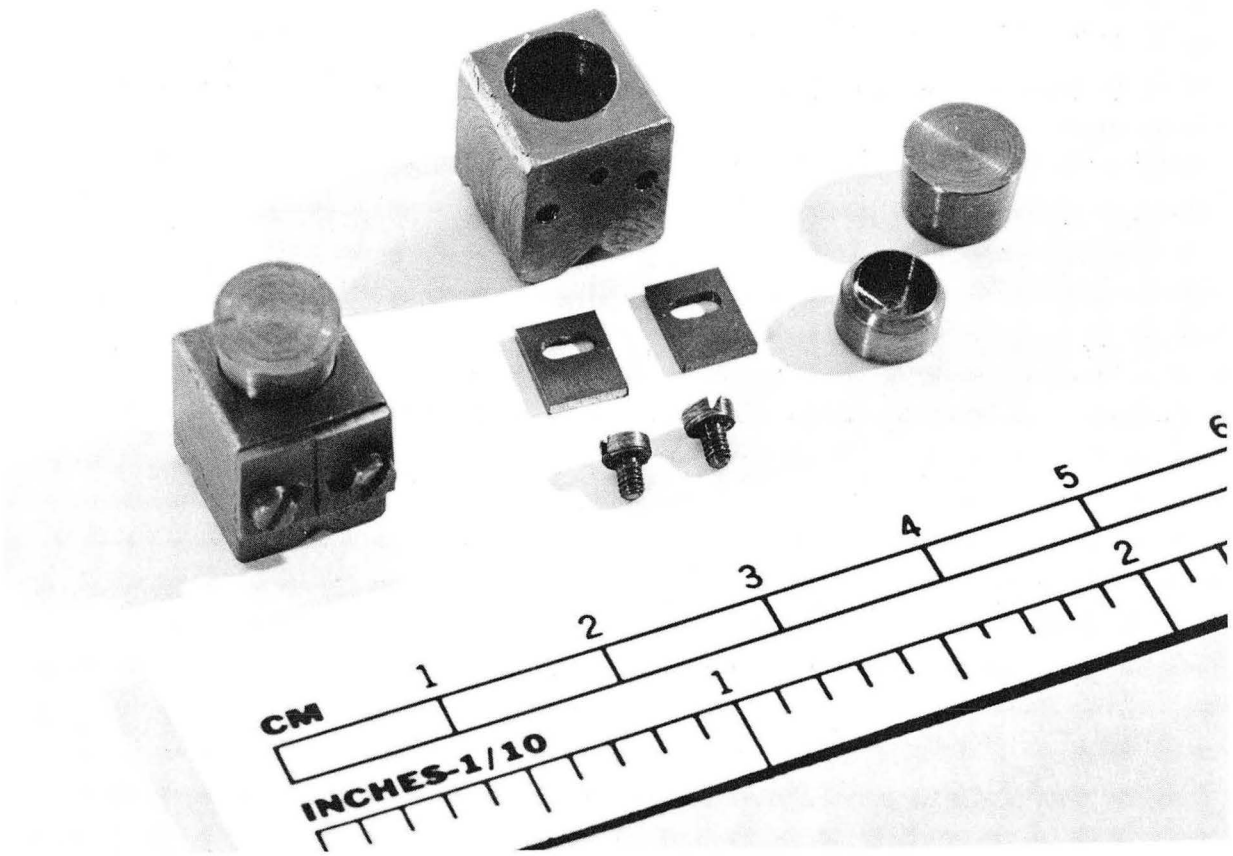

ZN-2679

Fig. 10. Electron bombardment Ta oven used for production of Y^{90}, La^{140}, and Lu^{177} atomic beams.

5 mils; 4 mils was the value most used. This type of oven produced very satisfactory atomic beams of Y^{90} and Lu^{177}.

La^{140} was quite another case, however. Without the tantalum crucible, results were completely obliterated by the very high background and erratic changes in beam intensity. The tantalum crucible alleviated this situation to some extent, and all the successful results were obtained with this type of oven.

Attempts were made to improve the stability and lower the machine background caused by the lanthanum beam. Carbon and tungsten ovens were tried. In both cases the lanthanum metal apparently diffused into or reacted with the oven walls at high temperatures. Both ovens lost their mechanical properties and crumbled into small pieces and dust shortly after their removal from the machine!

In another attempt a ceramic crucible was used in a tantalum oven. Again virtually all the material remained in the oven--apparently reacting with the ceramic crucible. In another case the use of a ThO_2 barrier around the tantalum crucible in a tantalum oven proved no more successful than the tantalum crucible alone. Further attempts to improve the beam stability and lower the background of La^{140} were interrupted in order to continue work on the other isotopes. However, these two problems must be solved before productive research on the hyperfine structure can be accomplished.

3. Radiofrequency Equipment

Frequencies in the 1-to-2500-Mc/sec region of the frequency spectrum were used in this research. Power requirements were of the order of 1 watt.

The signal generators used are listed below:

Signal Generator	Frequency Range
Tektronix Constant-Amplitude Signal Generator, Type 190	0.35 to 50 Mc/sec
Hewlett-Packard VHF Signal Generator, Model 608C	10 to 480 Mc/sec
Airborne Instruments Power Oscillator, Type 124C	200 to 2500 Mc/sec

Additional power for frequencies less than 200 Mc/sec was obtained from two "Instruments for Industry" Wide Band Amplifiers, Models 500 and 510.

Frequency-measuring equipment consisted of a Hewlett-Packard Electronic Counter, Model 524B, with Model 525A and 525B plug-in units. For frequencies higher than 220 Mc/sec, the rf signal was beat with a suitable harmonic from a Hewlett-Packard Transfer Oscillator, Model 540A. The fundamental of the transfer oscillator was then measured with the electronic counter. The 100-kc/sec internal-reference frequency in the electronic counter was calibrated weekly with a National Company Atomichron. Uncertainty in the counter crystal of this secondary standard was less than 1 part on 10^6. The radiofrequency was monitored continuously, and all measurements were made to the nearest kc/sec.

Signal-generator power output over a normal frequency sweep in the region less than 200 Mc/sec was essentially constant. The Airborne Instruments Power Oscillator, however, was quite power-sensitive. Consequently, the rf power was continuously monitored with a Hewlett-Packard

Microwave Power Meter, Model 430CR with which the rf power over a given frequency sweep was held constant. Much of the radiofrequency equipment is shown in Fig. 11.

A sketch of the rf hairpin is shown in Fig. 12. This hairpin worked very well for pi transitions but tended to give double-peaked resonances for sigma transitions. The atom, in passing through the hairpin, sees two rf components parallel to the C field and 180 deg out of phase with each other. The theoretical transition probability becomes zero at the resonant frequency (RAM 56, p. 132), thus giving rise to the double-peaked resonances. This hairpin characteristic has certain advantages, but is somewhat undesirable for radioactive detection, since greater resonance shape definition is required.

4. Beam-Detection Equipment

All atomic beams of the stable alkalies were detected by means of a surface ionization detector. The alkali atoms or molecules in the beam were ionized upon incidence upon a hot rhenium filament in the ratio usually taken as

$$n^+/n^0 = \exp[-e(I - \varphi)/kT], \qquad \text{(III-1)}$$

where I is the ionization potential of the incident atom and φ is the work function of the rhenium filament. If φ exceeds I by 0.5 volt, then all the atoms emerge from the filament as ions. The ions are accelerated to the collector surrounding the filament by 1.5 volts dc. The resulting current was measured with a Cary Vibrating Reed Electrometer. Currents as small as 10^{-13} amp could be measured without difficulty. Normal

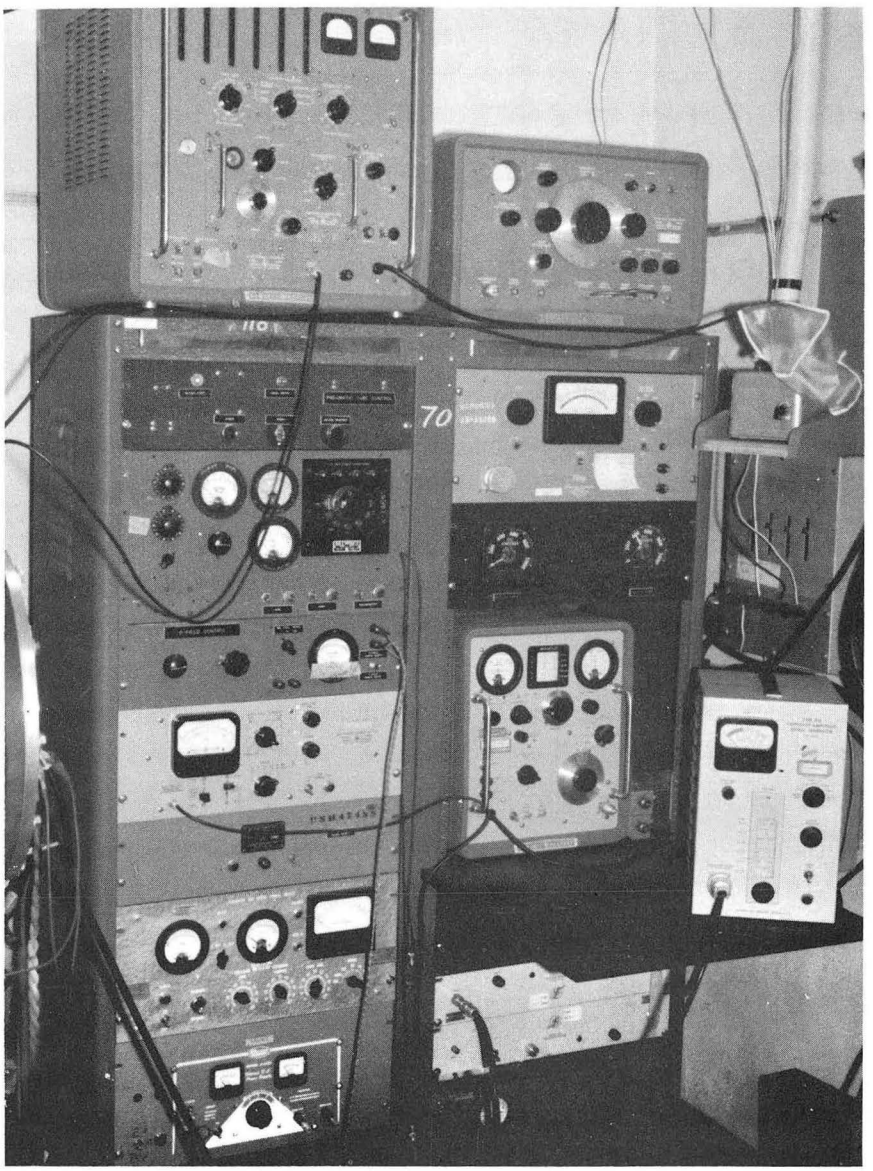

ZN-2365

Fig. 11. View of radiofrequency equipment.

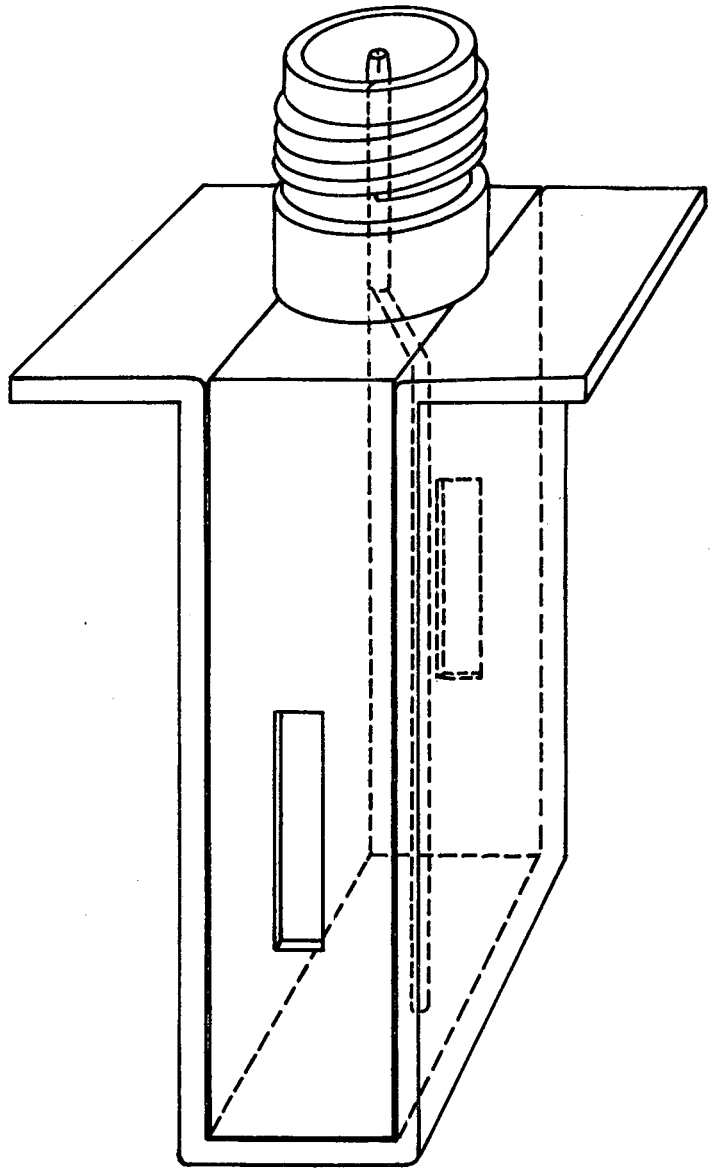

Fig. 12. Sketch of radiofrequency hairpin.

current at a resonance peak ranged from 10^{-12} to 10^{-11} amp.

All radioactive beams were detected by collecting the atoms in the beam on sulfur-coated surfaces or buttons for a short interval of time (usually 5 to 10 min). Since all the isotopes being discussed decay by β-particle emission, the activity on each button was detected by placing the sample in a continuous-flow β counter.

A cross section of a counting tube is shown in Fig. 13. Methane gas was allowed to flow slowly into the tube at the top of the chamber and out of the tube around the button at the bottom of the chamber. Slight positive pressure tended to flush out air which entered whenever the buttons were changed. The tubes were operated near the center of the Geiger voltage plateau (about 3200 volts). Thus, small variations in the high-voltage power supply did not change the counting efficiency.

The voltage pulse from the counting tube was amplified in a preamplifier before being counted in the scaling section of a recording pulse-height analyzer (shown in Fig. 14). A considerable amount of work was spent in reducing the background counting rate. The main source of difficulty was leakage current across the high-voltage capacitor that coupled the signal to the first stage of preamplification. When this difficulty was solved, counting backgrounds were reduced to 2 or 3 counts/min.

Instability in counting efficiency is a major problem with this type of β counter. This shortcoming appears to be due to the fact that the counting tube is an open system. The small amount of air introduced into the tube when the button is inserted tends to raise the initial counting rate. This problem can be diminished to some extent by allowing the tube

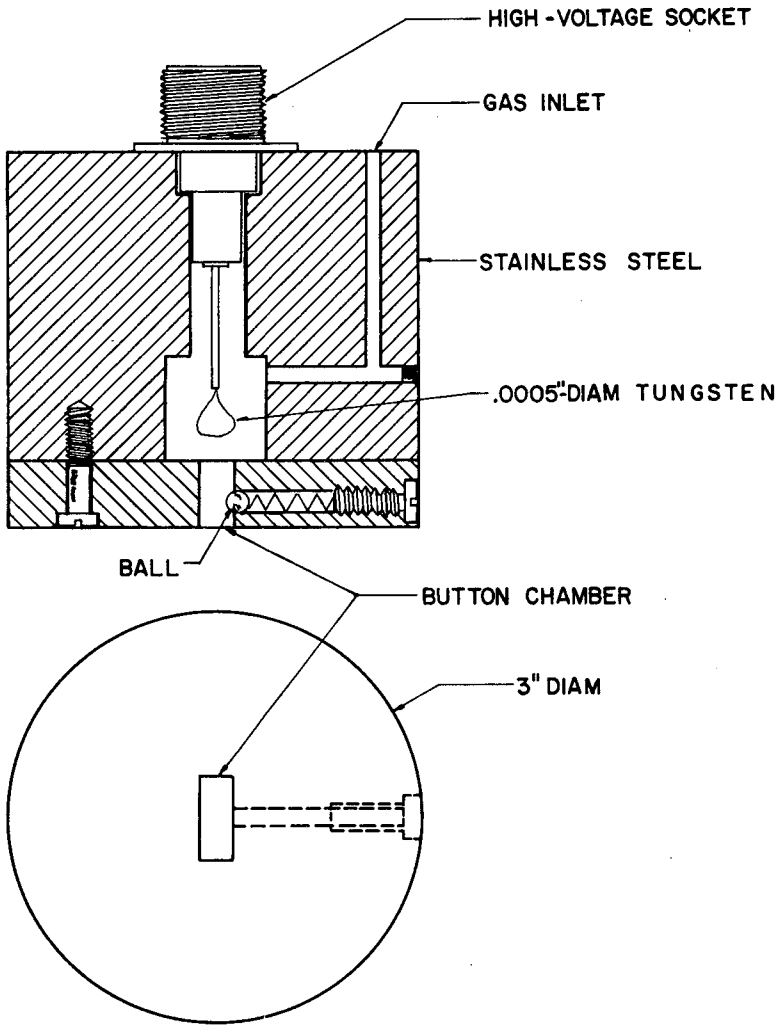

Fig. 13. Cross-sectional view of continuous-flow Geiger tube.

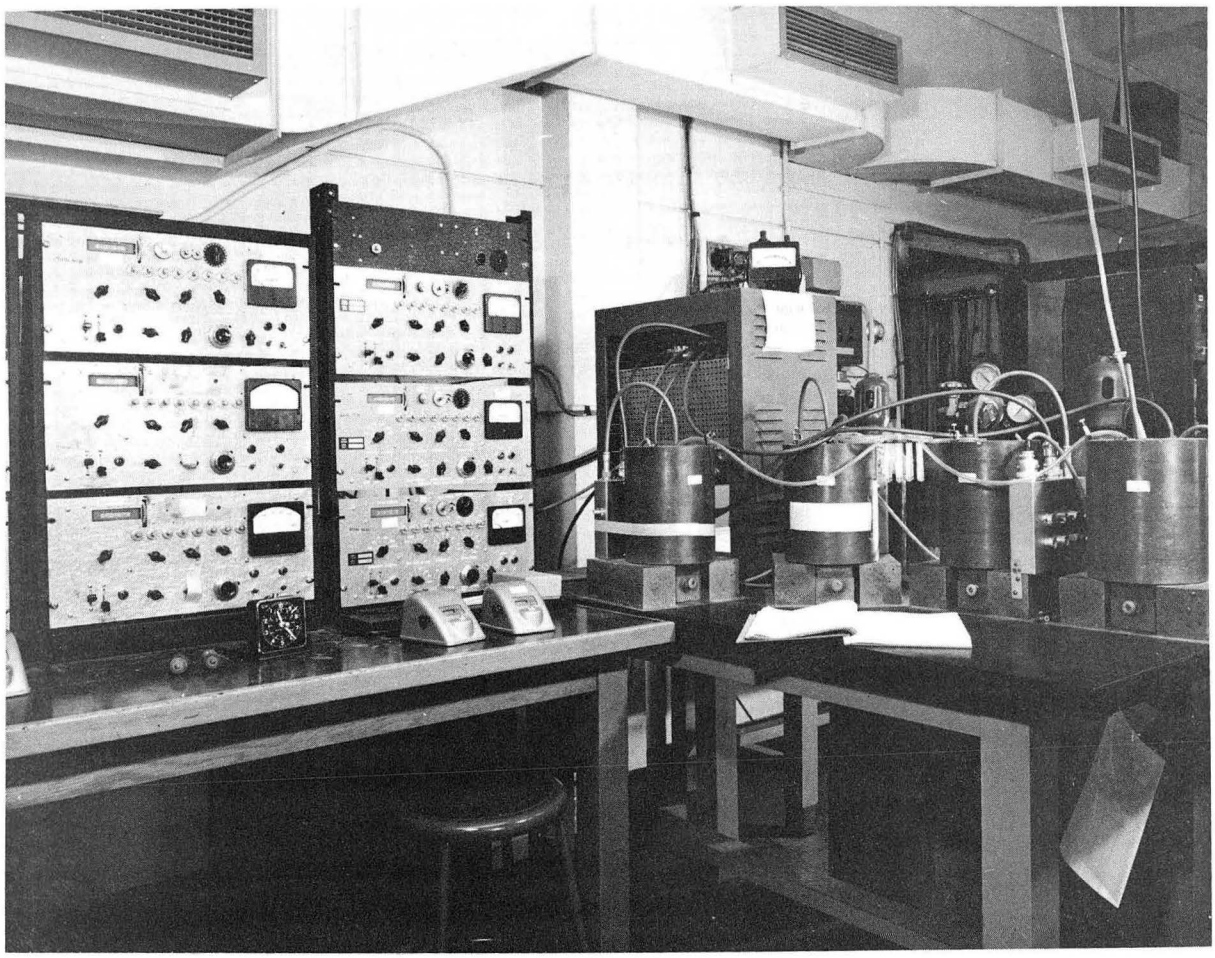

ZN-2675

Fig. 14. Scalers, high voltage supply, and shielded counting tubes used for detection of β-particle activity.

to flush out after the sample has been inserted. In addition, the high electric field inside the tube tends to accelerate lint and dust to the 1-mil high-voltage filament. A barely visible piece of lint on the filament can reduce counting efficiency by as much as 75%. Consequently, great care was exercised to insure that the buttons were dust-free before they were inserted into the counting chamber.

In spite of these difficulties, the increased efficiency (up to 10 times) over the more stable x-ray crystal counters justified use of the β counters for these experiments.

5. Pneumatic Tube

Since the counting rates for resonance buttons are generally less than 100 counts/min and since the γ-ray fields around the atomic beam machine are sometimes quite high, the counting of all resonance samples was done in a room four stories removed from the machine. As a result, sample transportation, especially when short half lives were involved, became a important problem.

The solution was to install an inexpensive pneumatic tube system. Approximately 450 ft of thin-walled war-surplus aluminum tubing (1/16 in. thick, i.d. 1-1/8 in.) was laid between the two research rooms, on the outside of the building. The tubing, in 12-ft lengths, was joined together by 4-in. lengths of high-pressure rubber tubing rigid enough to keep the sections properly aligned. Figure 15 shows the tubing extending along the roof of LeConte Hall.

A diagram of the control system is shown in Fig. 16. Four conductors were required between the two research rooms. Salient features of

ZN-2676

Fig. 15. View of aluminum tubing in pneumatic tube system connecting the two research rooms.

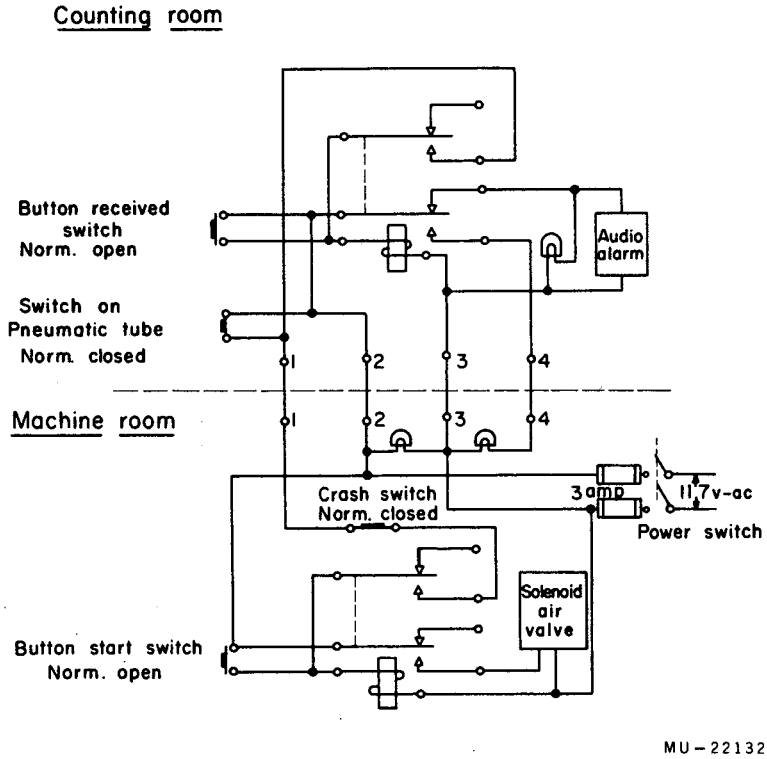

Fig. 16. Schematic of control system for pneumatic tube.

operation are as follows: (a) Button is placed in carrier shown in Fig. 17 and inserted in tube; (b) start switch is closed, thus opening solenoid air valve; (c) carrier opens microswitch on pneumatic tube upon arrival in counting room, thus closing solenoid air valve and actuating audio and visual signals; and (d) "received" switch is closed, thus turning off alarms and indicating reception of carrier to sender.

B. Isotope Production and Identification

With the exception of K^{43} (described in App. A), all the radioactive isotopes for which successful results were obtained in this research were pile-produced from the stable metal by (n,γ) reactions. Table I gives typical bombardment information. Bombardment conditions for Y^{90} and La^{140} provided enough activity to permit successful experimenting for periods of two to three half lives. In the case of Lu^{177}, the useful experimentation period was three to four half lives for each bombardment.

Table I

Typical bombardment conditions. The duration of bombardment is T_B; $T_{1/2}$ is the half life of each radioactive isotope.

Isotope (stable)	Abundance (%)	σ (barns)	Flux (n/cm^2-sec)	T_B	Reaction	$T_{1/2}$
Y^{89}	100	1.3	$2\text{-}9 \times 10^{13}$	60-120 hr	$Y^{89}(n,\gamma)Y^{90}$	64.2(3) hr[a]
La^{139}	99.911	8.9	2×10^{13}	60 hr	$La^{139}(n,\gamma)La^{140}$	40.22(2)hr[b]
Lu^{176}	2.60	3800	$.8\text{-}9 \times 10^{13}$	1-2 wk	$Lu^{176}(n,\gamma)Lu^{177}$	6.75(5) d[c]

[a](VOL 55) [b](KIR 54) [c](BET 58)

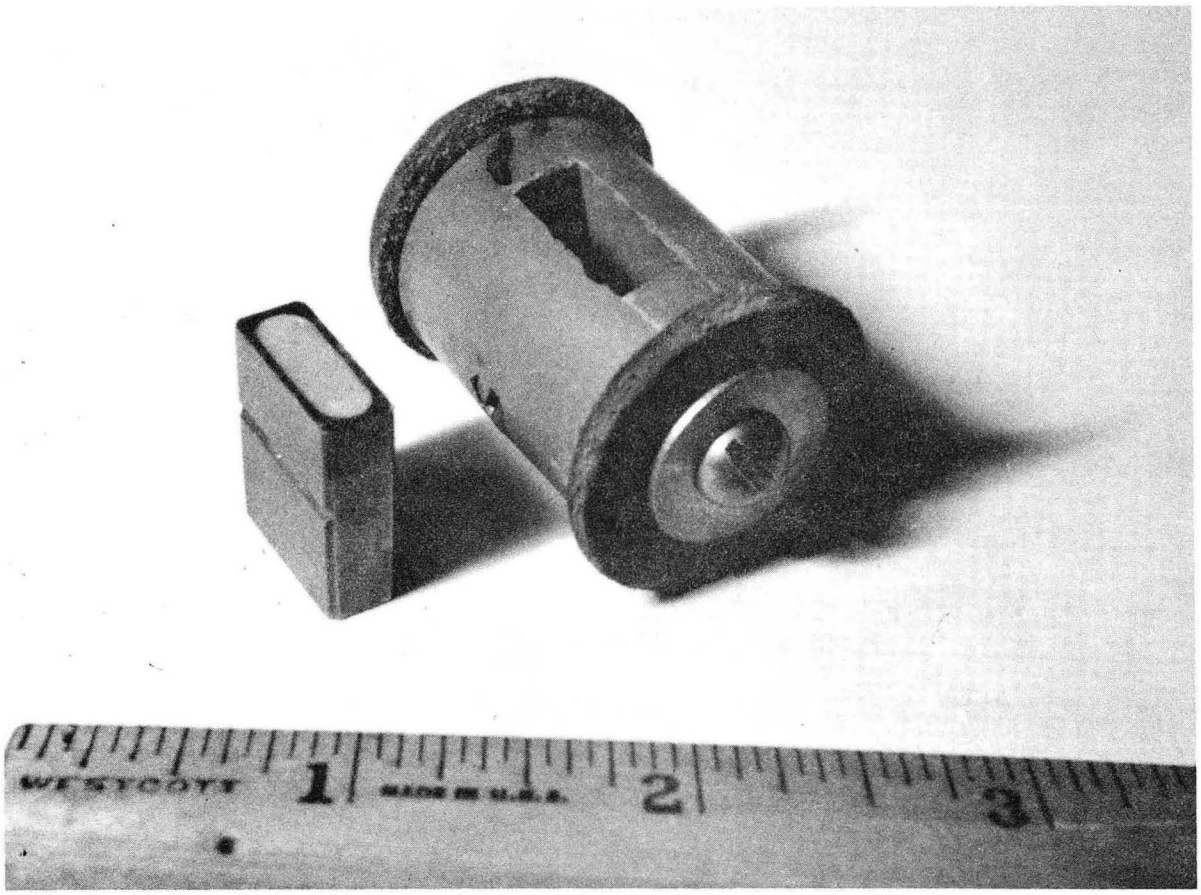

ZN-2367

Fig. 17. Collector button and carrier used to transport button through pneumatic tube.

During the early part of the research, all irradiations were done at the Livermore Pool-Type Reactor, where the maximum available flux was approximately 2×10^{13} n/cm^2-sec. Later bombardments were done in the General Electric Test Reactor at the Vallecitos Atomic Laboratory, where a somewhat higher flux ($\sim 9 \times 10^{13}$ n/cm^2-sec) was used.

Each sample consisted of approximately 200 mg of the stable metal contained in an evacuated quartz capsule (6 mm o.d. × 1.25 in. long). The quartz capsule in turn was enclosed in a special 99.999% pure aluminum capsule (1/2-in. o.d. × 2 in. long) for additional safety (see Fig. 18). The purity of the metals irradiated varied from 98% for lanthanum to 99.9% for yttrium and lutetium. The sample was transported from the reactor to the laboratory by the Health Chemistry Group from the Lawrence Radiation Laboratory.

The decay schemes for Y^{90}, La^{140}, and Lu^{177}, along with references to the original literature, are given in Strominger, Hollander, and Seaborg's Table of Isotopes (STR 58). (For recent work on the decay scheme of K^{43}, see the results of Benczer-Koller, Schwarzschild, and Wu (BEN 59).) These decay schemes along with the half lives were used to verify the identity of each of the radioactive samples. Figures 19 and 20 are decay curves for Y^{90} and Lu^{177} resonance buttons.

C. Experimental Procedure

Details of the K^{43} experiment are contained in App. A. Since the techniques involved with the other isotopes are identical, the following discussion applies with equal validity to Y^{90}, La^{140}, and Lu^{177}.

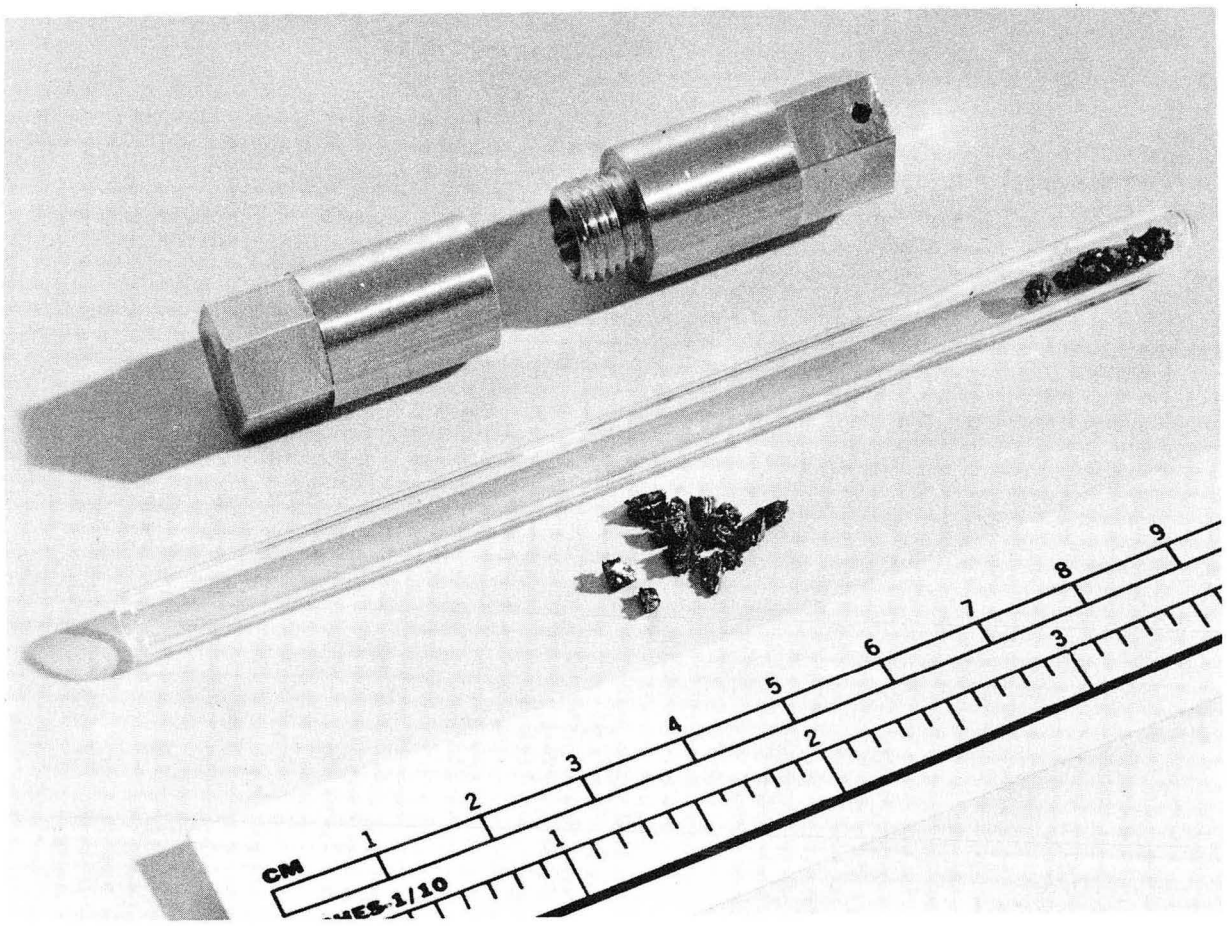

ZN-2680

Fig. 18. Metallic sample being prepared for neutron irradiation.

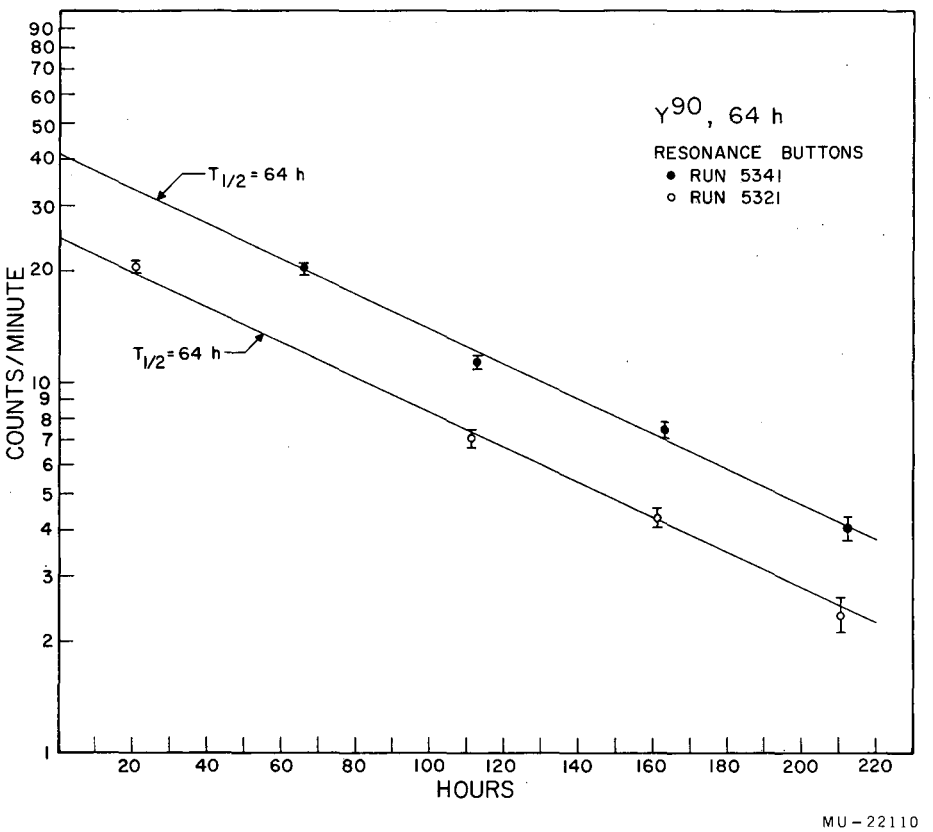

Fig. 19. Decay curves of Y^{90} resonance buttons.

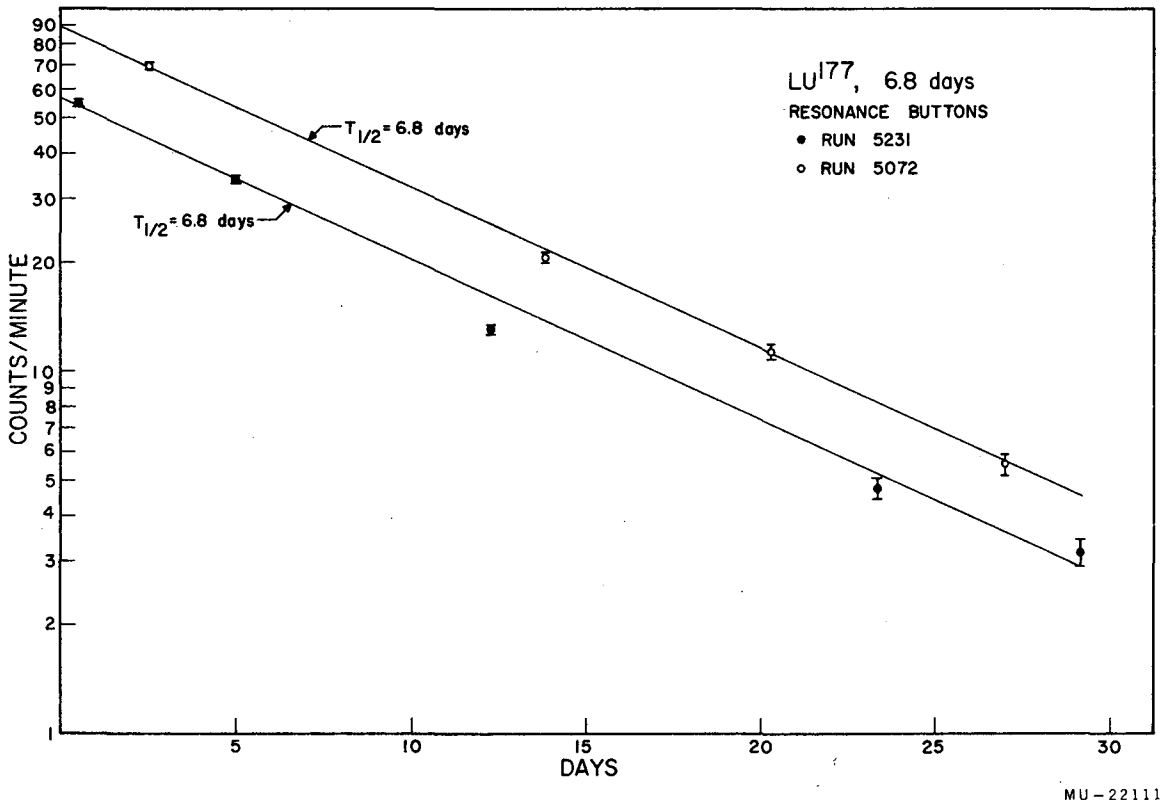

Fig. 20. Decay curves of Lu^{177} resonance buttons.

After irradiation, the radioactive sample was introduced into the "cave" shown in Fig. 21. When the aluminum capsule had been disassembled by means of a special wrench, the quartz capsule was removed. One end of the capsule was then broken off in a special jig and the radioactive contents were removed. Approximately 50 mg of the sample and a small amount of RbCl or CsCl, later used for alignment purposes, were then transported into an oven similar to the one shown in Fig. 10. All operations were done with specially constructed manipulators operated from outside the cave. Observations were made through a 4-in.-thick leaded-glass window. The γ-ray field outside the cave was negligible for Y^{90} and Lu^{177}. For La^{140} fields of about 1 r/hr were observed. However, the complete oven-loading operation could usually be accomplished with a maximum exposure to the experimenter of about 40 mr of radiation.

The oven was introduced into the vacuum of the atomic beam machine by means of an oven-loader assembly containing an electron-bombardment-type heater. The loader assembly permitted introduction and removal of the oven without disturbance of the vacuum in the machine. The oven power was raised to a point sufficient to produce a beam of alkali molecules. This beam was used to align the oven, since deflection of molecules in the beam was negligible even though the A and B deflecting magnets had been turned on several hours previously for stabilization purposes. After alignment, the temperature was raised enough to "blast out" the remaining alkali molecules, but was still far below the melting point of the isotope of interest. The temperature was then raised further until a beam of the radioactive isotope of adequate intensity was obtained.

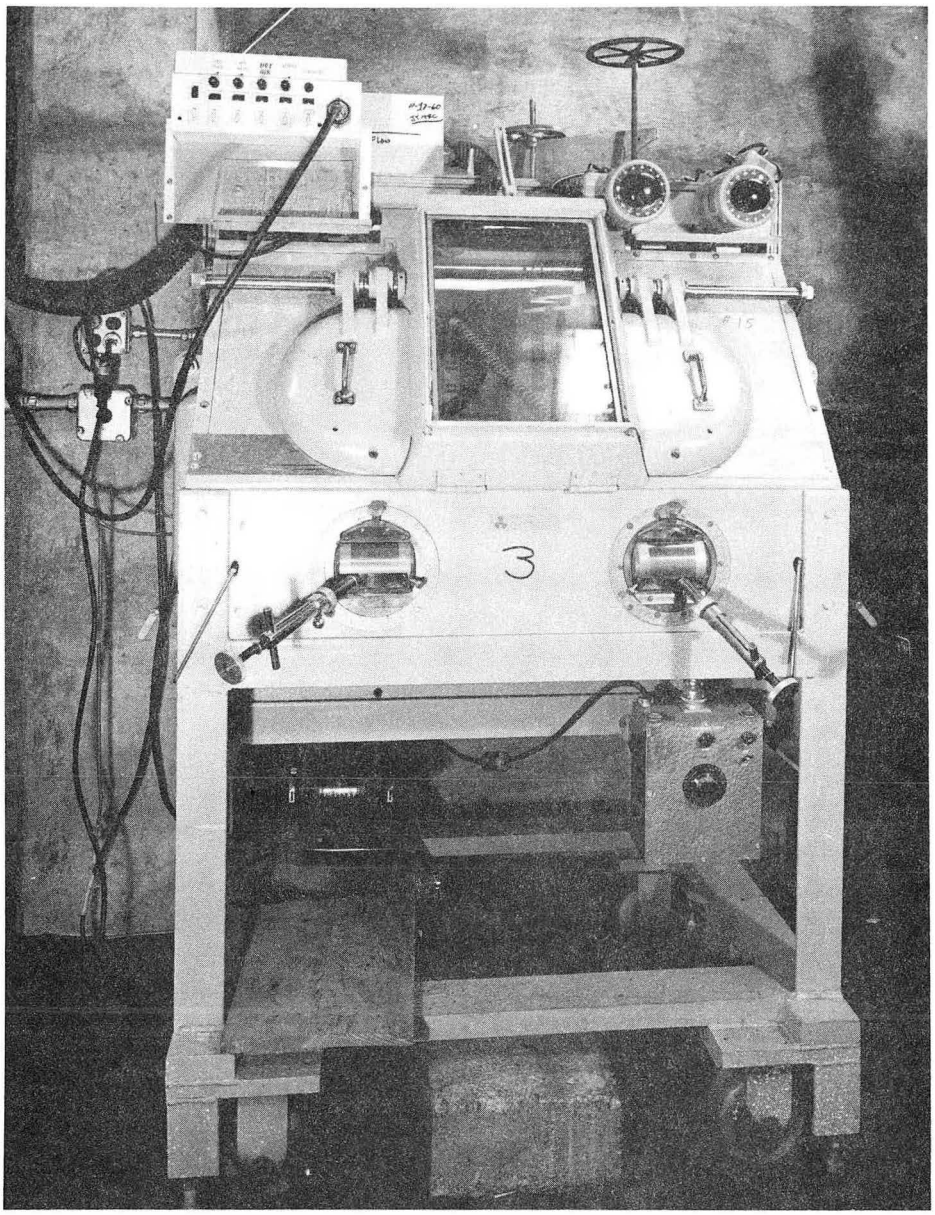

ZN-2677

Fig. 21. Lead "cave" used for handling highly radioactive materials.

The strength of the magnetic C field was measured by observation of the F,m = 3,-2 $\longleftrightarrow$ 3,-3 transition in Rb^{85}, and the F,m = 2,-1 $\longleftrightarrow$ 2,-2 transition in Rb^{87}. The beam of stable rubidium was produced from a calibration oven located on a special loader assembly immediately behind the radioactive oven. By removing the radioactive oven about 1/2 in. from the centerline, the rubidium beam was allowed to pass down the machine. The C field was usually set to the desired value about an hour before the experiment for stabilization purposes. Calibration measurements were made immediately before and immediately after each radioactive resonance. Usually, the drift in the magnetic field over the period required for obtaining one resonance was less than the uncertainty in the measurement.

Normally, enough buttons were exposed on a resonance to define its shape quite well. This procedure generally required 5 to 10 buttons, depending on the structure in the resonance. Each resonance button was normalized for fluctuations in beam intensity by dividing its counting rate (less counter background) by the average half-beam counting rate. Half-beam buttons were 1-min exposures taken before and after exposure of each resonance button, with the stop wire removed and no applied radiofrequency. Since the throwout, defined by

$$\text{Throwout} = 1 - \frac{\text{n/t, for half-beam exposure}}{\text{n/t, for full-beam exposure}},$$

was normally 60% to 70%, half-beam counting rates were high enough so that their statistical fluctuations were not important over 10- to 15-min counting periods.

The first task after production of a satisfactory beam of each new isotope was to measure the nuclear spin. The initial measurement was accomplished by observing $\Delta F = 0$ transitions at low magnetic fields. The predicted frequency of these transitions is given by Eq. (II-38):

$$\nu_\infty = -g_J \frac{F(F+1) + J(J+1) - I(I+1)}{2F(F+1)} \frac{\mu_0 H}{h} . \qquad \text{(III-2)}$$

The J and g_J for each isotope were known from atomic beam and optical spectroscopy measurements on the stable isotopes made by previous investigators. The magnetic field H was set at a value that separated the frequencies predicted for each value of I by at least one line width. Buttons were then exposed at the frequencies predicted by Eq. (III-2) for different theoretically possible values of I.

After determination of the nuclear spin, the next step was to observe the $\Delta F = 0$ transitions at higher magnetic fields. The predicted frequency of these transitions to second order in H is given by

$$\nu = \nu_\infty + \left[\frac{f_1(I,J,g_J)}{\Delta\nu_{F+1,F}} + \frac{f_2(I,J,g_J)}{\Delta\nu_{F,F-1}} \right] H^2; \qquad \text{(III-3)}$$

$f_1(I,J,g_J)$ and $f_2(I,J,g_J)$ were obtained with the assistance of second-order perturbation theory [Eq. (II-32)]. When the shift $(\nu - \nu_\infty)$ became appreciable, preliminary values of the hyperfine-structure separations between the levels F, F-1, F-2 were calculated. These values, and Eq. (II-30), enabled one to obtain preliminary values for the interaction constants a and b. These starting values were then used in Routine Hyperfine III (Sec. II.A.4) to obtain the best fit for the experimental

data.

Observation of the $\Delta F = 0$ transitions was continued to higher magnetic fields until the uncertainty in the predicted frequency for the $\Delta F = \pm 1$ transitions became less than 5 Mc/sec. Since these transitions provide the most accurate measurements of the zero-field hfs separations, the research was continued in this direction. Initially, the search was done at low magnetic fields. After observation of several of these transitions, uncertainties in the interaction constants became small enough to predict high-field $\Delta F = \pm 1$ transitions to within several hundred kc/sec. It was observed that the field dependence $\partial\nu/\partial H$ of several of these transitions became zero for particular values of H. Since inhomogeneity in the magnetic field was the principal reason for line broadening with this machine, the $\partial\nu/\partial H = 0$ points were used to obtain the best values for a and b.

From Eq. (II-59) we see that the frequency of each transition involves the term

$$-(m_1 - m_2)\,\frac{g_I \mu_0 H}{h}\,.$$

This term is zero for σ transitions, and consequently these transitions are much less g_I-dependent than π transitions. If the nuclear magnetic moment is appreciable, then one would expect the π transition frequency, based on interaction constants consistent with σ transitions, to be measurably different for plus and minus magnetic moments at high magnetic fields. This technique was used to determine the sign of the nuclear moments of Y^{90} and Lu^{177}.

IV. RESULTS

A. Results for K^{43}

Details of the results obtained for K^{43} (PET 58; PET 59a) are contained in App. A. The measured values are

$$I = 3/2,$$

$$\Delta\nu = 192.64(5) \text{ Mc/sec.}$$

The Fermi-Segrè formula was used in conjunction with the known constants of K^{39} or K^{41} to obtain the nuclear magnetic moment

$$|\mu_I| = 0.163(2) \text{ nm.}$$

B. Results for Y^{90}

Yttrium-90 has a $4d5s^2$ electronic ground-state configuration. The $^2D_{3/2}$ and $^2D_{5/2}$ states are the two lowest electronic states arising from this configuration. Since the $^2D_{5/2}$ state is only 530.36 cm^{-1} higher than the $^2D_{3/2}$ state (MEG 29), one would expect both states to be equally populated at the oven temperatures used.

The g_J factors for both these electronic states have been measured by Penselin (PEN 59). The values used in all calculations concerning this element are:

$$g_J(^2D_{3/2}) = -0.79927(11),$$

$$g_J(^2D_{5/2}) = -1.20028(19).$$

After the initial spin search in both electronic states, which confirmed the expected value I = 2 (PET 59b), low-frequency $\Delta F = 0$ resonances were attempted. Figures 22 and 23 are examples of the $\Delta F = 0$ transitions observed in the $^2D_{5/2}$ state. The transition F,m = $5/2,1/2 \longleftrightarrow 5/2,-1/2$ shown in Fig. 24 was also observed near the end of the research on this isotope. Figures 25 and 26 are examples of $\Delta F = 0$ transitions observed in the $^2D_{3/2}$ state.

The established value of the nuclear spin was expected for several theoretical reasons. From nuclear shell structure, the 39th proton should be in the $p_{1/2}$ level. The $g_{9/2}$ level is filled at 50, and the next level, filled by neutrons, is the $d_{5/2}$ level. Since one nucleon is in a level with intrinsic spin and orbital angular momentum parallel, and the other is in a level with intrinsic spin and orbital angular momentum antiparallel, the total spin of the nuclear ground state, according to rule N2 or rule BB2 from Sec. II.B.1, should be the difference between the individual angular momenta, or I = 2. Also, since the asymptotic quantum numbers given by Gallagher and Moszkowski (GAL 58) are $\Omega_p = 1/2$ (parallel spin) and $\Omega_n = 5/2$ (antiparallel spin), rule GM2 of the collective model predicts I = 2. In addition, since Y^{90} β^- decays to the 0^+ ground state of Zr^{90}, and since the unique spectrum shape corresponds to $\Delta I = 2$ with change of parity, one would expect the ground state to be 2 minus.

Observation of $\Delta F = 0$ resonances in the $^2D_{5/2}$ state at high magnetic fields reduced uncertainties in the interaction constants to such an extent that a search for the observable $\Delta F = \pm 1$ transitions became

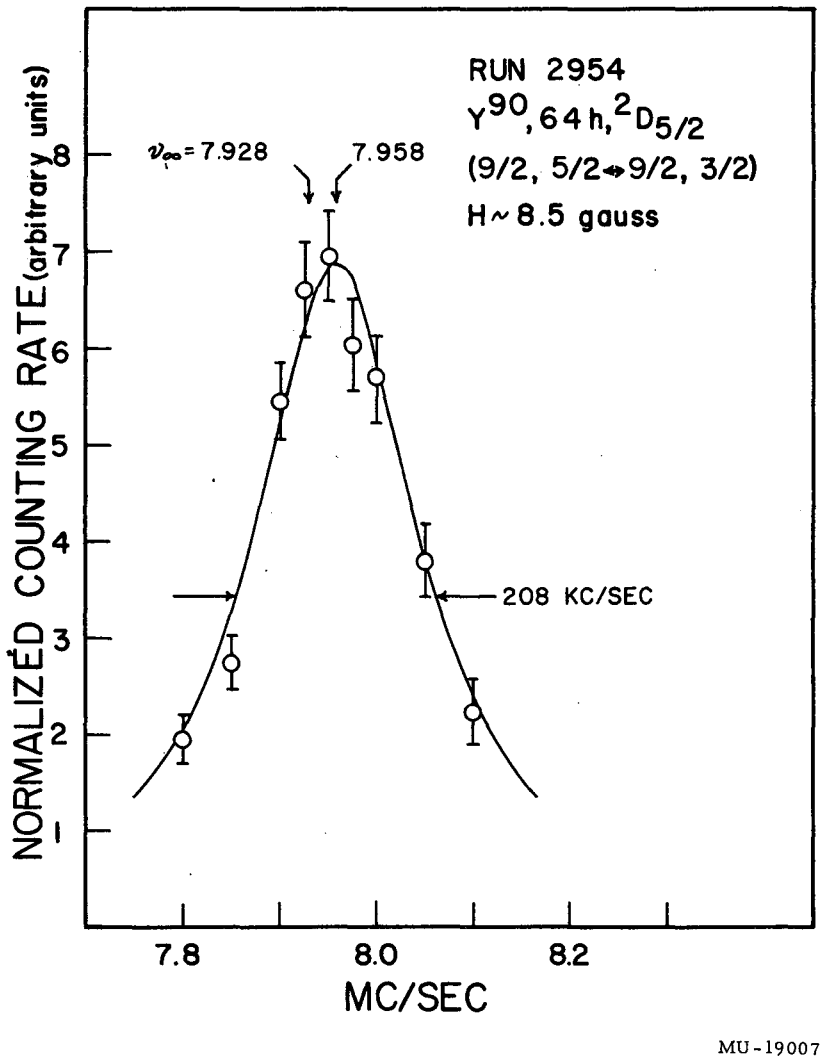

Fig. 22. Resonance corresponding to the transition F, m=9/2, 5/2 ⟷ 9/2, 3/2 in the $^2D_{5/2}$ state of Y^{90}.

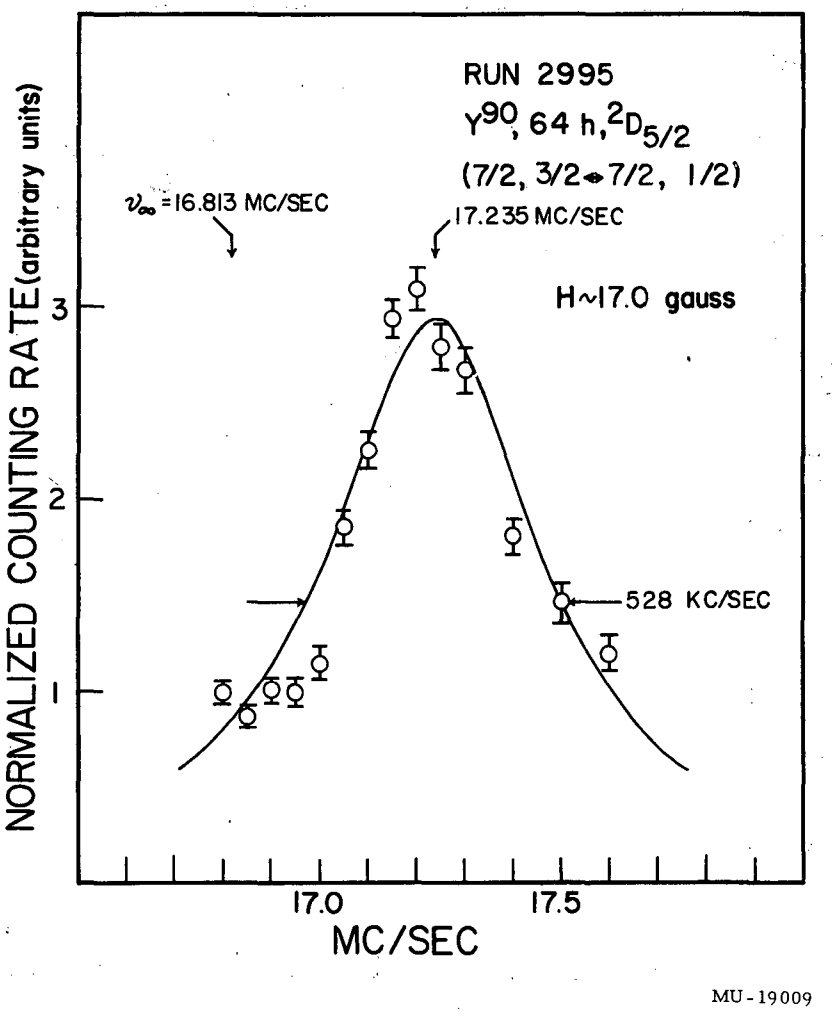

Fig. 23. Resonance corresponding to the transition F, m=7/2, 3/2 ⟷ 7/2, 1/2 in the $^2D_{5/2}$ state of Y^{90}.

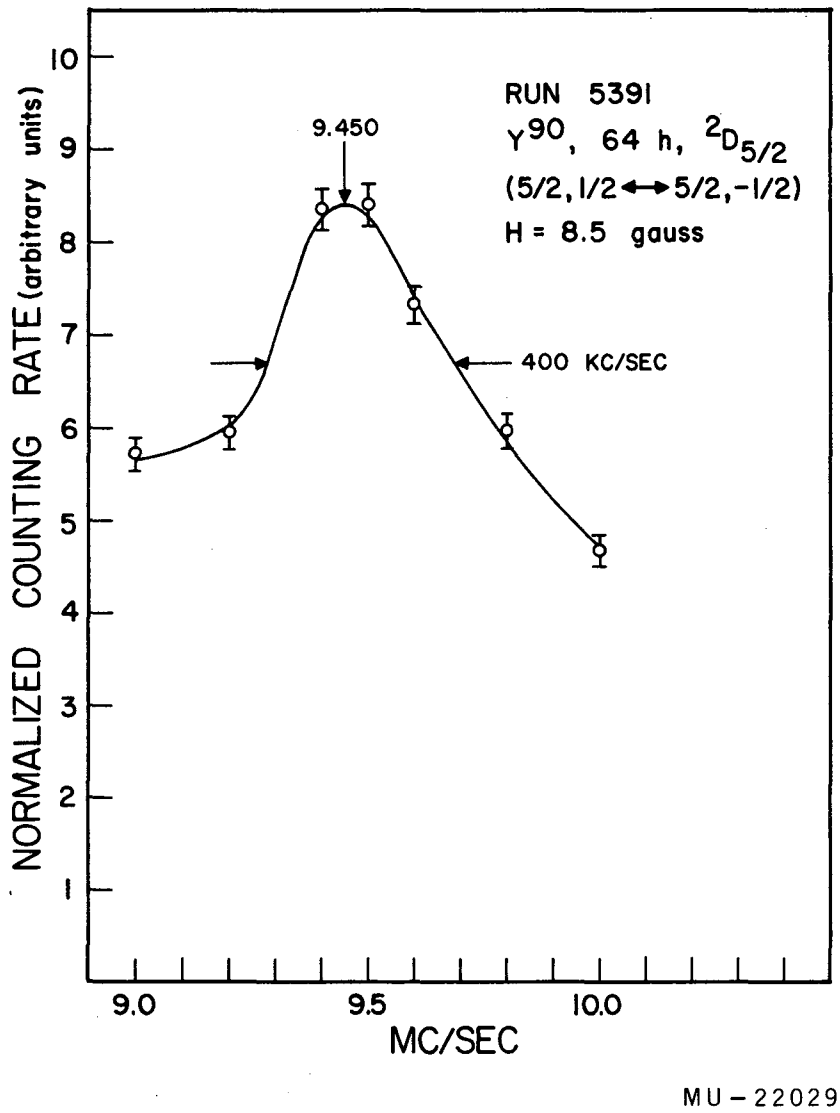

Fig. 24. Resonance corresponding to the transition F, m=5/2, 1/2 ⟷ 5/2, -1/2 in the $^2D_{5/2}$ state of Y^{90}.

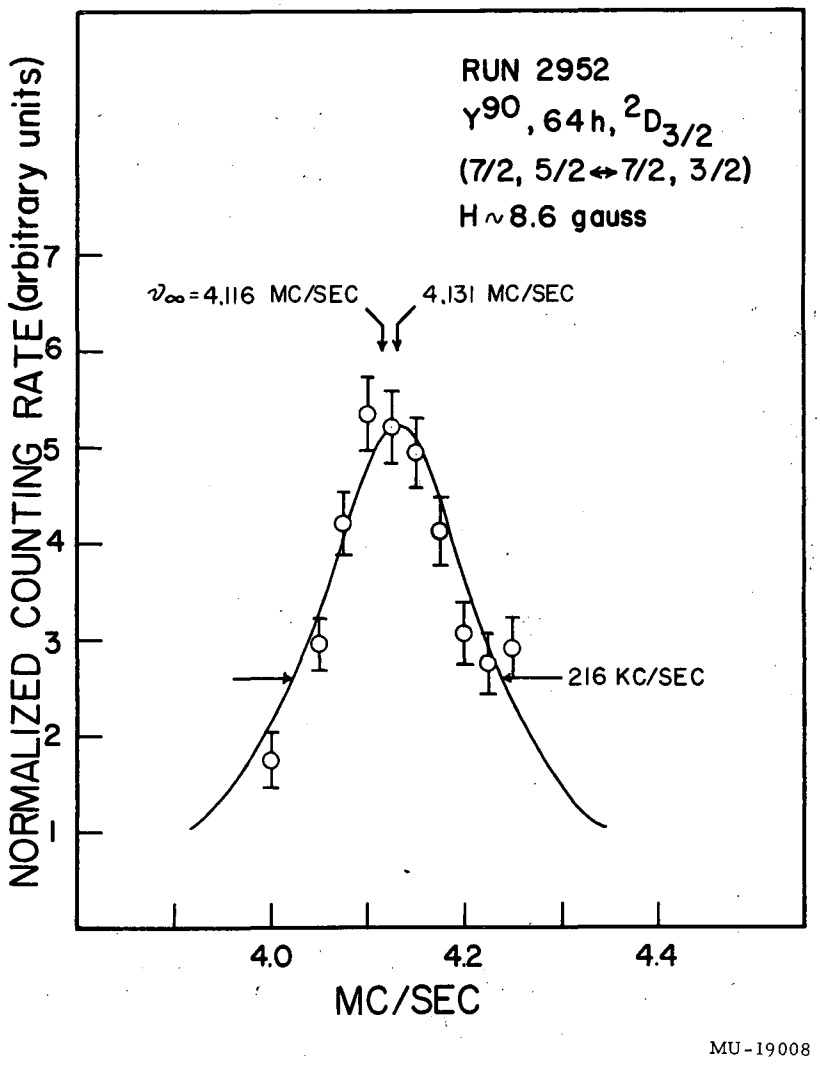

Fig. 25. Resonance corresponding to the transition F, m=7/2, 5/2 ⟷ 7/2, 3/2 in the $^2D_{3/2}$ state of Y^{90}.

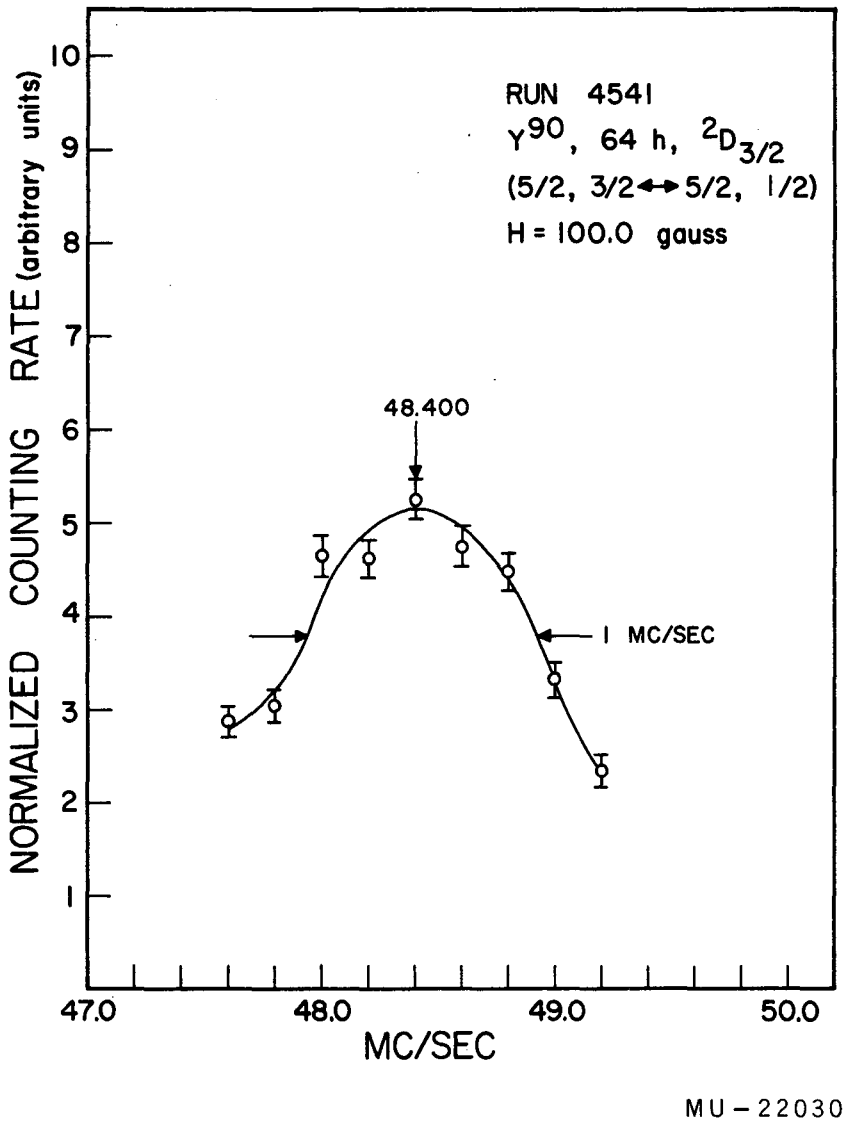

Fig. 26. Resonance corresponding to the transition F, m=5/2, 3/2 ⟷ 5/2, 1/2 in the $^2D_{3/2}$ state of Y^{90}.

feasible. The ratio b/a ascertained a normal level ordering (Fig. 3), so that there was no ambiguity concerning observable transitions. These transitions were initially observed at low magnetic fields. With the improved values for the interaction constants, transition frequencies $\nu(H)$ were calculated with Routine JO-9. Table II shows where these $\Delta F = \pm 1$ transitions are least field-dependent. Since the line width is narrowest at these points, future work was concentrated in this area. Figures 27 through 33 are examples of the transitions observed at their field-dependent minima.

Table II

The most field-independent positions of the observable $\Delta F = \pm 1$ transitions in the $^2D_{5/2}$ electronic state of Y^{90}. The calculations were performed for a = -85.258 Mc/sec and b = -29.716 Mc/sec.

Transition $(F_1,m_1 \leftrightarrow F_2,m_2)$	$(\partial\nu/\partial H)_{min}$ (Mc/sec-gauss)	H (gauss)	$\nu(g_I +)$ (Mc/sec)	$\nu(g_I -)$ (Mc/gauss)
7/2,3/2 ↔ 9/2,3/2	0.016	51.5	405.718	405.718
5/2,1/2 ↔ 7/2,1/2	0	8.6 63.2	293.451 289.572	293.451 289.572
3/2,-3/2 ↔ 5/2,-1/2	0	32.5	171.408	171.368
3/2,-3/2 ↔ 5/2,-3/2	0	13.6	194.660	194.660
3/2,-1/2 ↔ 5/2,-1/2	0	48.8	176.485	176.485
3/2,-3/2 ↔ 5/2,-5/2	0.576	0	198.287	198.287
3/2,-1/2 ↔ 5/2,-3/2	0.134	29.9	211.731	211.768

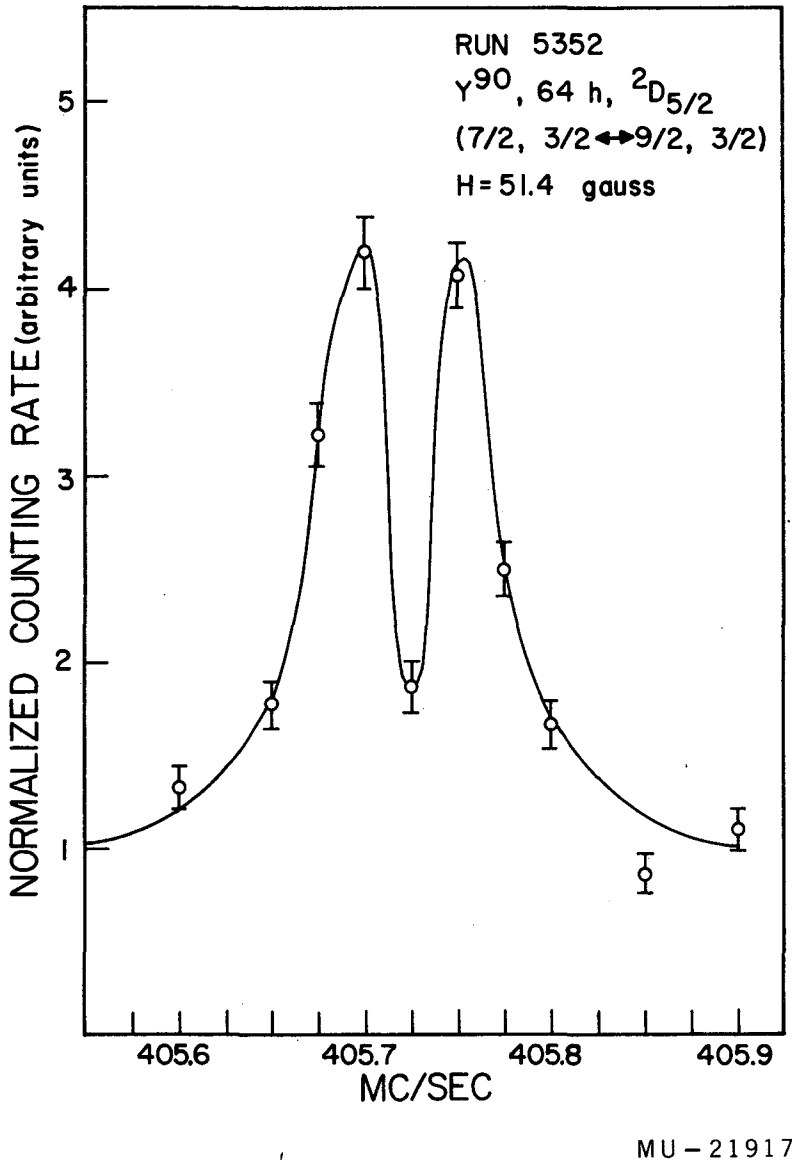

Fig. 27. Resonance corresponding to the transition F, m=7/2, 3/2 ⟷ 9/2, 3/2 in the $^2D_{5/2}$ state of Y^{90}.

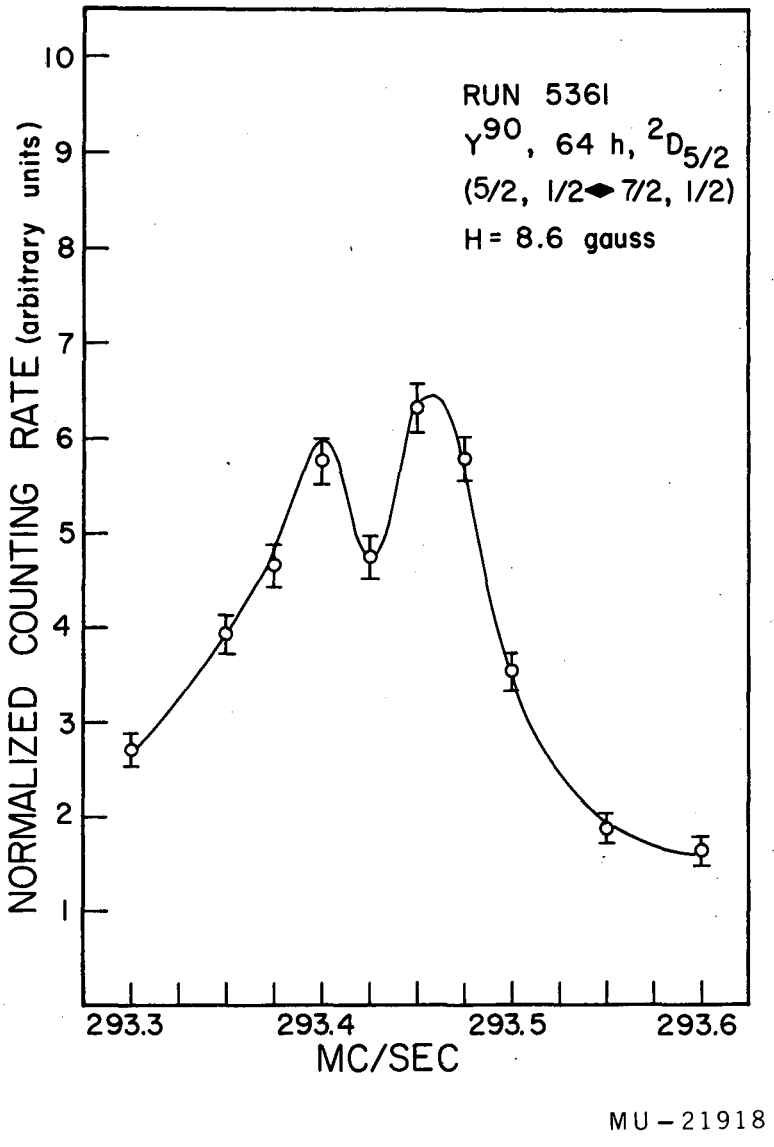

Fig. 28. Resonance corresponding to the transition F, m=5/2, 1/2 ⟷ 7/2, 1/2 in the $^2D_{5/2}$ state of Y^{90}.

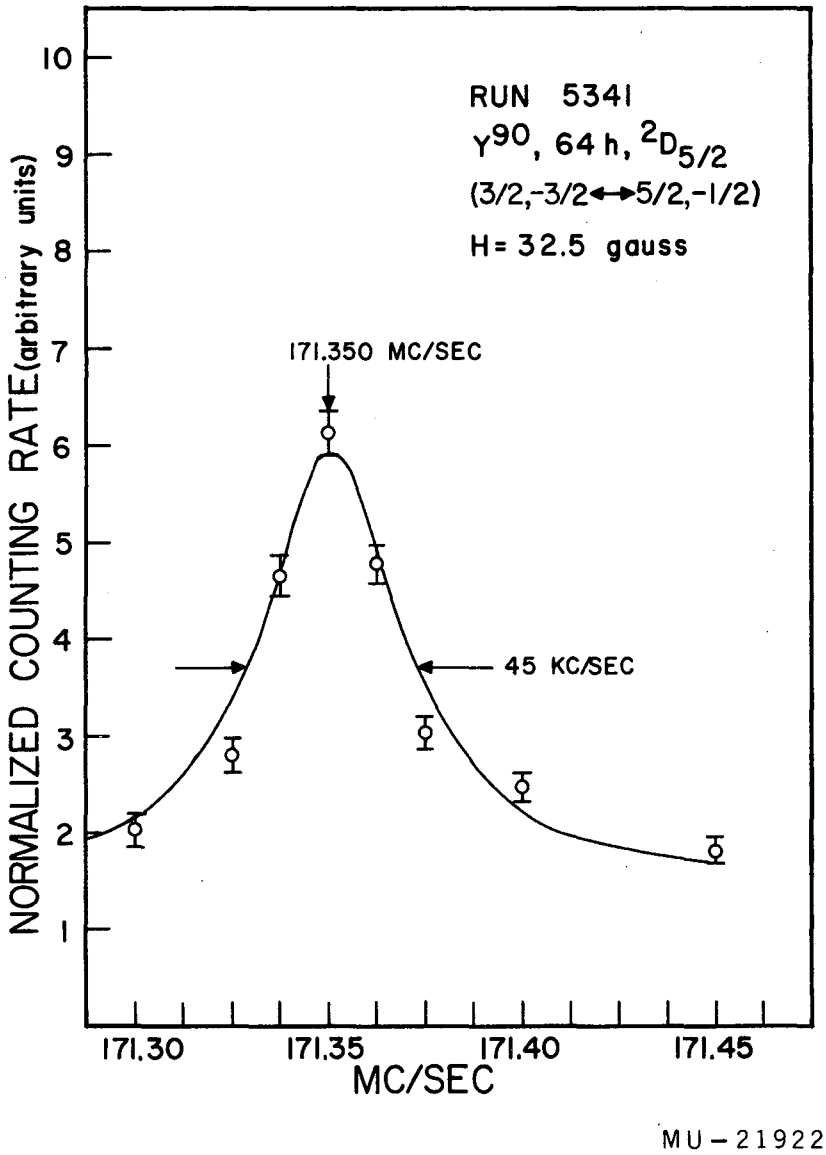

Fig. 29. Resonance corresponding to the transition F, m=3/2, -3/2 ⟷ 5/2, -1/2 in the $^2D_{5/2}$ state of Y^{90}.

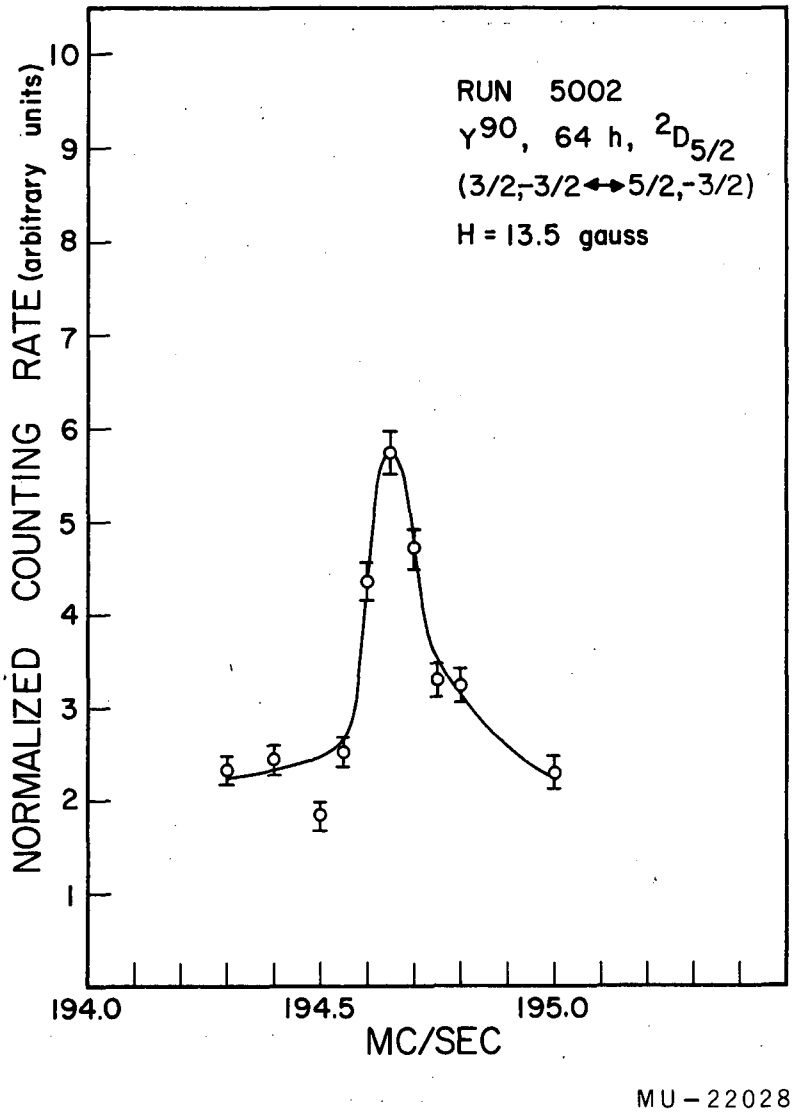

Fig. 30. Resonance corresponding to the transition F, m=3/2, -3/2 ⟷ 5/2, -3/2 in the $^2D_{5/2}$ state of Y^{90}.

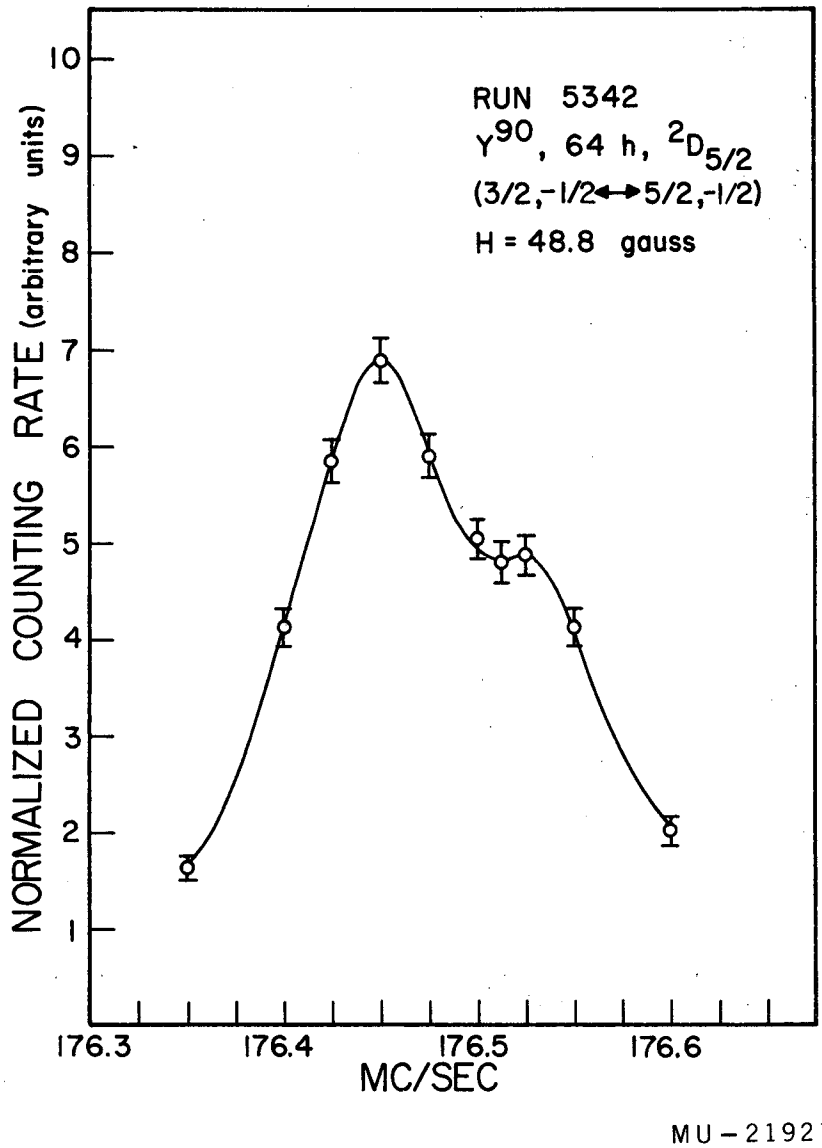

Fig. 31. Resonance corresponding to the transition F, m=3/2, -1/2 ⟷ 5/2, -1/2 in the $^2D_{5/2}$ state of Y^{90}.

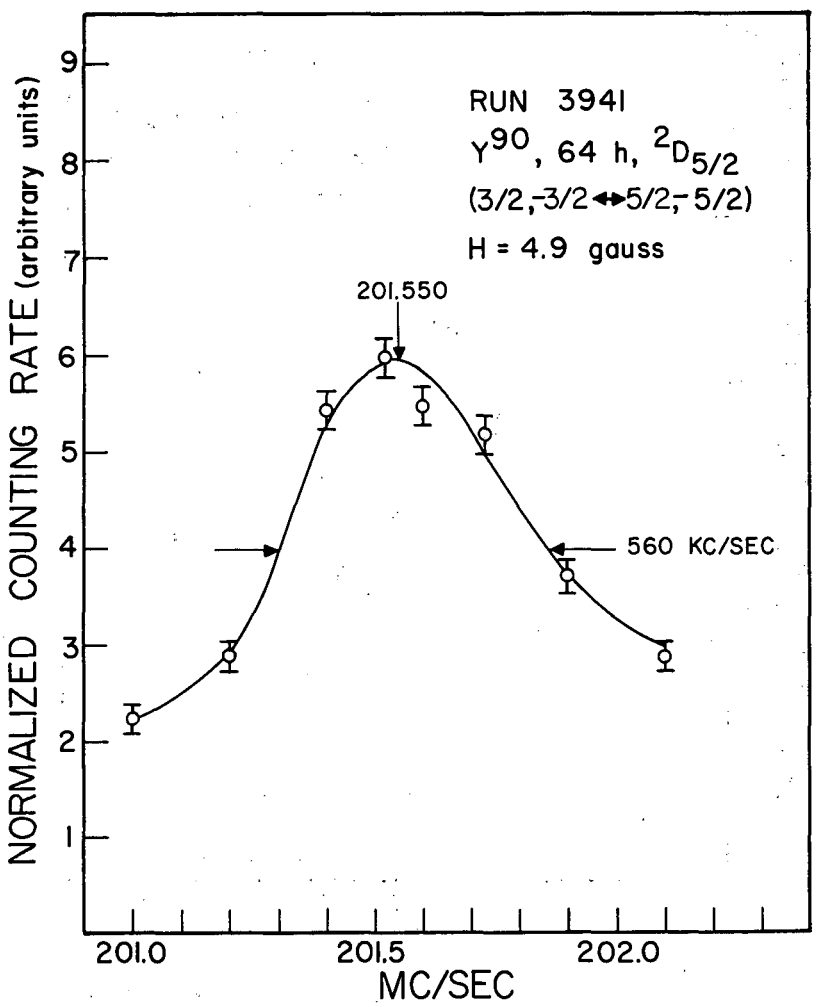

Fig. 32. Resonance corresponding to the transition F, m=3/2, -3/2 ⟷ 5/2, -5/2 in the $^2D_{5/2}$ state of Y^{90}.

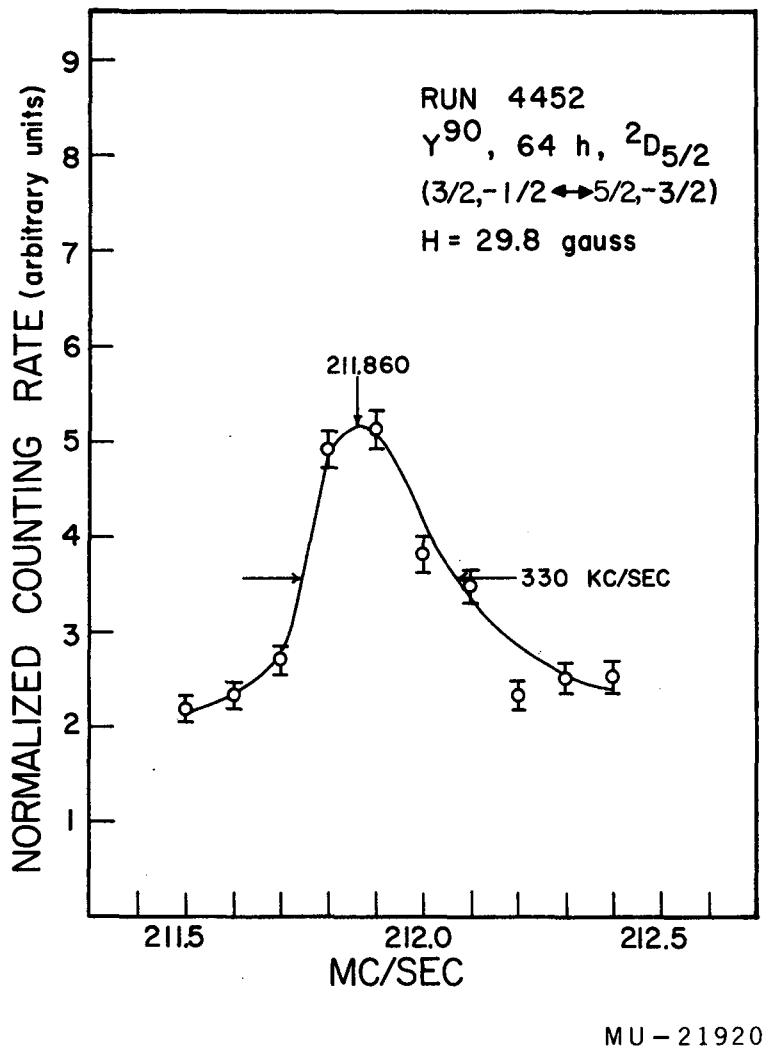

Fig. 33. Resonance corresponding to the transition F, $m = 3/2, -1/2 \leftrightarrow 5/2, -3/2$ in the $^2D_{5/2}$ state of Y^{90}.

Since the atom sees two rf fields parallel to the magnetic field H and 180 deg out of phase in the hairpin used, the transition probability goes through zero at the "peak" for σ transitions (Sec. III.A.3). The resulting double-peaked structure was observed for all σ transitions carefully done at their field-dependent minima. When $(\partial\nu/\partial H)$ is not very close to zero, however, the field inhomogeneities "wash out" the structure and the resultant shape is similar to a π transition, but somewhat broadened and flattened. The position of the peak and other characteristics of the line were checked with K^{39} for the transition F,m = 2,-1 $\longleftrightarrow$ 1,-1.

During the investigation in the $^2D_{5/2}$ state, a resonance at about 410 Mc/sec was identified as the transition F,m = 7/2,3/2 $\longleftrightarrow$ 9/2,3/2. Because the data fit was poor, however, this was suspected to be a resonance in the $^2D_{3/2}$ state. A short frequency search soon revealed all eight observable transitions in the $^2D_{3/2}$ state as well as the F,m = 7/2,3/2 $\longleftrightarrow$ 9/2,3/2 transition in the $^2D_{5/2}$ state in this frequency region. This information, and the known interaction constants of Y^{89} (FRI 59), permitted observation of all observable transitions within a short time. Again, Routine JO-9 was used to obtain transition frequencies as a function of the magnetic field for all observable ΔF = ±1 transitions. Table III shows where these transitions are least field-dependent. Resonances corresponding to these transitions, observed in most cases at the field-dependent minima, are shown in Fig. 34 through 41.

The final results, in which Routine Hyperfine III has been used to vary the parameters a, b, and g_I to fit all observed resonances, are shown

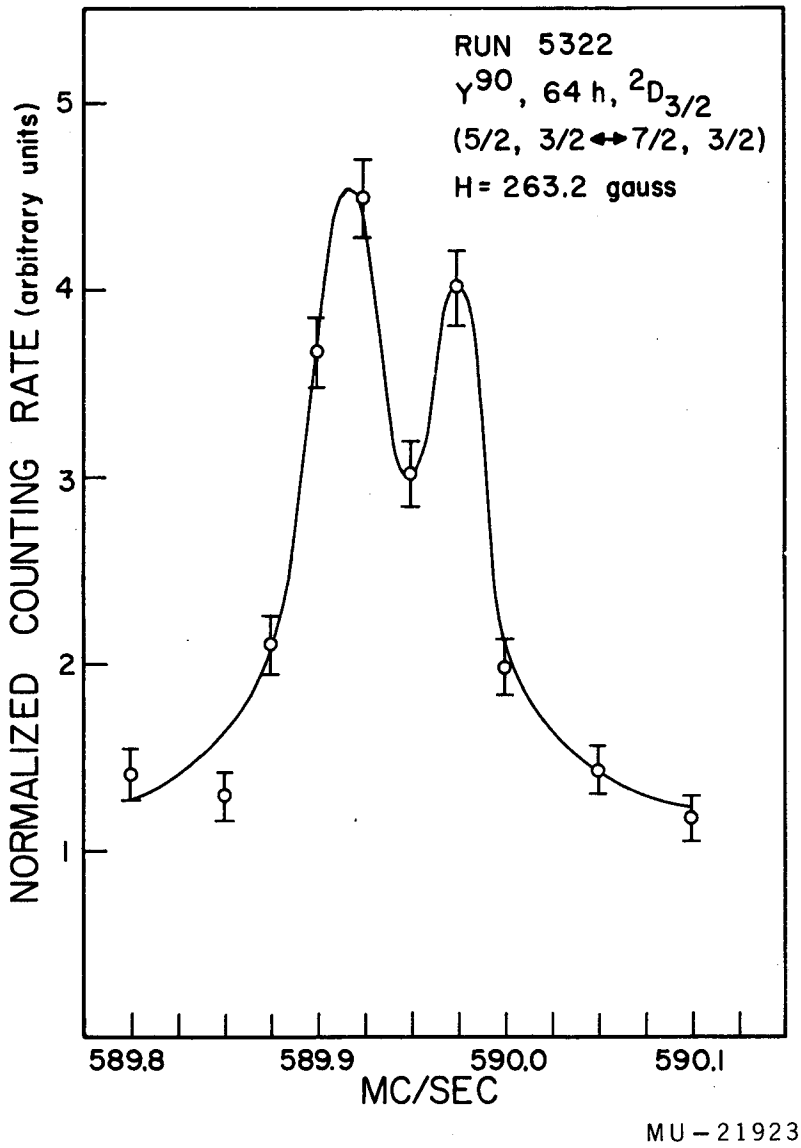

Fig. 34. Resonance corresponding to the transition F, m=5/2, 3/2 ↔ 7/2, 3/2 in the $^2D_{3/2}$ state of Y^{90}.

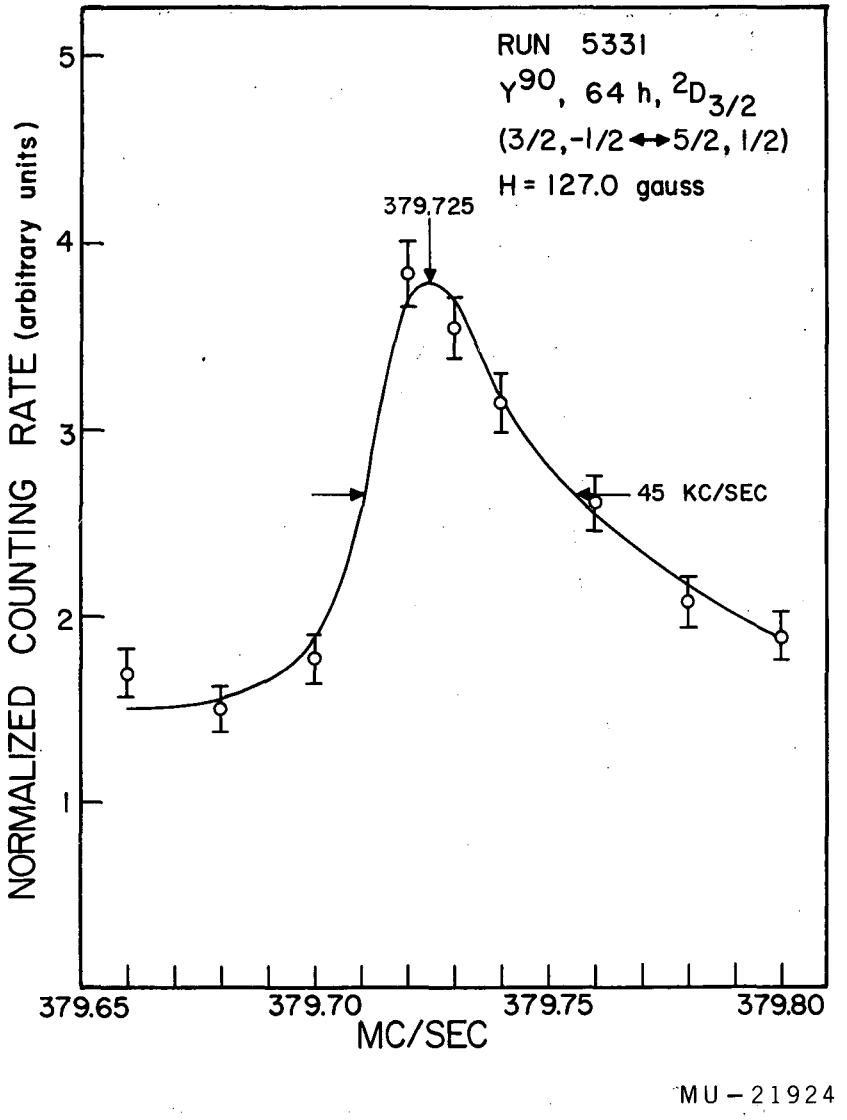

Fig. 35. Resonance corresponding to the transition F, $m=3/2, -1/2 \leftrightarrow 5/2, 1/2$ in the $^2D_{3/2}$ state of Y^{90}.

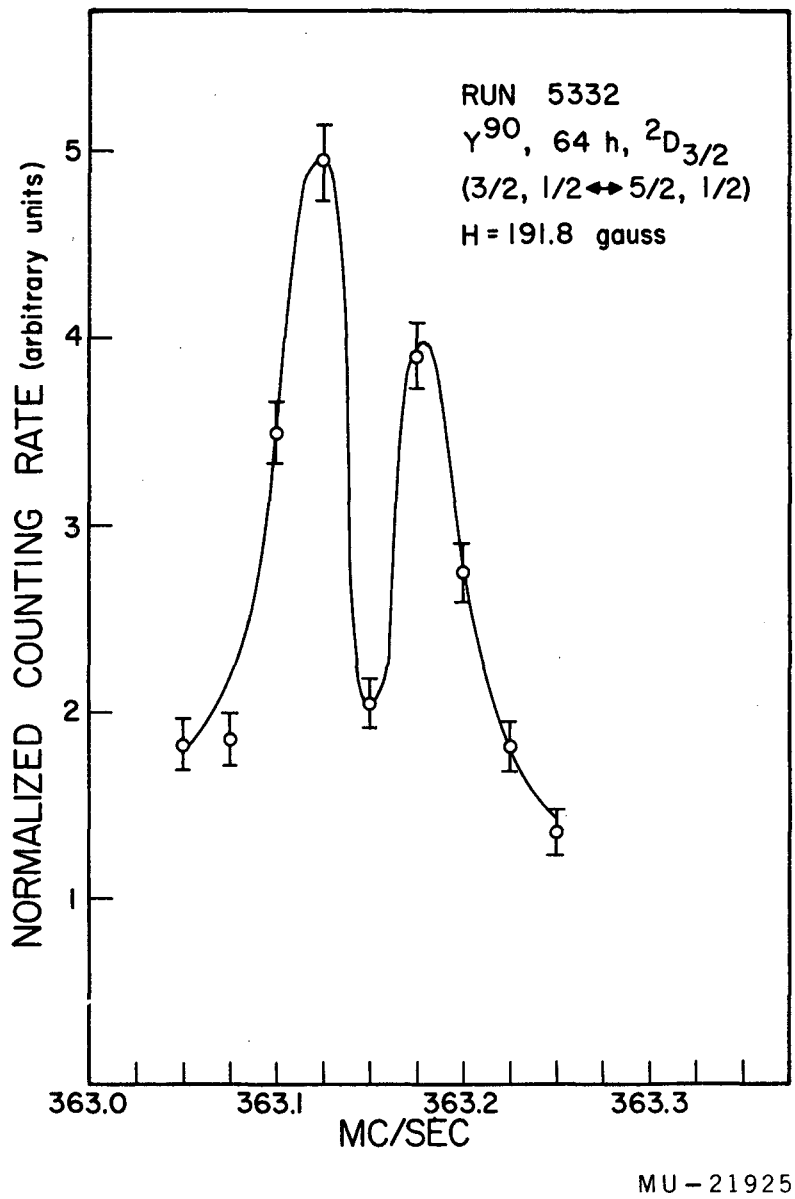

Fig. 36. Resonance corresponding to the transition F_0 m=3/2, +1/2 ↔ 5/2, +1/2 in the $^2D_{3/2}$ state of Y^{90}.

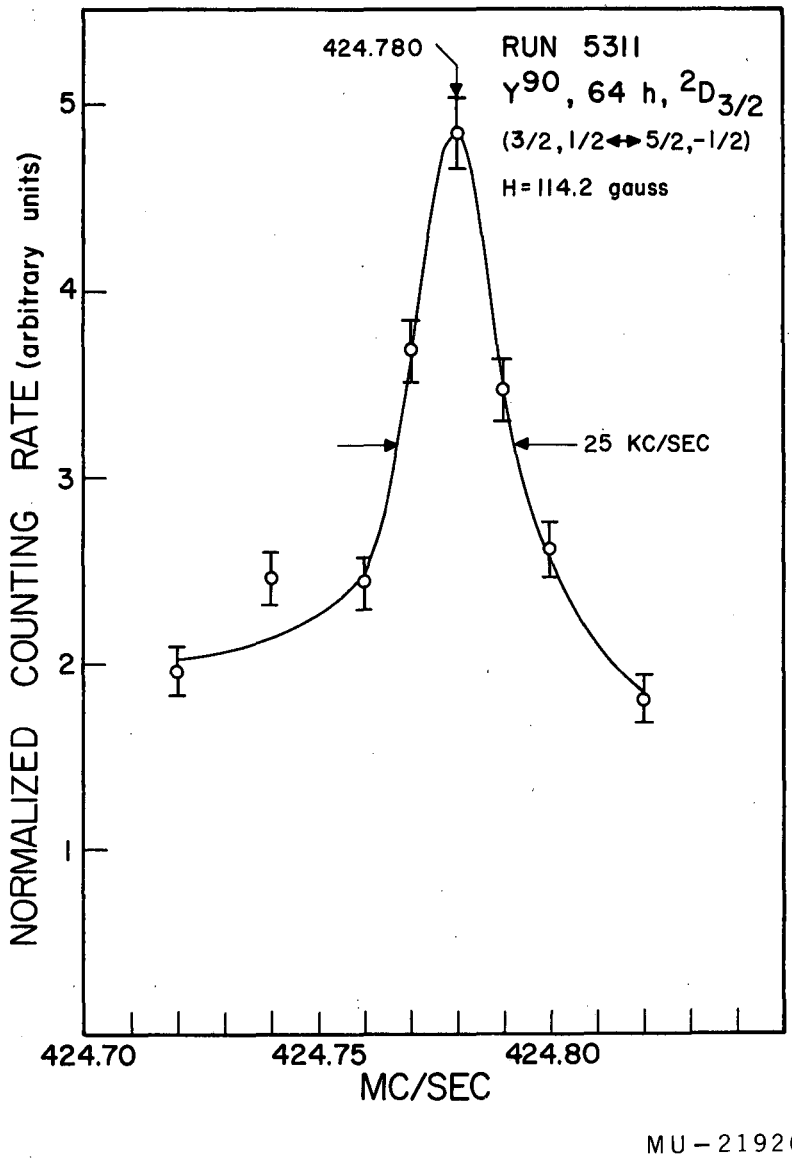

Fig. 37. Resonance corresponding to the transition F, $m=3/2,\ 1/2 \leftrightarrow 5/2,\ -1/2$ in the $^2D_{3/2}$ state of Y^{90}.

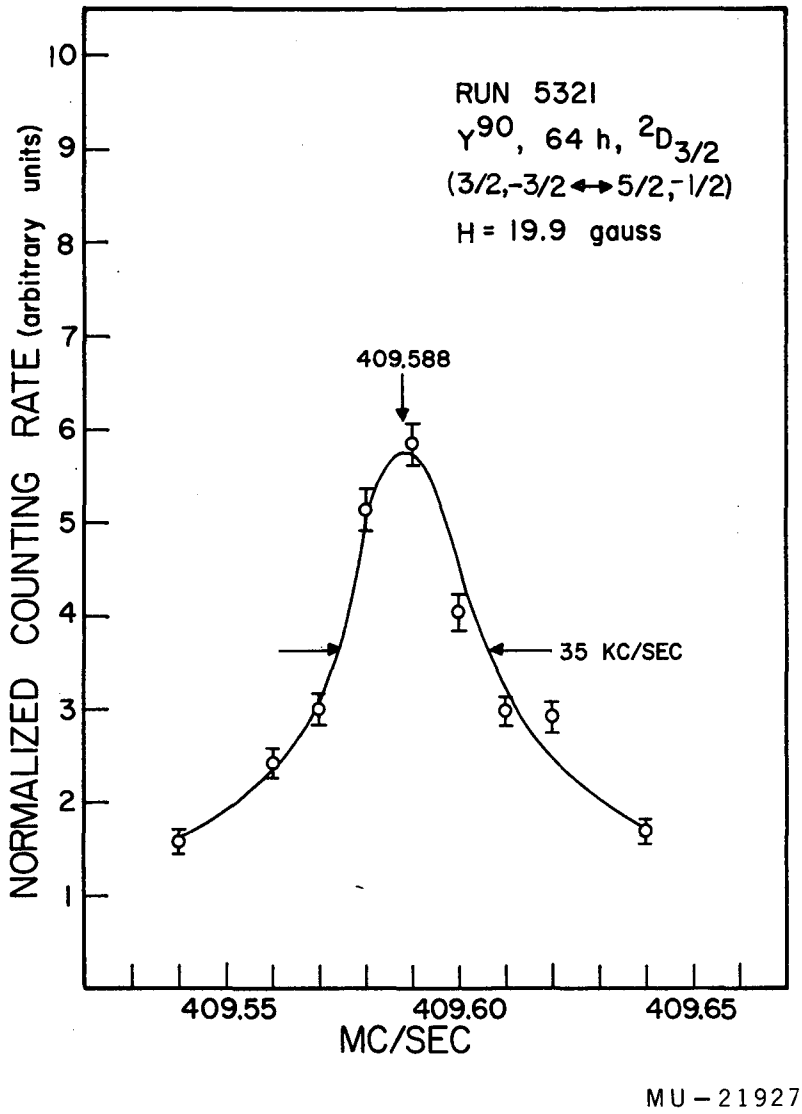

Fig. 38. Resonance corresponding to the transition F, $m=3/2,\ -3/2 \leftrightarrow 5/2,\ -1/2$ in the $^2D_{3/2}$ state of Y^{90}.

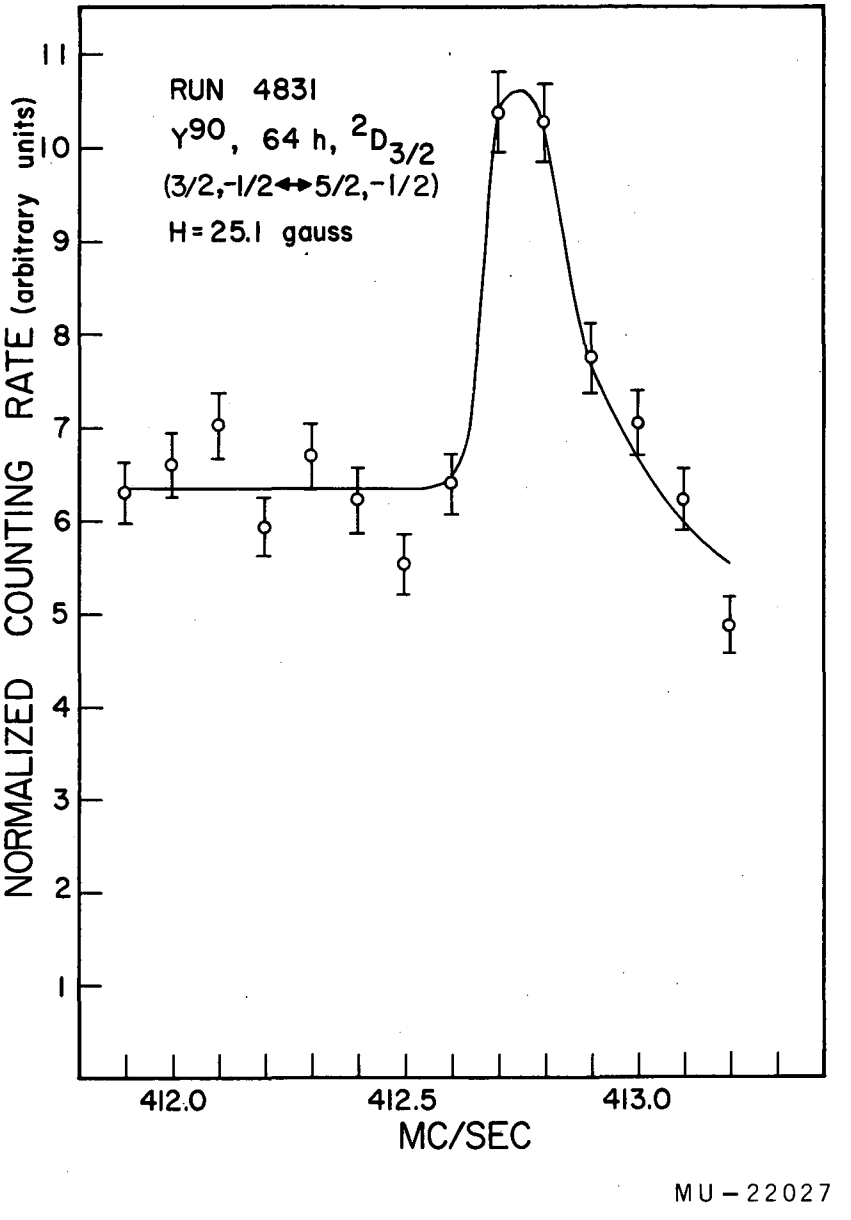

Fig. 39. Resonance corresponding to the transition F, m=3/2, -1/2 ↔ 5/2, -1/2 in the $^2D_{3/2}$ state of Y^{90}.

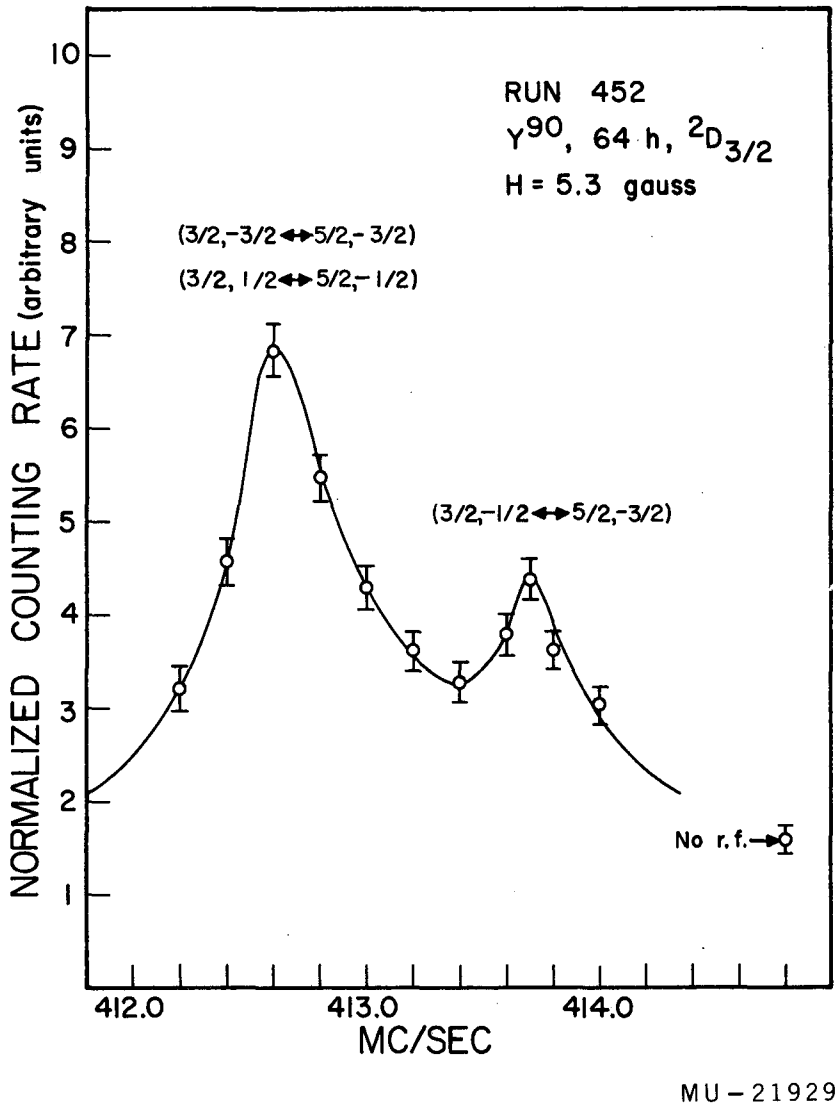

Fig. 40. Resonance corresponding to the unresolved transitions F, m=3/2, -3/2 ↔ 5/2, -3/2 and F, m=3/2, 1/2 ↔ 5/2, -1/2, in the $^2D_{3/2}$ state of Y^{90}. The transition F, m=3/2, -1/2 ↔ 5/2, -3/2 in the same electronic state is just separated from the doublet.

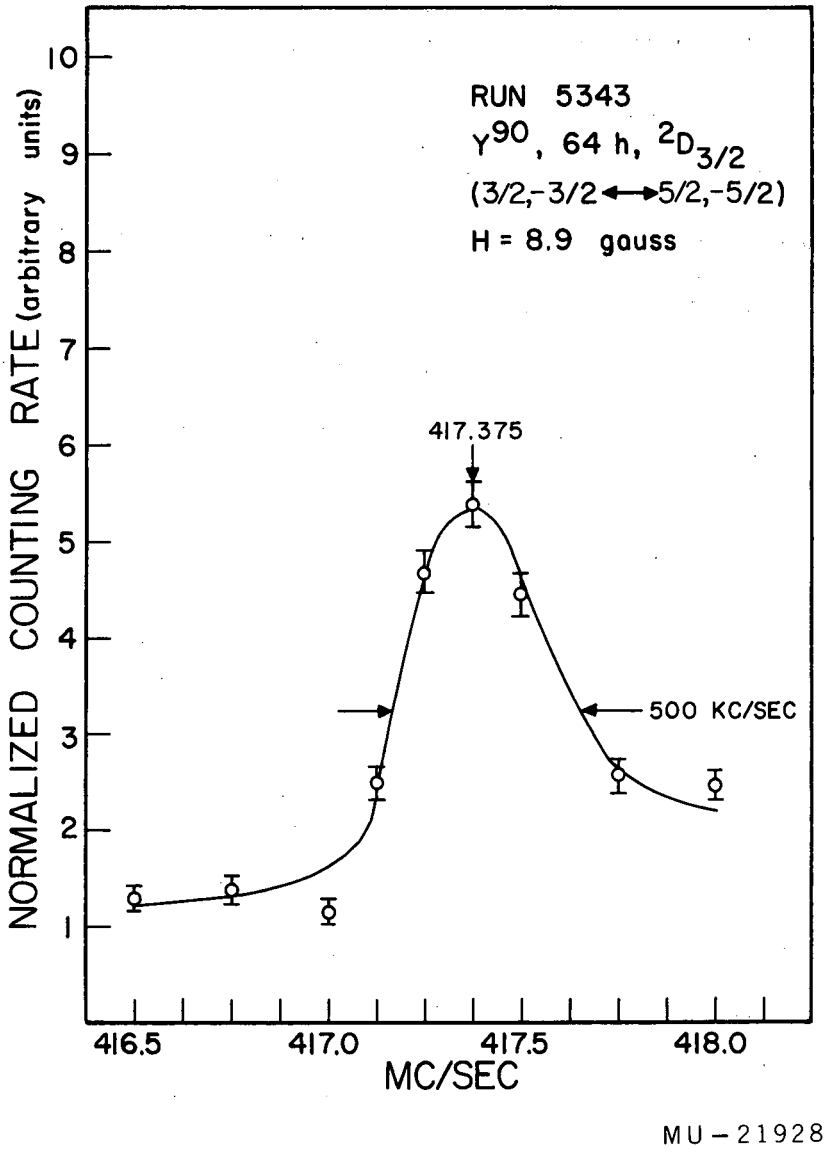

Fig. 41. Resonance corresponding to the transition F, m=3/2, -3/2 ⟷ 5/2, -5/2 in the $^2D_{3/2}$ state of Y^{90}.

in Tables IV and V. Both positive and negative starting values for g_I were used. It should be noted that g_I converges to the same negative value for both cases in each electronic state.

The value of g_I calculated in this manner provides an independent check on the value calculated with the aid of the Fermi-Segrè formula and the interaction constants of Y^{89}. Uncertainty in the $^2D_{5/2}$ measurement was very large, since the field-independent π transitions occur at approximately 30 gauss. The $^2D_{3/2}$ state gives greater accuracy, since these transitions occur in the region of 120 gauss.

Table III

The most field-independent positions of the observable $\Delta F = \pm 1$ transitions in the $^2D_{3/2}$ electronic state of Y^{90}. The calculations were performed for $a = -169.749$ Mc/sec and $b = -21.602$ Mc/sec.

Transition $(F_1,m_1 \leftrightarrow F_2,m_2)$	$(\partial\nu/\partial H)_{min}$ (Mc/sec-gauss)	H (gauss)	$\nu(g_I +)$ (Mc/sec)	$\nu(g_I -)$ (Mc/sec)
$5/2,3/2 \leftrightarrow 7/2,3/2$	0	263.3	589.909	589.909
$3/2,-1/2 \leftrightarrow 5/2,1/2$	0	127.1	379.885	379.728
$3/2,1/2 \leftrightarrow 5/2,1/2$	0	191.7	363.144	363.144
$3/2,1/2 \leftrightarrow 5/2,-1/2$	0	96.6 114.4	424.679 424.628	424.799 424.770
$3/2,-3/2 \leftrightarrow 5/2,-1/2$	0	19.9	409.618	409.593
$3/2,-1/2 \leftrightarrow 5/2,-1/2$	0.064	27.0	412.879	412.879
$3/2,-3/2 \leftrightarrow 5/2,-3/2$	0.288	0	410.871	410.871
$3/2,-1/2 \leftrightarrow 5/2,-3/2$	0.426	47.5	432.389	432.443
$3/2,-3/2 \leftrightarrow 5/2,-5/2$	0.703	0	410.871	410.871

Table IV

Summary of Y^{90} data for the $^2D_{3/2}$ electronic state.

Comparing isotope	Calibrating isotope
Y^{89}, $^2D_{3/2}$, $I = 1/2$	Rb^{85}, $^2S_{1/2}$, $I = 5/2$
$g_J = -0.79927$	$g_J = -2.00238$
$g_I = -1.49037 \times 10^{-4}$	$g_I = 2.93704 \times 10^{-4}$
$a = -57.217$ Mc/sec	$\Delta\nu = 3035.735$ Mc/sec

Iteration No.	a (Mc/sec)	δa (Mc/sec)	b (Mc/sec)	δb (Mc/sec)	$g_I \times 10^4$	$\delta g_I \times 10^4$	χ^2
1	-169.749	0.000	-21.599	0.000	4.42	0.000	375.9
2	-169.749	0.003	-21.602	0.013	-4.89	0.35	9.4
3	-169.749	0.003	-21.602	0.013	-4.89	0.35	9.4
1	-169.749	0.000	-21.599	0.000	-4.42	0.000	10.3
2	-169.749	0.003	-21.602	0.013	-4.89	0.35	9.4
3	-169.749	0.003	-21.602	0.013	-4.89	0.35	9.4

Run	Calibrating isotope	ν_c (Mc/sec)	$\delta\nu_c$ (Mc/sec)	H (gauss)	δH (gauss)	F_1	m_1	F_2	m_2	ν (Mc/sec)	$\delta\nu$ (Mc/sec)	Residual (Mc/sec)	Weight Factor
2952	RB85	4.034	0.040	8.585	0.084	7/2	5/2	7/2	3/2	4.131	0.030	-0.013	387.4
2953	RB85	7.905	0.040	16.718	0.084	7/2	5/2	7/2	3/2	8.101	0.045	-0.014	270.2
4531	RB85	50.724	0.085	100.406	0.156	7/2	5/2	7/2	3/2	51.480	0.150	-0.078	33.6
4532	RB85	179.192	0.150	300.127	0.199	7/2	5/2	7/2	3/2	175.600	0.200	-0.178	16.8
4541	RB85	50.520	0.130	100.032	0.238	5/2	3/2	5/2	1/2	48.400	0.300	-0.108	9.3
4581	RB85	2.146	0.040	4.581	0.085	5/2	3/2	7/2	3/2	612.480	0.100	-0.103	99.3
5322	RB85	152.225	0.060	263.189	0.085	5/2	3/2	7/2	3/2	589.940	0.040	0.031	625.0
4792	RB85	152.239	0.090	263.209	0.127	5/2	3/2	7/2	3/2	589.900	0.040	-0.009	625.0
4512	RB85	2.642	0.040	5.636	0.085	3/2	-1/2	5/2	1/2	408.920	0.150	-0.112	42.9
4504	RB85	4.765	0.040	10.129	0.084	3/2	-1/2	5/2	1/2	407.400	0.150	-0.123	42.9
5331	RB85	65.581	0.045	127.044	0.079	3/2	-1/2	5/2	1/2	379.725	0.015	0.005	4444.4
4791	RB85	65.680	0.050	127.218	0.088	3/2	-1/2	5/2	1/2	379.720	0.040	0.000	625.0
4961	RB85	12.062	0.045	25.339	0.093	3/2	1/2	5/2	1/2	407.375	0.175	-0.100	32.4
5332	RB85	104.443	0.140	191.807	0.222	3/2	1/2	5/2	1/2	363.140	0.040	-0.004	625.0
4831	RB85	11.923	0.060	25.053	0.124	3/2	-1/2	5/2	-1/2	412.750	0.100	-0.004	99.4
4521	RB85	2.485	0.070	5.302	0.149	3/2	1/2	5/2	-1/2	412.620	0.200	0.087	23.8

Run	Calibrating Isotope	ν_c (Mc/sec)	$\delta\nu_c$ (Mc/sec)	H (gauss)	δH (gauss)	F_1	m_1	F_2	m_2	ν (Mc/sec)	$\delta\nu$ (Mc/sec)	Residual (Mc/sec)	Weight Factor
5311	RB85	58.357	0.065	114.232	0.116	3/2	1/2	5/2	-1/2	424.780	0.010	0.002	10000.0
4501	RB85	2.189	0.040	4.673	0.085	3/2	-3/2	5/2	-1/2	410.260	0.200	-0.082	25.0
4121	RB85	2.330	0.100	4.973	0.213	3/2	-3/2	5/2	-1/2	410.150	0.200	-0.163	24.7
4511	RB85	2.659	0.040	5.672	0.085	3/2	-3/2	5/2	-1/2	410.200	0.200	-0.048	25.0
4503	RB85	4.770	0.040	10.139	0.084	3/2	-3/2	5/2	-1/2	409.700	0.200	-0.202	25.0
5321	RB85	9.423	0.035	19.880	0.073	3/2	-3/2	5/2	-1/2	409.588	0.010	-0.004	9999.9
4821	RB85	11.860	0.040	24.923	0.082	3/2	-3/2	5/2	-1/2	409.670	0.050	0.003	398.9
4522	RB85	2.485	0.070	5.302	0.149	3/2	-1/2	5/2	-3/2	413.700	0.100	0.166	65.1
5343	RB85	4.160	0.040	8.852	0.084	3/2	-3/2	5/2	-5/2	417.375	0.175	0.183	29.1

Table V

Summary of Y^{90} data for the $^2D_{5/2}$ electronic state.

Comparing isotope	Calibrating isotopes	
Y^{89}, $^2D_{5/2}$, I = 1/2	Rb^{85}, $^2S_{1/2}$, I = 5/2	Rb^{87}, $^2S_{1/2}$, I = 3/2
$g_J = -1.20028$	$g_J = -2.00238$	$g_J = -2.00238$
$g_I = -1.49037 \times 10^{-4}$	$g_I = 2.93704 \times 10^{-4}$	$g_I = 9.95359 \times 10^{-4}$
a = -28.749 Mc/sec	$\Delta\nu$ = 3035.735 Mc/sec	$\Delta\nu$ = 6834.685 Mc/sec

Iteration No.	a (Mc/sec)	δa (Mc/sec)	b (Mc/sec)	δb (Mc/sec)	$g_I \times 10^4$	$\delta g_I \times 10^4$	χ^2
1	-85.255	0.000	-29.738	0.000	4.42	0.00	36.5
2	-85.258	0.003	-29.716	0.019	-8.70	2.88	14.0
3	-85.258	0.003	-29.716	0.019	-8.75	2.88	14.0
1	-85.255	0.000	-29.738	0.000	-4.42	0.00	15.1
2	-85.258	0.003	-29.716	0.019	-8.75	2.88	14.0
3	-85.258	0.003	-29.716	0.019	-8.75	2.88	14.0

Run	Calibrating isotope	ν_c (Mc/sec)	$\delta\nu_c$ (Mc/sec)	H (gauss)	δH (gauss)	F_1	m_1	F_2	m_2	ν (Mc/sec)	$\delta\nu$ (Mc/sec)	Residual (Mc/sec)	Weight Factor
2954	RB85	3.990	0.030	8.492	0.063	9/2	5/2	9/2	3/2	7.958	0.030	-0.035	221.7
2955	RB85	8.078	0.030	17.079	0.063	9/2	5/2	9/2	3/2	16.190	0.045	-0.013	176.9
2991	RB85	20.023	0.030	41.534	0.060	9/2	5/2	9/2	3/2	40.280	0.105	-0.022	68.0
2996	RB85	34.889	0.030	70.721	0.058	9/2	5/2	9/2	3/2	70.485	0.190	-0.041	25.1
3291	RB85	64.916	0.030	125.876	0.053	9/2	5/2	9/2	3/2	132.150	0.300	-0.258	10.7
3391	RB87	133.524	0.050	180.438	0.064	9/2	5/2	9/2	3/2	199.600	0.750	-0.631	1.8
2994	RB85	3.946	0.030	8.399	0.063	7/2	3/2	7/2	1/2	8.334	0.085	-0.053	88.3
2995	RB85	8.059	0.030	17.039	0.063	7/2	3/2	7/2	1/2	17.235	0.075	0.011	101.9
3191	RB85	12.000	0.030	25.211	0.062	7/2	3/2	7/2	1/2	25.880	0.200	0.088	22.6
3192	RB85	16.795	0.030	35.016	0.061	7/2	3/2	7/2	1/2	36.500	0.200	0.133	22.5
3193	RB85	24.398	0.030	50.262	0.059	7/2	3/2	7/2	1/2	53.540	0.200	0.011	22.4
3194	RB85	34.568	0.030	70.104	0.058	7/2	3/2	7/2	1/2	77.600	0.300	0.213	10.5
3401	RB87	68.313	0.040	94.816	0.054	7/2	3/2	7/2	1/2	109.800	0.300	-0.066	10.5
3421	RB87	113.131	0.040	154.143	0.052	7/2	3/2	7/2	1/2	199.650	0.500	-0.345	3.9
5391	RB85	4.002	0.035	8.518	0.074	5/2	1/2	5/2	-1/2	9.450	0.150	0.023	34.2
4991	RB85	12.089	0.030	25.395	0.062	7/2	3/2	9/2	3/2	405.120	0.080	-0.013	156.1
5352	RB85	24.993	0.030	51.440	0.059	7/2	3/2	9/2	3/2	405.725	0.025	0.007	1597.7
5351	RB85	25.297	0.310	52.042	0.612	7/2	3/2	9/2	3/2	405.725	0.025	-0.002	1386.6

Run	Calibrating isotope	ν_c (Mc/sec)	$\delta\nu_c$ (Mc/sec)	H (gauss)	δH (gauss)	F_1	m_1	F_2	m_2	ν (Mc/sec)	$\delta\nu$ (Mc/sec)	Residual (Mc/sec)	Weight Factor
5361	RB85	4.020	0.040	8.556	0.085	5/2	1/2	7/2	1/2	293.435	0.035	-0.016	816.3
5001	RB85	4.026	0.035	8.568	0.074	5/2	1/2	7/2	1/2	293.425	0.075	-0.026	177.8
4992	RB85	12.146	0.080	25.512	0.165	5/2	1/2	7/2	1/2	292.600	0.150	-0.052	44.0
3931	RB85	1.721	0.030	3.677	0.064	3/2	-3/2	5/2	-5/2	200.750	0.150	0.227	41.4
3751	RB85	1.729	0.040	3.694	0.085	3/2	-3/2	5/2	-5/2	200.525	0.100	-0.008	77.2
3941	RB85	2.278	0.030	4.862	0.064	3/2	-3/2	5/2	-5/2	201.545	0.200	0.252	23.9
4111	RB85	2.845	0.050	6.067	0.106	3/2	-3/2	5/2	-5/2	202.100	0.300	0.000	10.5
4101	RB85	1.672	0.050	3.572	0.106	3/2	-1/2	5/2	-3/2	201.550	0.200	0.127	21.0
4112	RB85	2.845	0.050	6.067	0.106	3/2	-1/2	5/2	-3/2	203.650	0.300	0.282	10.4
4452	RB85	14.250	0.050	29.831	0.102	3/2	-1/2	5/2	-3/2	211.860	0.075	0.086	172.0
5002	RB85	6.382	0.040	13.530	0.084	3/2	-3/2	5/2	-3/2	194.650	0.070	-0.010	204.1
3942	RB85	2.279	0.030	4.864	0.064	3/2	-1/2	5/2	-1/2	196.850	0.200	-0.354	24.8
4451	RB85	23.633	0.040	48.745	0.079	3/2	-1/2	5/2	-1/2	176.450	0.050	-0.036	400.0
5342	RB85	23.676	0.050	48.830	0.099	3/2	-1/2	5/2	-1/2	176.480	0.040	-0.006	625.0
4441	RB85	9.494	0.030	20.027	0.062	3/2	-3/2	5/2	-1/2	175.375	0.200	-0.004	24.0
5341	RB85	15.572	0.030	32.530	0.061	3/2	-3/2	5/2	-1/2	171.350	0.015	0.001	4444.4
4442	RB85	15.574	0.030	32.534	0.061	3/2	-3/2	5/2	-1/2	171.350	0.025	0.001	1600.0
4443	RB85	15.699	0.050	32.788	0.102	3/2	-3/2	5/2	-1/2	171.350	0.015	0.000	4414.0

The small value of the χ^2 reflects the conservative errors placed on the experimental resonance frequencies. Since computer uncertainty in each parameter is the standard deviation of that parameter, there should be a 95% probability (for a normal distribution) that the true value lies within two standard deviations of the measured value. With this uncertainty, the measured values of the interaction constants and g_I were:

$^2D_{3/2}$ state: $a = -169.749(7)$ Mc/sec,

$b = -21.602(27)$ Mc/sec,

$g_I = -4.9(7) \times 10^{-4}$;

$^2D_{5/2}$ state: $a = -85.258(6)$ Mc/sec,

$b = -29.716(38)$ Mc/sec,

$g_I = -9(6) \times 10^{-4}$.

From these values for a and b, the zero-field hyperfine-structure separations were:

$^2D_{3/2}$ state: $\Delta\nu_{1/2-3/2} = 235.722(26)$ Mc/sec,

$\Delta\nu_{3/2-5/2} = 410.872(24)$,

$\Delta\nu_{5/2-7/2} = 613.022(34)$;

$^2D_{5/2}$ state: $\Delta\nu_{1/2-3/2} = 114.515(19)$ Mc/sec,

$\Delta\nu_{3/2-5/2} = 198.288(24)$,

$\Delta\nu_{5/2-7/2} = 293.202(22)$,

$\Delta\nu_{7/2-9/2} = 403.718(37)$.

Figures 42 and 43 show the energy level diagrams for both electronic states in the region 0 to 1000 gauss.

From Eqs. (II-9) and (II-18), one would expect the ratio of the a's in the doublet (primed quantities imply $^2D_{5/2}$; double-primed quantities imply $^2D_{3/2}$) to be

$$\frac{a'}{a''} = \frac{3}{7}\frac{F'}{F''},$$

and the ratio of the b's to be

$$\frac{b'}{b''} = \frac{10}{7}\frac{R'}{R''}.$$

From the interaction constants and nuclear magnetic moment for Y^{89}, the value $Z_1 = 25.5$ was determined with the aid of Eq. (II-9a). With this value for Z_1, the relativistic correction factors (KOP 58, pp. 445-448) were:

$$F' = 1.0059, \qquad R' = 1.0114,$$
$$F'' = 1.0137, \qquad R'' = 1.0374.$$

Thus, the ratios become

$$\frac{a'}{a''} = 0.4253,$$

and

$$\frac{b'}{b''} = 1.3928.$$

From the experimental measurements,

$$\frac{a'}{a''} = 0.5023,$$

and

$$\frac{b'}{b''} = 1.3756.$$

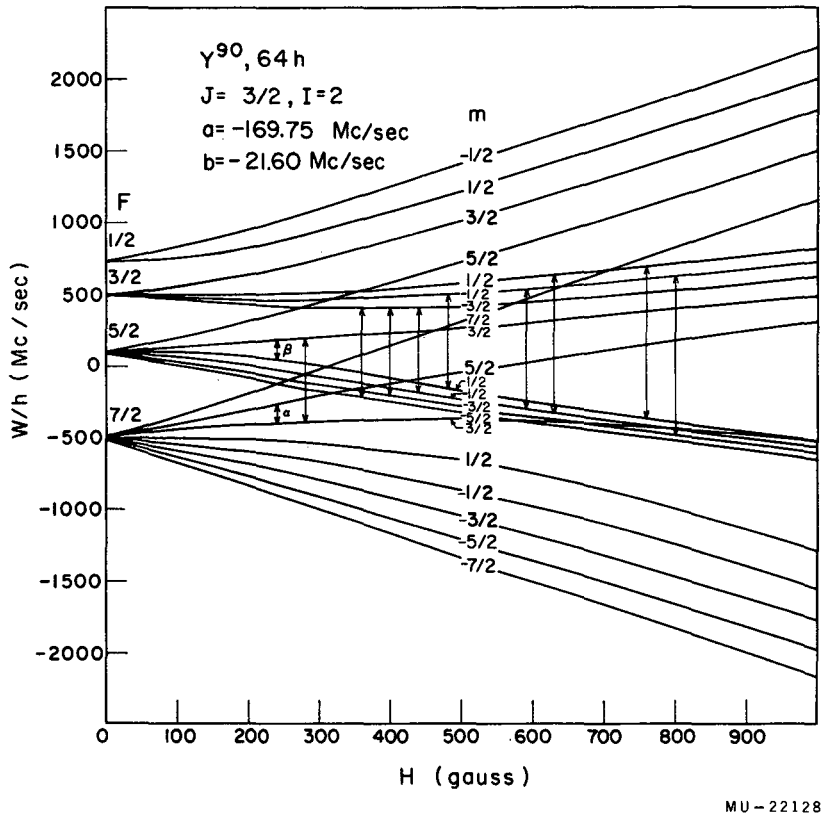

Fig. 42. Energy level diagram of the hyperfine structure in the $^2D_{3/2}$ electronic state of Y^{90}.

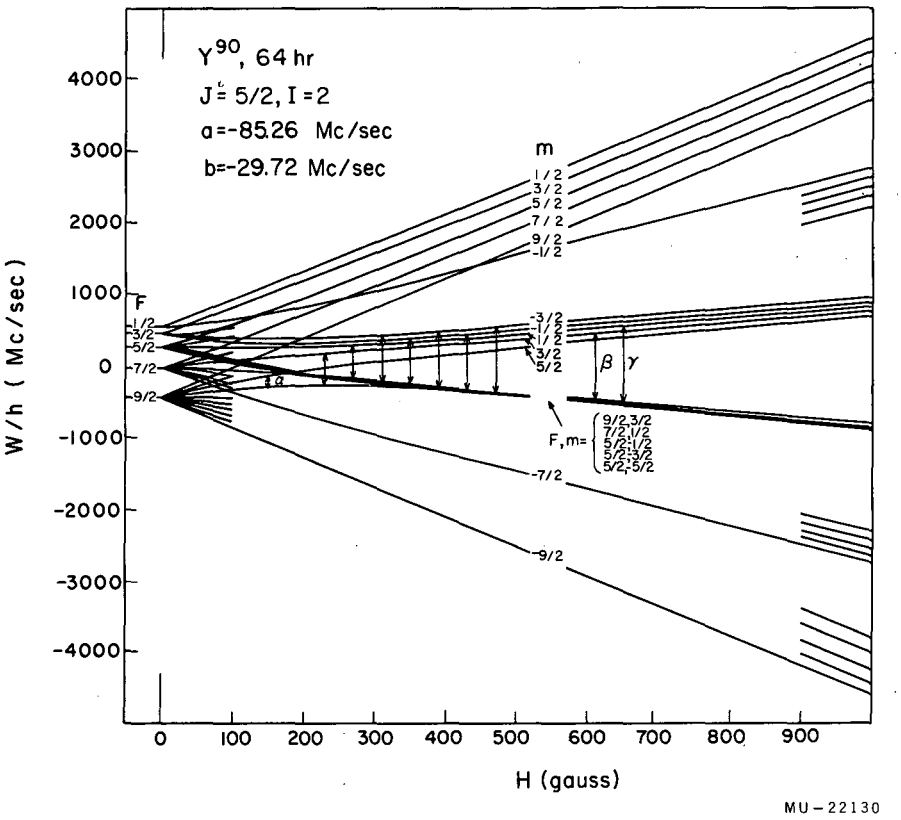

Fig. 43.2 Energy level diagram of the hyperfine structure in the $^2D_{5/2}$ electronic state of Y^{90}.

The large deviation, especially in the ratio of the a's, suggests a configuration mixing effect of the type discussed in Sec. II.A.5. The electronic configuration that meets the requirements for an effect of this type is the $4d5s6s$ configuration.

From the measured a values for both electronic states we calculate the corrections that must be made. With the same notation as in Sec. II.A.5, we have the relations

$$\frac{a_0'}{a_0''} = \frac{3}{7\theta},$$

$$\delta' = -\delta'',$$

$$a' = a_0' + \delta',$$

$$a'' = a_0'' + \delta'',$$

$$\theta = \frac{F''}{F'} \left| \frac{C''}{C'} \right|^2.$$

We may estimate $|C''/C'|^2$ from Eq. (II-73). Taking $n^* = 1.444$, we obtain

$$\left| \frac{C''}{C'} \right|^2 = 1.0140.$$

Thus, $\theta = 1.0219$ and

$$a_0' = -75.347 \text{ Mc/sec},$$

$$a_0'' = -179.660 \text{ Mc/sec}.$$

The interaction constants of Y^{89} are (FRI 59):

$$a' = -28.749(30) \text{ Mc/sec},$$

and

$$a'' = -57.217(15) \text{ Mc/sec}.$$

The corrected values are

$$a_0' = -25.401 \text{ Mc/sec},$$

and

$$a_0'' = -60.565 \text{ Mc/sec}.$$

Since $g_I^*(Y^{89})_{expt}^{uncorr} = -0.273650(8)$ (BRU 54), we can now use the Fermi-Segrè relation to calculate the nuclear g_I^* factor for Y^{90}. For both electronic states, the value is

$$g_I^*(Y^{90})_{expt}^{uncorr} = -0.812(4).$$

The uncorrected nuclear magnetic moment, therefore, is

$$\mu_I(Y^{90})_{expt}^{uncorr} = g_I^* I = -1.623(8) \text{ nm}.$$

The 0.5% uncertainty has been assigned to the calculated nuclear magnetic moment because of assumptions involved in the Fermi-Segrè relation.

Fricke, Kopfermann, and Penselin (FRI 59) have calculated effective nuclear charge numbers for yttrium based on their hyperfine-structure results for Y^{89}. Their results are:

$$^2D_{3/2} \text{ state: } Z_1 = Z - 12.5,$$

$$^2D_{5/2} \text{ state: } Z_1 = Z - 16.4.$$

Here the configuration mixing effect is reflected in the two different values for Z_i. If we use these values and the uncorrected a's for Y^{90} to calculate the magnetic moment from Eq. (II-9a), the result for both electronic states is

$$\mu_I = -1.621 \text{ nm.}$$

This result agrees very well with the previous one.

The uncorrected nuclear electric quadrupole moment can best be obtained from Eq. (II-20). For the $^2D_{5/2}$ state,

$$Q(^2D_{5/2}) = -0.1551 \text{ barns,}$$

and for the $^2D_{3/2}$ state,

$$Q(^2D_{3/2}) = -0.1549 \text{ barns.}$$

We shall take

$$Q(Y^{90})^{\text{uncorr}}_{\text{expt}} = -0.155(3) \text{ barns}$$

as the best uncorrected value of the nuclear electric quadrupole moment for Y^{90}. A 2% uncertainty has been assigned to the nuclear quadrupole moment because of the uncertainty in g_I and because the ratio of the b's for the two electronic states differs from the theoretical ratio by 1.2%.

Since nuclear deformation is not large in the case of Y^{90}, the experimental nuclear moment results are comparable with the single-particle shell model. Since the odd proton in a $p_{1/2}$ level couples with the odd neutron in a $d_{5/2}$ level to give I = 2, we obtain from Eq. (II-77),(II-78), and

(II-79)

$$g_p = +0.528,$$

$$g_n = -0.765,$$

$$\mu_s = -1.609 \text{ nm}.$$

The diamagnetic correction factor $\kappa = (1 - \sigma)^{-1} = 1.00359$ (KOP 58, p.450); thus,

$$\mu_I(Y^{90})^{\text{corr}}_{\text{expt}} = \kappa\mu_I(Y^{90})^{\text{uncorr}}_{\text{expt}} = -1.629(8) \text{ nm}.$$

The experimental and theoretical values for μ_I are seen to be in remarkable agreement (approx. 1%). Since the odd proton is in a $p_{1/2}$ level, the single-particle shell model would predict $Q = 0$ for the quadrupole moment of Y^{90} [Eq. (II-83)]. Therefore, the spin and magnetic moment are predicted very well by this model, whereas the quadrupole moments are not in very good agreement.

From Eqs. (II-83), (II-84), and (II-86), the collective model predicts

$$\mu_c = +0.30 \text{ nm}.$$

The collective model predicts the spin correctly but gives a much poorer prediction for the magnetic moment than the independent-particle model.

From nuclear spin and magnetic moment considerations, one can finally say that the independent-particle shell model is a better representation than the collective model for Y^{90}.

C. Results for La^{140}

Lanthanum-140 has a $5d6s^2$ electronic ground-state configuration, giving rise to the $^2D_{3/2}$ and $^2D_{5/2}$ electronic states. Since the $^2D_{5/2}$ state is only 1053.20 cm^{-1} higher than the $^2D_{3/2}$ ground state (MEC 32), one would expect approximately 60% of the atoms to be in the $^2D_{3/2}$ state and 40% to be in the $^2D_{5/2}$ state at the temperatures required to produce a beam.

The g_J factors required for Eq. (III-2) were obtained from the atomic beam work by Yu Ting (TIN 57) on stable La^{139}. His results are

$$g_J(^2D_{3/2}) = -0.7988(5),$$

$$g_J(^2D_{5/2}) = -1.201(2).$$

The difficulties discussed in Sec. III.A.2 in producing a satisfactory atomic beam precluded making extensive measurements on the hyperfine structure of this isotope. However, observation of the $\Delta F = 0$ transitions corresponding to the $F = I + J$ levels at low magnetic fields established the nuclear spin. Figures 44 and 45 show the results of spin searches, which indicated the spin to be $I = 3$. Observation of resonances in both electronic states, one of which is shown in Fig. 46, established this result (PET 60b).

Beta- and gamma-ray spectroscopic evidence previously indicated the probable ground state of La^{140} to be 4 minus. However, recent work (LAN 60) has eliminated this possibility. It shows the shape of the β-ray spectrum of the highest-energy transition to be consistent with a transition from 3- to 2+, in agreement with the value determined by means of atomic beams.

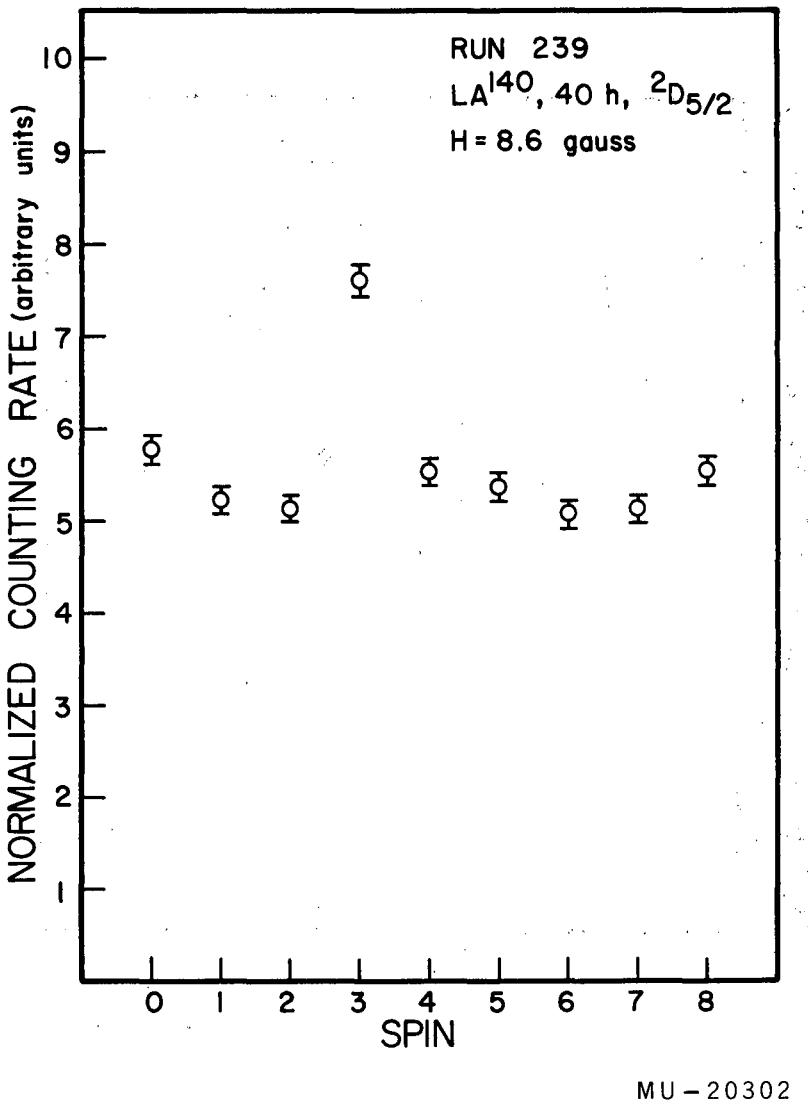

Fig. 44. Results of a spin search in the $^2D_{5/2}$ electronic state of La^{140} for the $\Delta F = 0$ transition in the $F = I + J$ level.

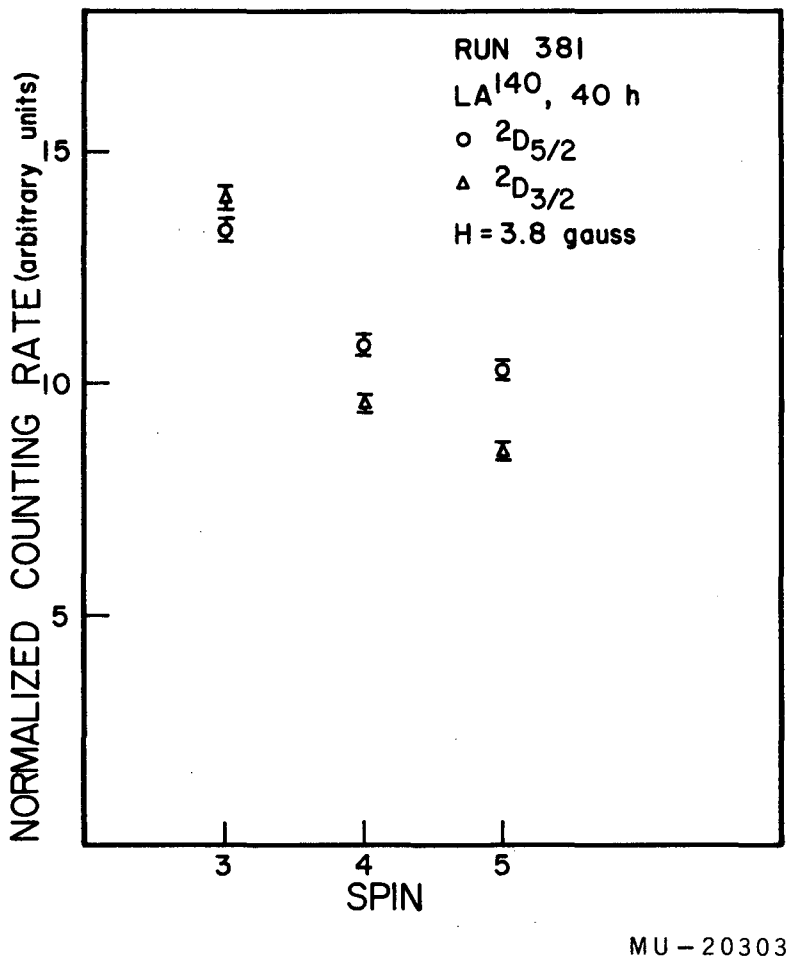

Fig. 45. Results of a spin search in the $^2D_{3/2}$ and $^2D_{5/2}$ electronic states of La^{140} for the $\Delta F = 0$ transition in the F = I + J level.

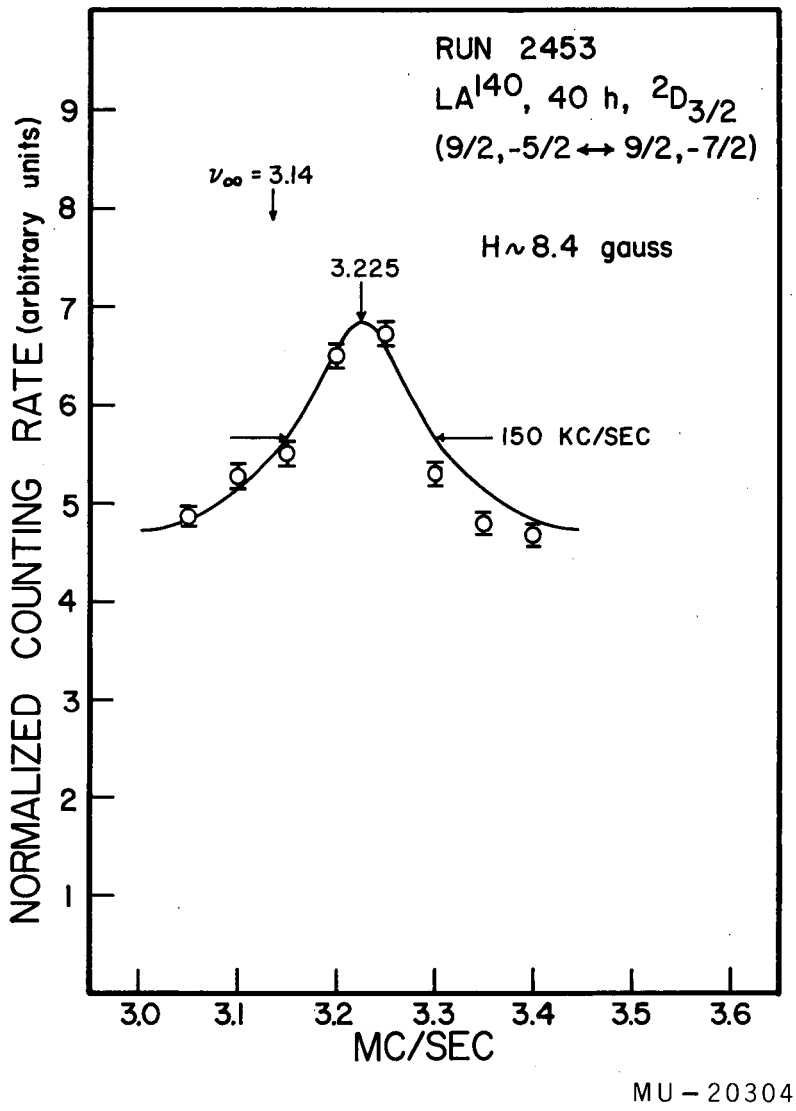

Fig. 46. Resonance corresponding to the transition F, $m=9/2, -5/2 \leftrightarrow 9/2, -7/2$ in the $^2D_{3/2}$ state of La^{140}.

D. Results for Lu^{177}

As with lanthanum, lutetium has a $5d6s^2$ electronic ground-state configuration giving rise to the $^2D_{3/2}$ and $^2D_{5/2}$ electronic states. Since the $^2D_{5/2}$ state is only 1993.9 cm^{-1} higher (MEG 30) than the $^2D_{3/2}$ ground state, one would expect approximately 75% of the atoms to be in the lower state and 25% to be in the upper state at the oven temperatures used.

The initial g_J factors required for Eq. (III-2) were assumed to be the LS coupling values. These values fitted the first experimental data to within about 1%. Later, Ritter of the National Research Council, Ottawa, Canada, kindly provided unpublished experimental information on stable Lu^{175} which permitted calculation of more accurate values with Routine Hyperfine III (RIT 60). The values used for final analysis of the data are:

$$g_J(^2D_{3/2}) = -0.79911(10),$$

$$g_J(^2D_{5/2}) = -1.20035(20).$$

Although the irradiated sample was 99.9% pure lutetium metal, very high beams at low temperatures with no throwout were initially observed. This phenomenon proved to be a temporary effect, and probably was caused by $LuCl_3$ or LuF_3 molecules. After about half an hour of running, an atomic beam with 60 to 70% throwout was observed.

The initial spin search in both electronic states confirmed the expected spin I = 7/2. Figures 47 through 51 are examples of resonances corresponding to the $\Delta F = 0$ transitions in the $^2D_{5/2}$ and $^2D_{3/2}$ states, which verified this result (PET 60a).

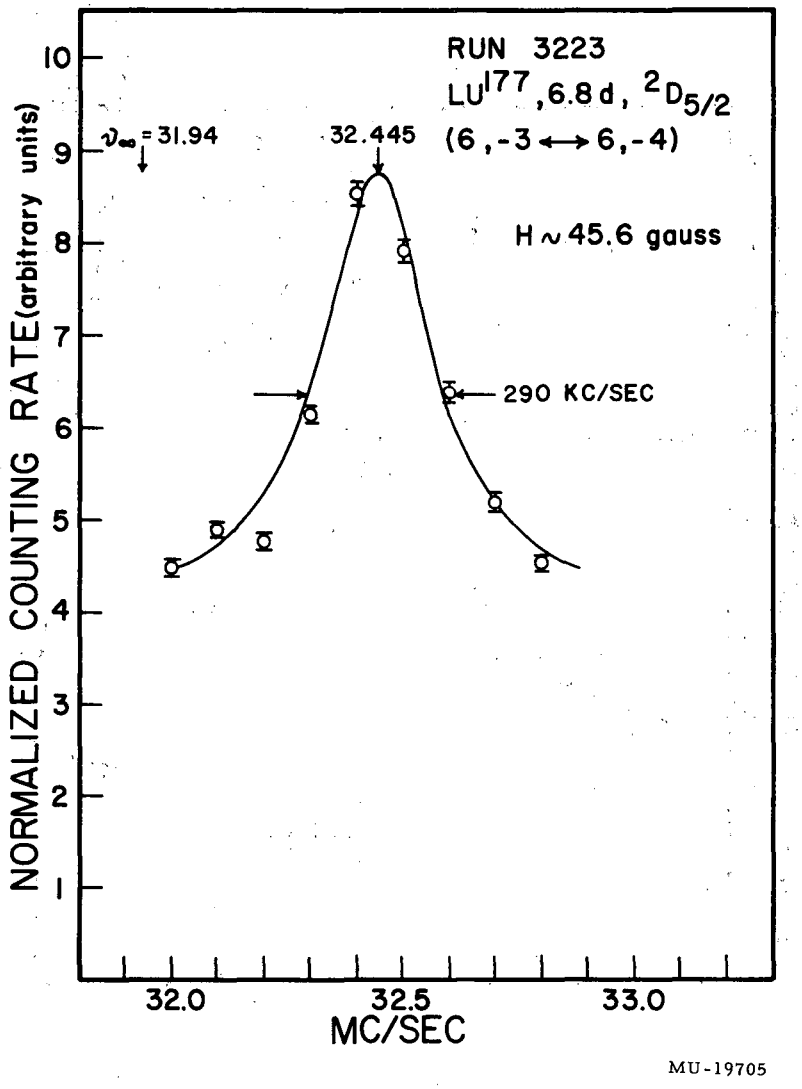

Fig. 47. Resonance corresponding to the transition F, m=6, -3 ↔ 6, -4 in the $^2D_{5/2}$ state of Lu^{177}.

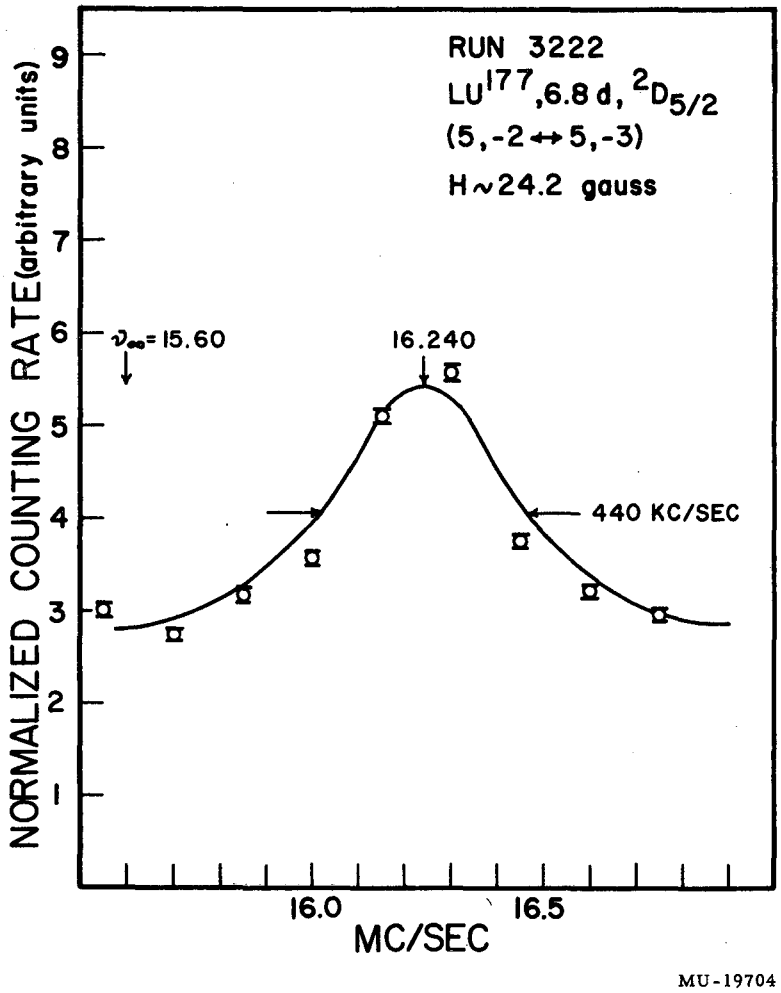

Fig. 48. Resonance corresponding to the transition F, m=5, -2 ↔ 5, -3 in the $^2D_{5/2}$ state of Lu^{177}.

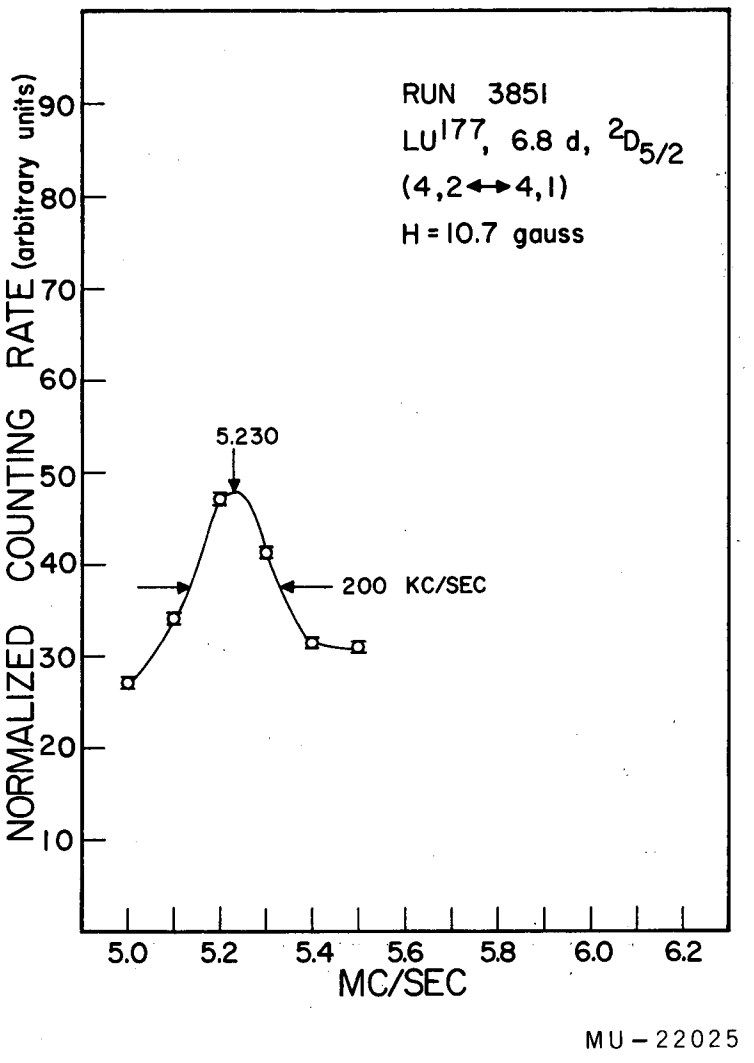

Fig. 49. Resonance corresponding to the transition F, m=4, 2↔4, 1 in the $^2D_{5/2}$ state of Lu^{177}.

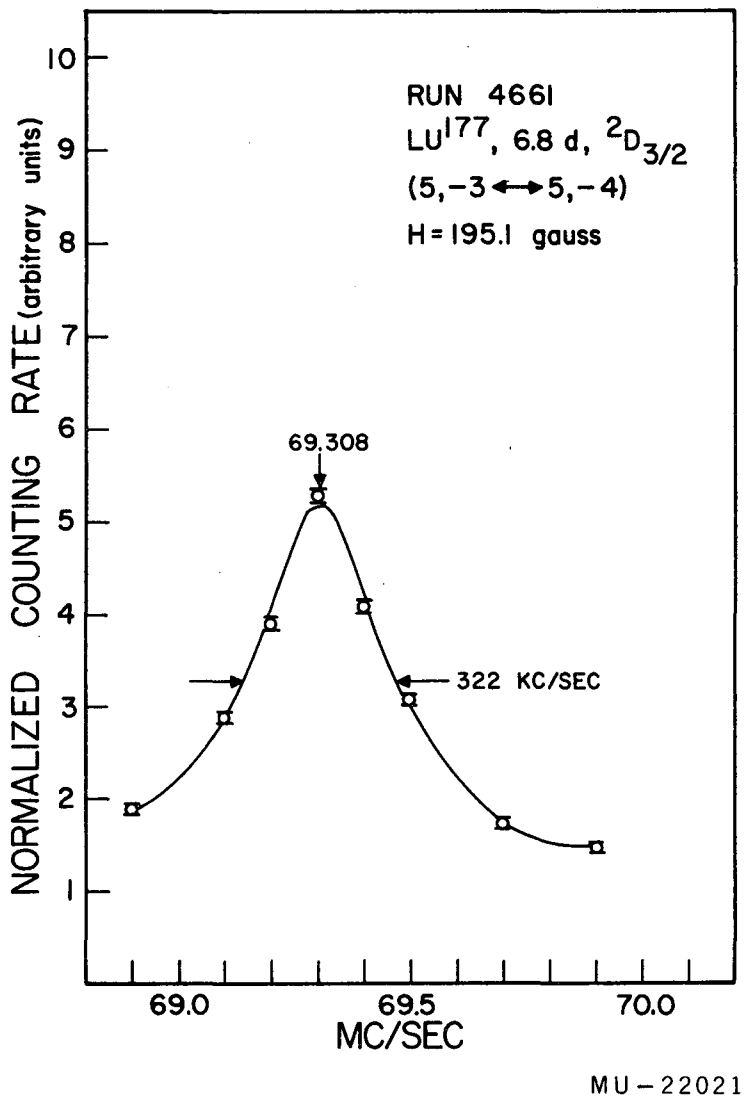

Fig. 50. Resonance corresponding to the transition F, m=5, -3 ↔ 5, -4 in the $^2D_{3/2}$ state of Lu^{177}.

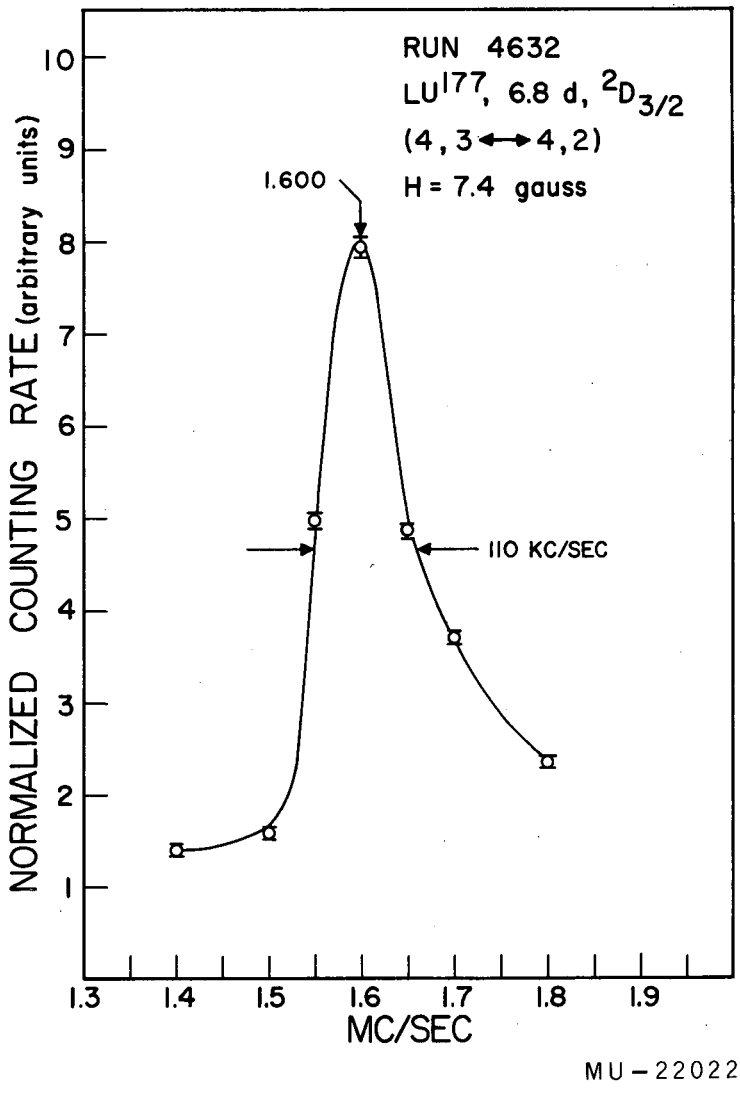

Fig. 51. Resonance corresponding to the transition F, m=4, 3 ↔ 4, 2 in the $^2D_{3/2}$ state of Lu^{177}.

The $^2D_{5/2}$ electronic state was investigated first. In accordance with the usual procedure, $\Delta F = 0$ transitions were carried to higher magnetic fields in order to reduce the uncertainty in the zero-field hfs separations. After appreciable quadratic shifts had been observed, preliminary a and b values were calculated. These values were then used as starting values in Routine Hyperfine III, and all future fits of experimental data were made with the computer program. Since the ratio b/a was found to be 12.3, the level ordering in this electronic state has been inverted to F = 6, 5, 1, 4, 2, and 3 (see Fig. 5).

In order to increase the accuracy of the interaction constants, an attempt was next made to observe the $\Delta F = \pm 1$ transitions at low magnetic fields. These observations reduced the uncertainties in a and b to a few hundred kc/sec. With these values, Routine JO-9 was used to predict transition frequencies as a function of the magnetic field. Table VI shows where these transitions are least field-dependent. Since the resonance line width is narrowest at these points, future work was concentrated in this area. Figures 52 through 56 are examples of resonances observed, where possible, at their least field-dependent points. Again, double-peaked σ transitions of the type discussed in Sec. IV.B were observed.

With the aid of Ritter's hfs interaction constants for Lu^{175} (RIT 60, unpublished data), the $^2D_{5/2}$ interaction constants were used to estimate the interaction constants in the $^2D_{3/2}$ electronic state. These values predicted the ratio b/a to be 7.5, which resulted in the level ordering F = 5, 2, 4, and 3 (see Fig. 4). The accuracy of the estimate made possible a direct search for the $\Delta F = \pm 1$ transitions. Examples of resonances

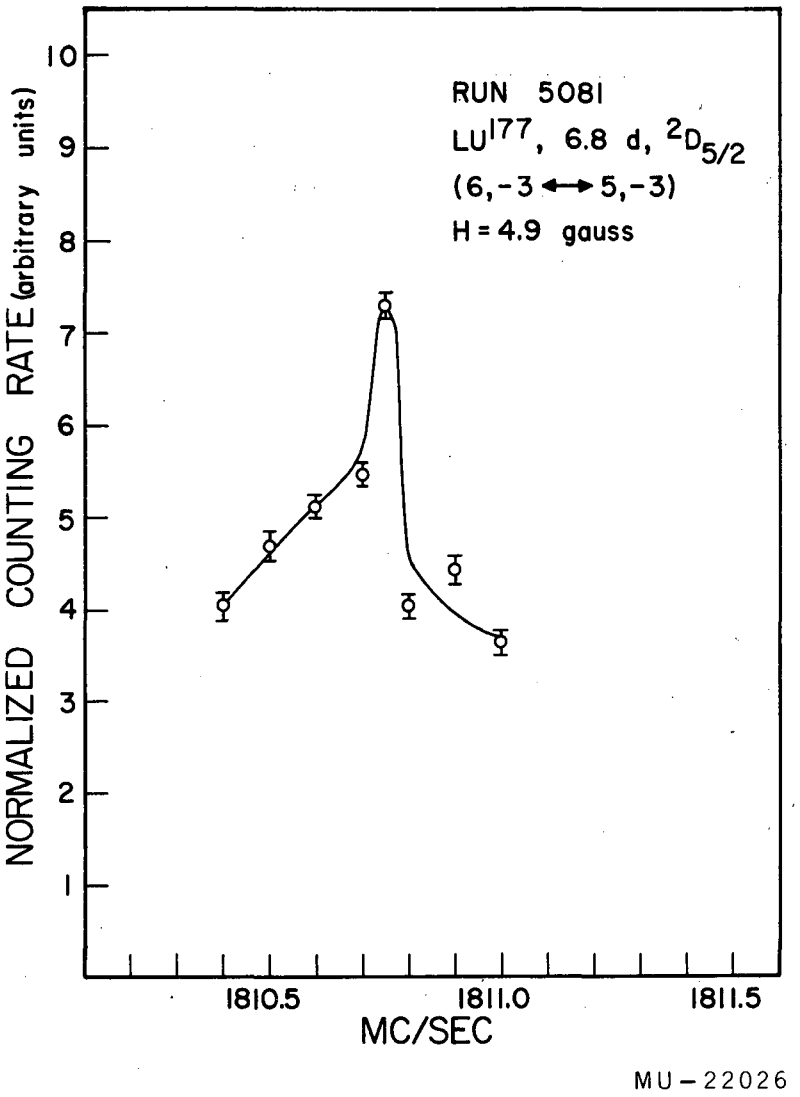

Fig. 52. Resonance corresponding to the transition F, m=6, -3 ↔ 5, -3 in the $^2D_{5/2}$ state of Lu^{177}.

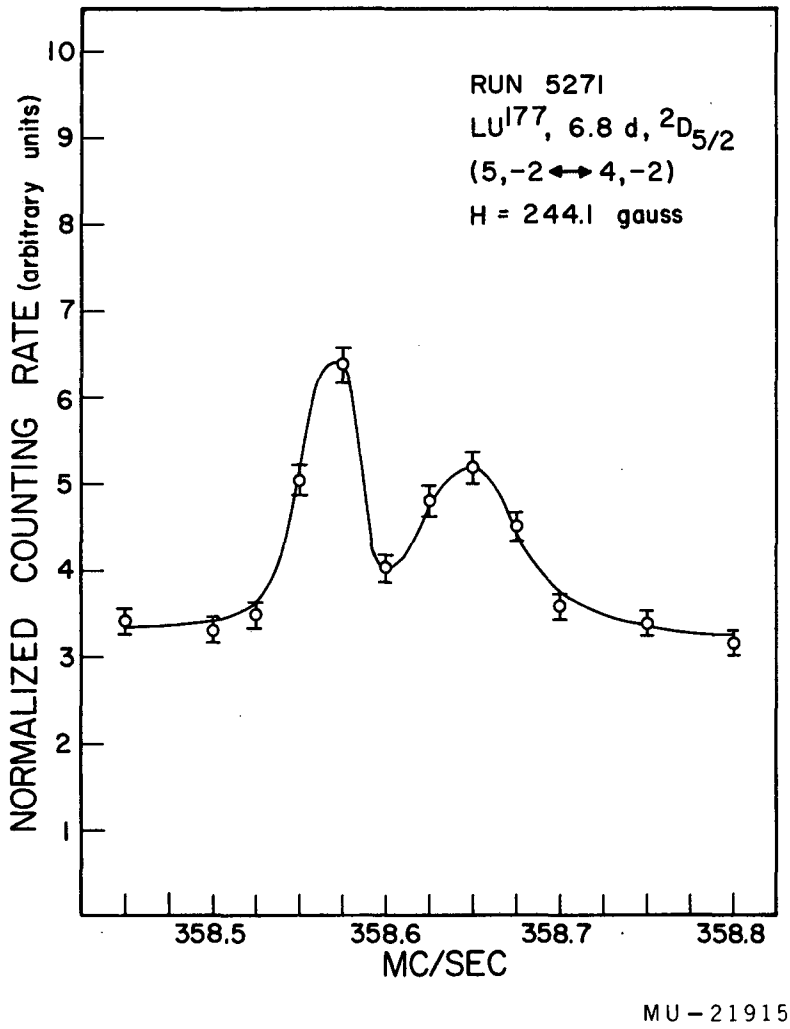

Fig. 53. Resonance corresponding to the transition F, m=5, -2 ↔ 4, -2 in the $^2D_{5/2}$ state of Lu^{177}.

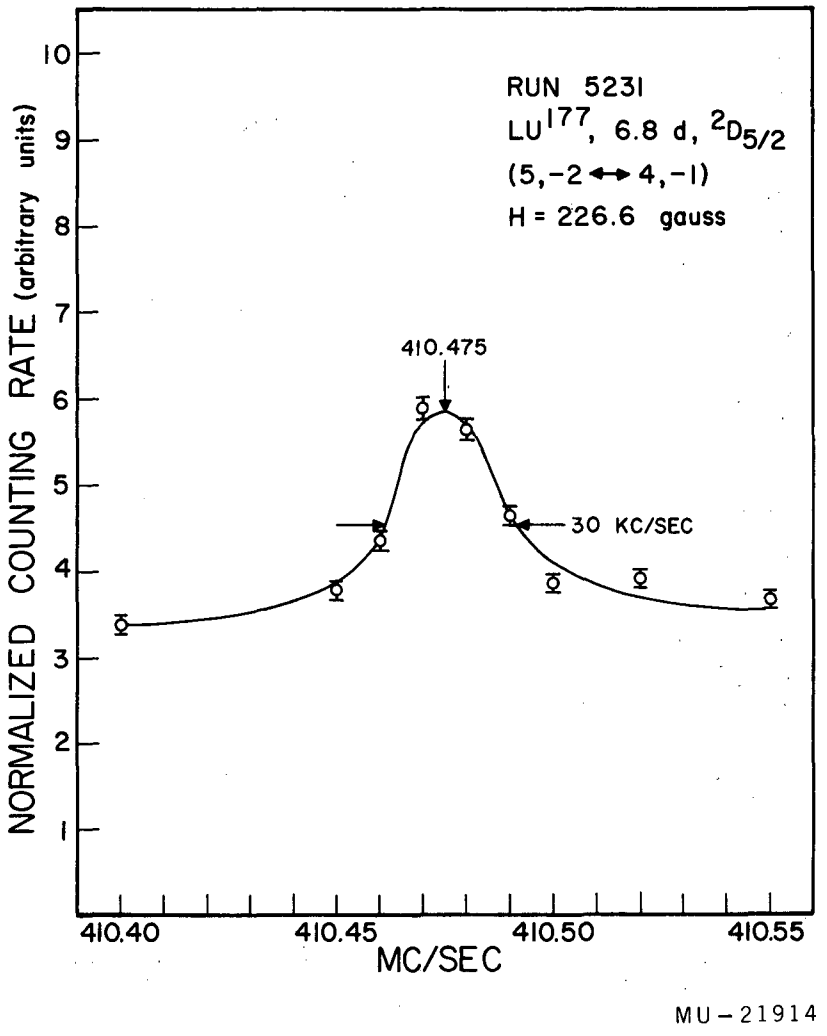

Fig. 54. Resonance corresponding to the transition F, m=5, -2 ↔ 4, -1 in the $^2D_{5/2}$ state of Lu^{177}.

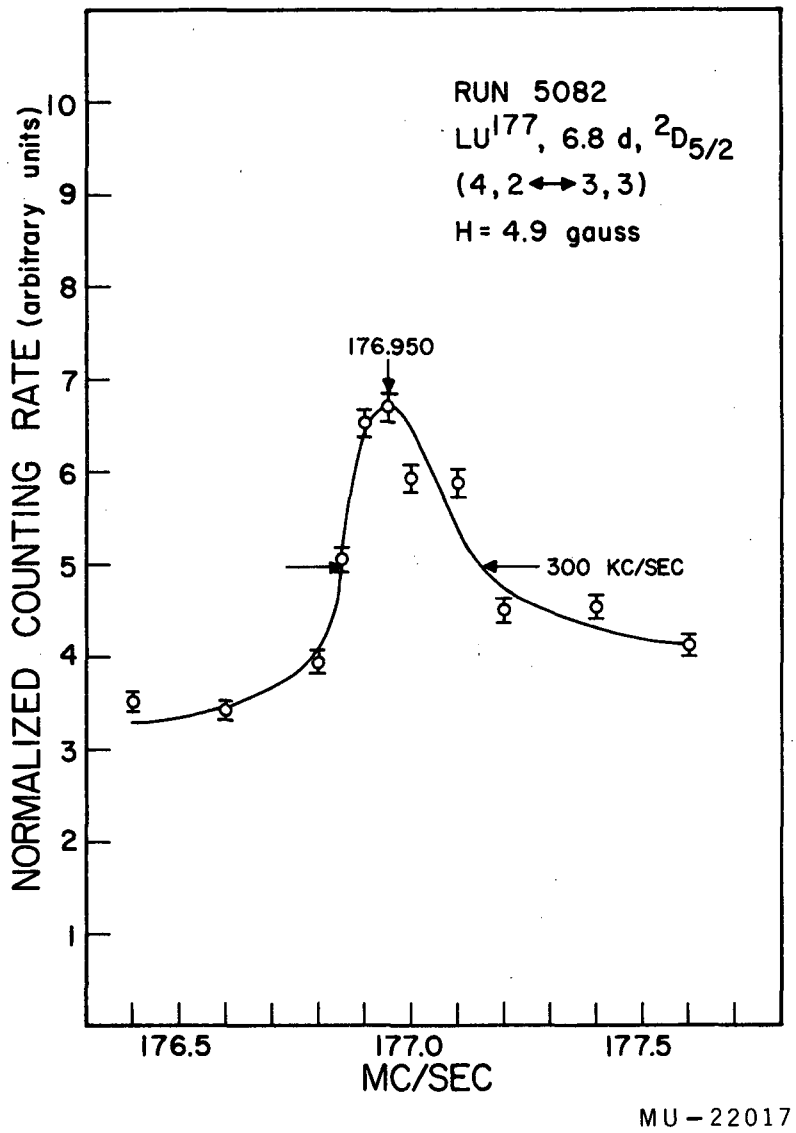

Fig. 55. Resonance corresponding to the transition F, m=4, 2 ↔ 3, 3 in the $^2D_{5/2}$ state of Lu^{177}.

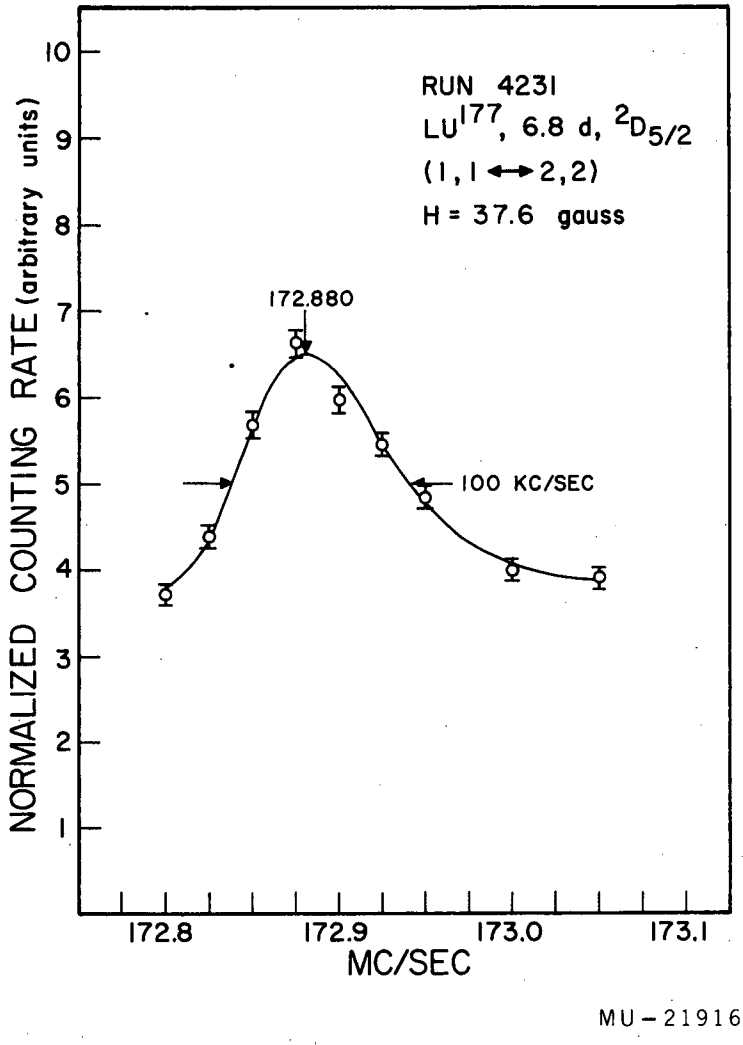

Fig. 56. Resonance corresponding to the transition F, m=1, 1 ↔ 2, 2 in the $^2D_{5/2}$ state of Lu^{177}.

corresponding to these transitions are shown in Figs. 57 through 61.

The only transition for which $\partial\nu/\partial H$ is 0 in this electronic state for magnetic fields less than 1000 gauss is shown in Fig. 61 ($\partial\nu/\partial H = 0$ at approx. 62 gauss). The field-independent advantage of this transition was partially lost because of interference with the transition $F,m = 4,3 \longleftrightarrow 3,3$. Good resolution, however, was finally obtained at about 60 gauss.

The final results, in which all experimental data have been fitted by Routine Hyperfine III, are shown in Tables VII and VIII. Both positive and negative starting values for g_I were used. It should be noted that g_I converges to the same positive value for both cases in each electronic state.

The value of g_I calculated in this manner provides an independent check on the values calculated from Eq. (II-9a) and the a's for both electronic states. Uncertainty in the $^2D_{3/2}$ measurement is very large because the observed field-independent π transition occurs at only 60 gauss. The $F,m = 5,-2 \longleftrightarrow 4,-1$ field-independent transition in the $^2D_{5/2}$ state occurring at 227 gauss provided the best directly measured value of g_I.

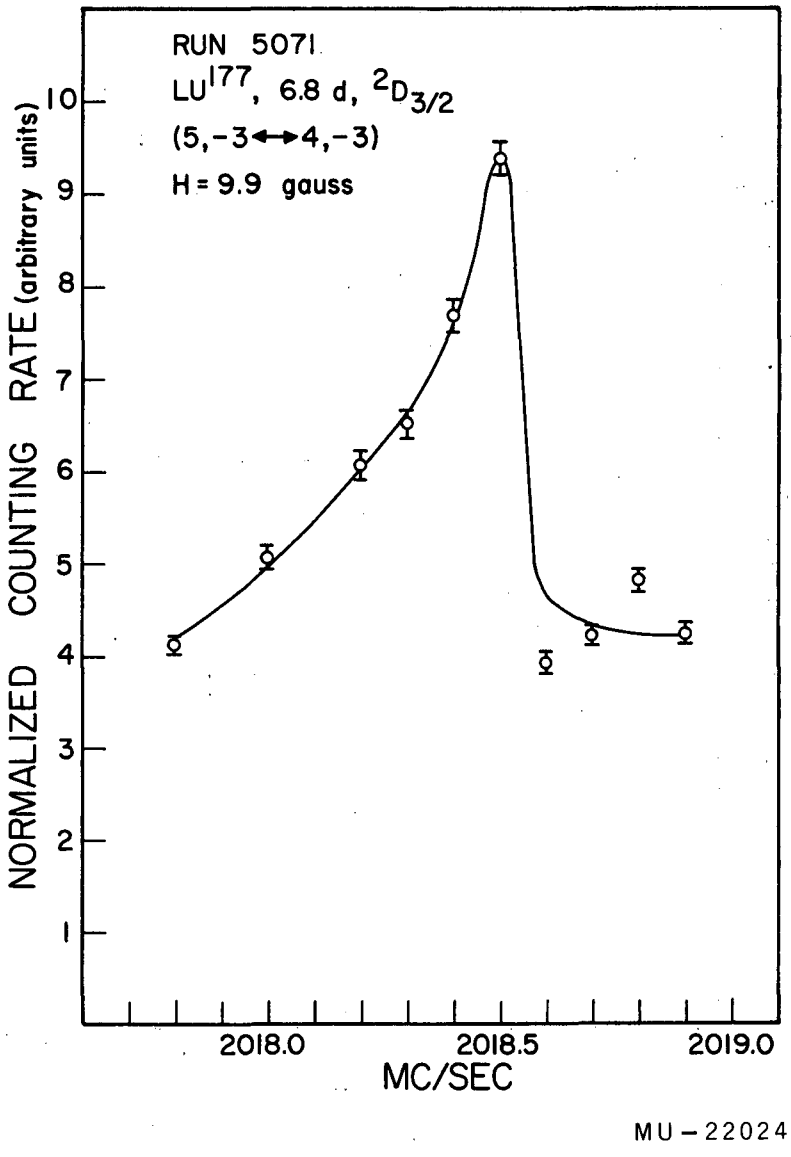

Fig. 57. Resonance corresponding to the transition F, m=5, -3↔4, -3 in the $^2D_{3/2}$ state of Lu^{177}.

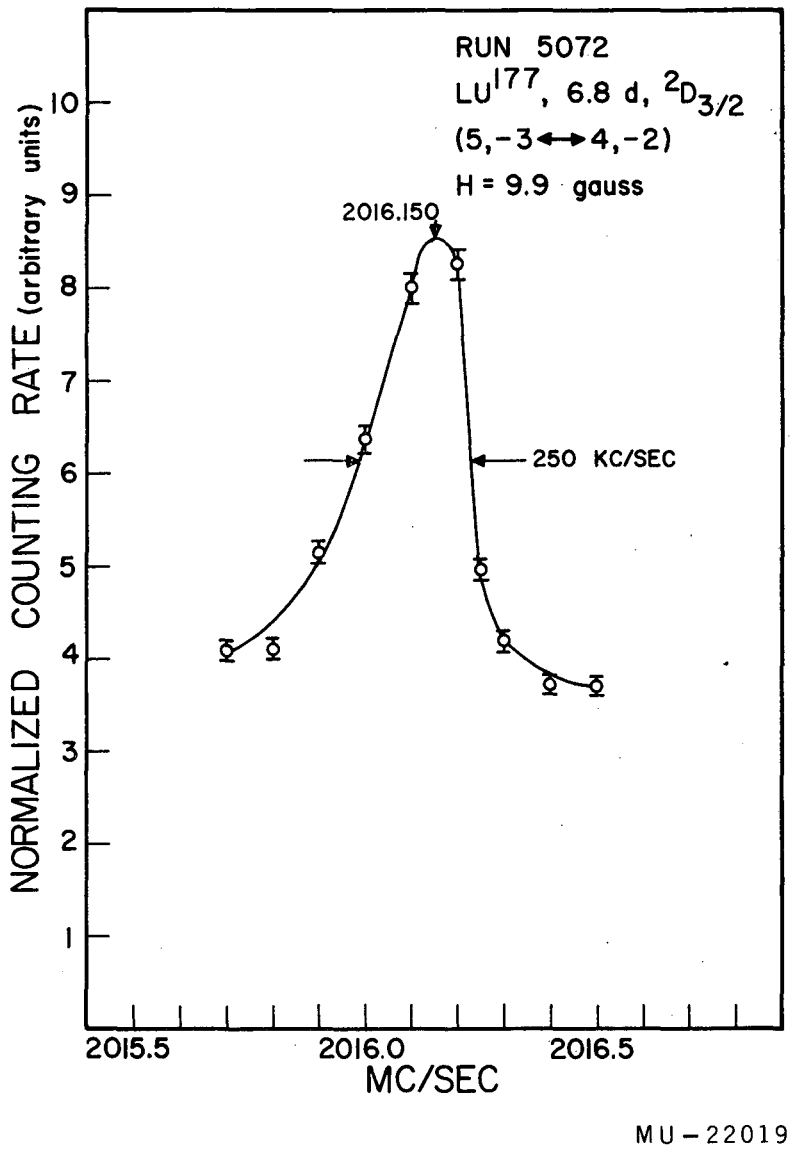

Fig. 58. Resonance corresponding to the transition F, m=5, -3 ↔ 4, -2 in the $^2D_{3/2}$ state of Lu^{177}.

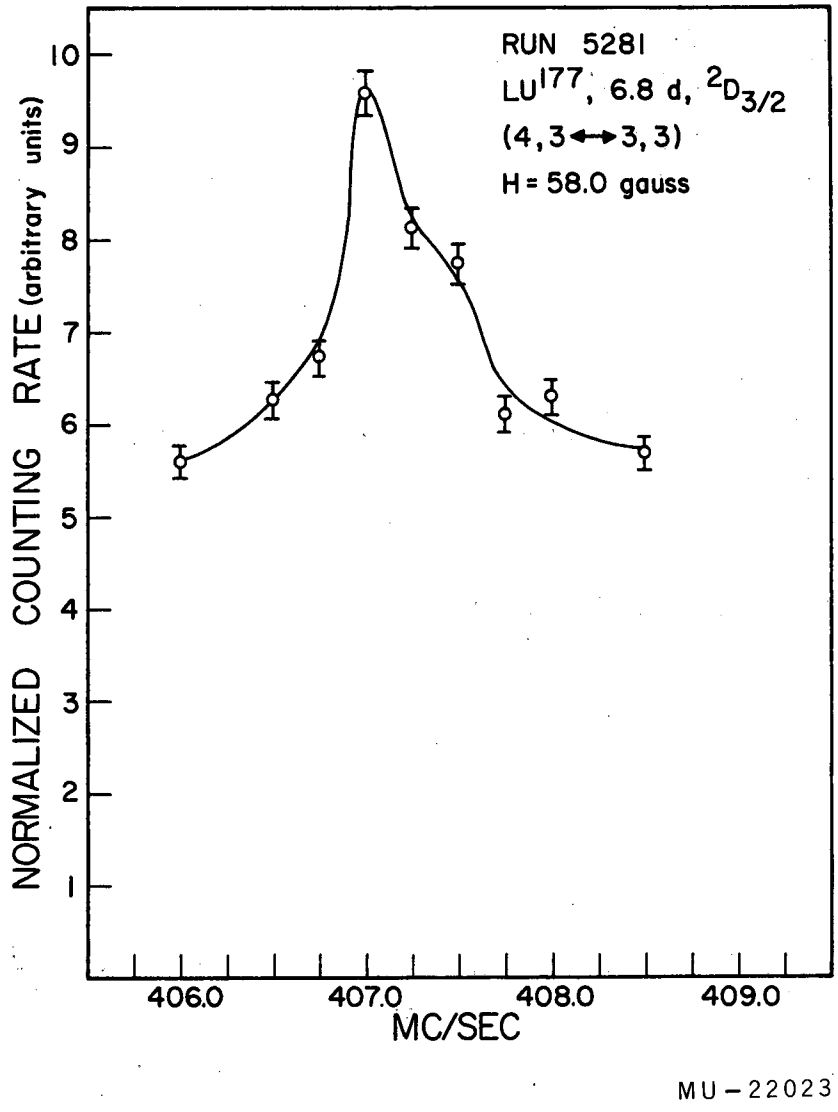

Fig. 59. Resonance corresponding to the transition F, m=4, 3 ↔ 3, 3 in the $^2D_{3/2}$ state of Lu^{177}.

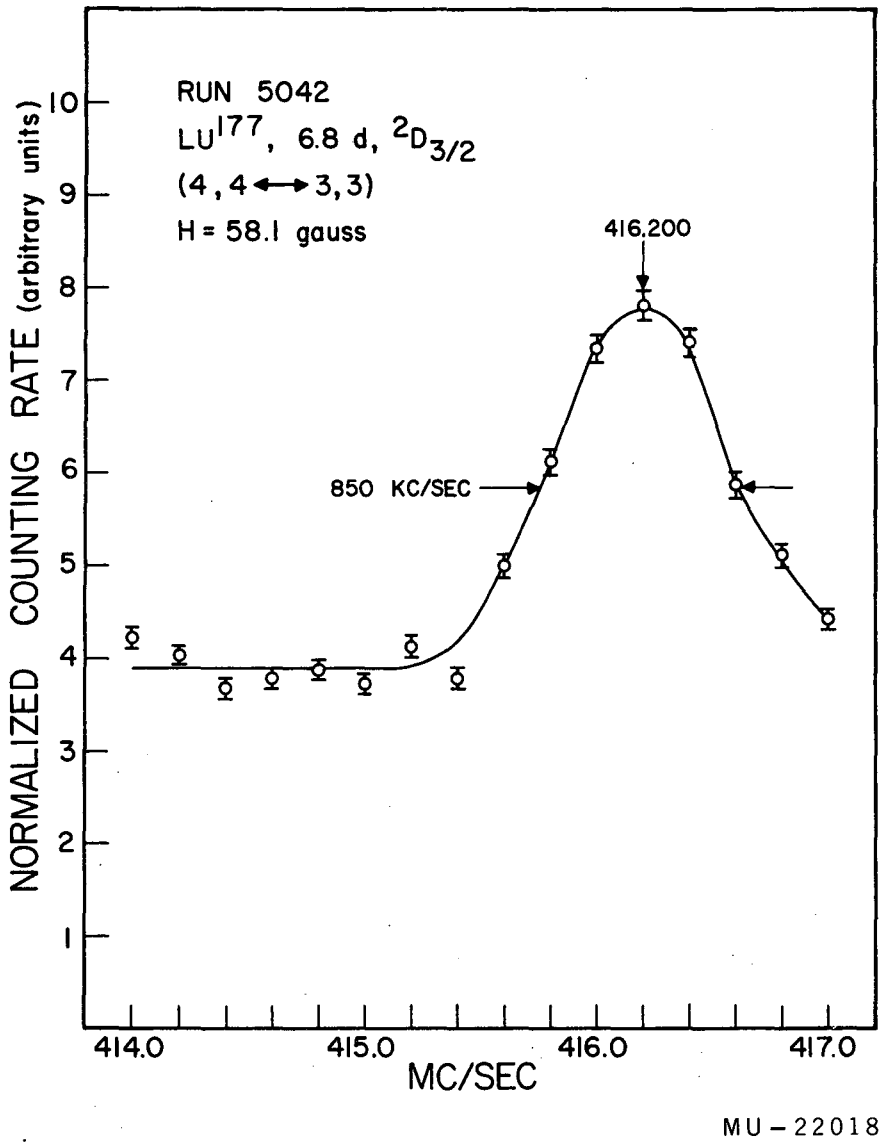

Fig. 60. Resonance corresponding to the transition F, m=4, 4 ↔ 3, 3 in the $^2D_{3/2}$ state of Lu^{177}.

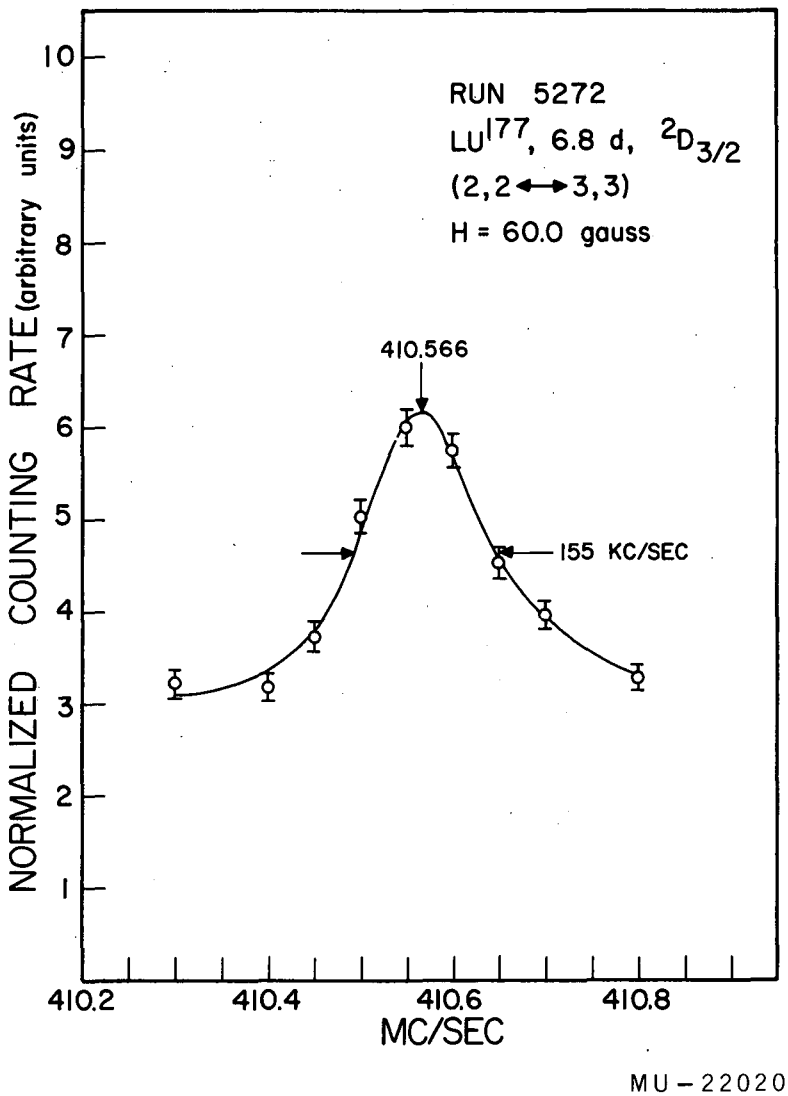

Fig. 61. Resonance corresponding to the transition F, m=2, 2 ↔ 3, 3 in the $^2D_{3/2}$ state of Lu^{177}.

Table VI

The most field-independent positions of the observable $\Delta F = \pm 1$ transitions in the $^2D_{5/2}$ electronic state of Lu^{177}. The calculations were performed for a = 147.167 and b = 1805.928.

Transition $(F_1,m_1 \longleftrightarrow F_2,m_2)$	$(\partial\nu/\partial H)_{min}$ (Mc/sec-gauss)	H (gauss)	$\nu(g_I +)$ (Mc/sec)	$\nu(g_I -)$ (Mc/sec)
6,-3 ⟷ 5,-3	0	805.2	1230.572	1230.572
5,-2 ⟷ 4,-2	0	243.9	358.595	358.595
5,-2 ⟷ 4,-1	0	226.5	410.476	410.279
4, 2 ⟷ 3, 3	0.042	0	175.885	175.885
4, 4 ⟷ 3, 3	1.134	0	175.885	175.885
4, 3 ⟷ 3, 3	0.588	0	175.885	175.885
1, 1 ⟷ 2, 2	0	37.2	172.868	172.835

Table VII

Summary of Lu^{177} data for the $^2D_{3/2}$ electronic state.

Comparing isotope	Calibrating isotopes	
Lu^{175}, $^2D_{3/2}$, I = 7/2	Rb^{85}, $^2S_{1/2}$, I = 5/2	Rb^{87}, $^2S_{1/2}$, I = 3/2
g_J = -0.79911	g_J = -2.00238	g_J = -2.00238
$g_I = 3.1 \times 10^{-4}$	$g_I = 2.93704 \times 10^{-4}$	$g_I = 9.95359 \times 10^{-4}$
a = 194.3317 Mc/sec	$\Delta\nu$ = 3035.735 Mc/sec	$\Delta\nu$ = 6834.685 Mc/sec

Iteration No.	a (Mc/sec)	δa (Mc/sec)	b (Mc/sec)	δb (Mc/sec)	$g_I \times 10^4$	$\delta g_I \times 10^4$	χ^2
1	194.840	0.000	1466.725	0.000	3.11	0.00	2.93
2	194.842	0.010	1466.713	0.058	4.15	2.86	2.86
3	194.842	0.010	1466.713	0.058	4.15	2.86	2.86
1	194.840	0.000	1466.725	0.000	-3.11	0.00	6.70
2	194.842	0.010	1466.713	0.058	4.20	2.88	2.86
3	194.842	0.010	1466.713	0.058	4.14	2.86	2.86

Run	Calibrating isotope	ν_c (Mc/sec)	$\delta\nu_c$ (Mc/sec)	H (gauss)	δH (gauss)	F_1	m_1	F_2	m_2	ν (Mc/sec)	$\delta\nu$ (Mc/sec)	Residual (Mc/sec)	Weight Factor
4631	RB85	3.460	0.040	7.371	0.085	5	-3	5	-4	2.470	0.050	-0.006	301.5
4651	RB85	28.660	0.070	58.653	0.137	5	-3	5	-4	20.000	0.050	-0.007	209.8
4661	RB85	106.545	0.110	195.126	0.173	5	-3	5	-4	69.308	0.075	-0.024	101.2
4632	RB85	3.463	0.040	7.377	0.085	4	3	4	2	1.600	0.050	0.005	355.1
4652	RB85	28.652	0.070	58.637	0.137	4	3	4	2	13.400	0.200	0.039	21.2
3261	RB85	50.618	0.030	100.211	0.055	4	3	4	2	74.600	0.200	-0.186	20.7
5071	RB85	4.667	0.030	9.922	0.063	5	-3	4	-3	2018.450	0.200	0.021	24.7
5072	RB85	4.668	0.030	9.924	0.063	5	-3	4	-2	2016.150	0.120	0.032	63.1
5061	RB85	4.688	0.030	9.966	0.063	5	-3	4	-2	2016.050	0.150	-0.043	41.8
5281	RB85	28.340	0.035	58.027	0.068	4	3	3	3	407.125	0.350	-0.090	7.9
4741	RB87	20.234	0.100	28.666	0.140	4	4	3	3	387.200	0.300	0.227	9.2
5042	RB85	28.364	0.030	58.074	0.059	4	4	3	3	416.200	0.300	0.004	10.7
4742	RB85	1.403	0.040	2.999	0.085	2	2	3	3	459.000	0.750	-0.800	1.8
5041	RB85	28.364	0.030	58.074	0.059	2	2	3	3	411.030	0.120	-0.029	67.7
5021	RB85	29.356	0.040	60.013	0.078	2	2	3	3	410.550	0.080	-0.027	152.2
5272	RB85	29.371	0.030	60.042	0.058	2	2	3	3	410.566	0.080	-0.006	154.0
5111	RB85	30.883	0.030	62.986	0.058	2	2	3	3	410.510	0.100	0.014	99.6
5101	RB85	30.931	0.030	63.079	0.058	2	2	3	3	410.525	0.100	0.018	99.5

Table VIII

Summary of Lu^{177} data for the $^2D_{5/2}$ electronic state.

Comparing isotope	Calibrating isotopes	
Lu^{175}, $^2D_{5/2}$, I = 7/2	Rb^{85}, $^2S_{1/2}$, I = 5/2	Rb^{87}, $^2S_{1/2}$, I = 3/2
g_J = -1.20035	g_J = -2.00238	g_J = -2.00238
$g_I = 3.1 \times 10^{-4}$	$g_I = 2.93704 \times 10^{-4}$	$g_I = 9.95359 \times 10^{-4}$
a = 146.779 Mc/sec	$\Delta\nu$ = 3035.735 Mc/sec	$\Delta\nu$ = 6834.685 Mc/sec

Iteration No.	a (Mc/sec)	δa (Mc/sec)	b (Mc/sec)	δb (Mc/sec)	$g_I \times 10^4$	$\delta g_I \times 10^4$	χ^2
1	147.166	0.000	1805.909	0.000	3.11	0.00	25.1
2	147.167	0.005	1805.928	0.072	3.01	0.51	25.0
3	147.167	0.005	1805.928	0.072	3.01	0.51	25.0
1	147.166	0.000	1805.909	0.000	-3.11	0.00	942.0
2	147.166	0.005	1805.911	0.072	3.19	0.52	25.1
3	147.167	0.005	1805.928	0.072	3.11	0.51	25.0
4	147.167	0.005	1805.928	0.072	3.01	0.51	25.0

Run	Calibrating isotope	ν_c (Mc/sec)	$\delta\nu_c$ (Mc/sec)	H (gauss)	δH (gauss)	F_1	m_1	F_2	m_2	ν (Mc/sec)	$\delta\nu$ (Mc/sec)	Residual (Mc/sec)	Weight Factor
3221	RB85	11.506	0.025	24.193	0.052	6	-3	6	-4	17.150	0.075	0.079	143.4
3223	RB85	22.070	0.025	45.633	0.050	6	-3	6	-4	32.445	0.050	0.009	263.2
3262	RB85	50.625	0.030	100.224	0.055	6	-3	6	-4	72.560	0.200	-0.008	24.0
3271	RB87	173.599	0.070	230.907	0.087	6	-3	6	-4	174.480	0.250	-0.248	14.8
3222	RB85	11.520	0.025	24.222	0.052	5	-2	5	-3	16.240	0.075	0.146	145.4
3224	RB85	22.082	0.020	45.656	0.040	5	-2	5	-3	31.400	0.100	0.219	92.3
3341	RB87	94.650	0.070	129.941	0.092	5	-2	5	-3	99.250	0.300	-0.263	10.3
3351	RB87	129.137	0.030	174.817	0.038	5	-2	5	-3	144.750	0.300	-0.013	10.9
3352	RB87	156.861	0.030	210.017	0.038	5	-2	5	-3	187.500	0.600	-0.276	2.8
4051	RB85	2.327	0.040	4.966	0.085	4	2	4	1	2.700	0.100	0.129	85.4
3851	RB85	5.045	0.030	10.719	0.063	4	2	4	1	5.230	0.100	0.128	94.3
3911	RB85	7.077	0.030	14.987	0.063	4	2	4	1	6.640	0.100	0.058	96.4
4021	RB85	7.111	0.040	15.058	0.084	4	2	4	1	6.690	0.075	0.086	159.2
4022	RB85	7.588	0.040	16.056	0.084	4	2	4	1	7.000	0.075	0.099	161.0
4031	RB85	8.718	0.040	18.413	0.083	4	2	4	1	7.630	0.100	0.086	95.6
5081	RB85	2.282	0.040	4.871	0.085	6	-3	5	-3	1810.730	0.150	-0.183	44.0
5241	RB85	138.837	0.070	244.001	0.102	5	-2	4	-2	358.610	0.050	0.014	400.0
5131	RB85	138.869	0.070	244.048	0.102	5	-2	4	-2	358.600	0.050	0.004	400.0

Run	Calibrating isotope	ν_c (Mc/sec)	$\delta\nu_c$ (Mc/sec)	H (gauss)	δH (gauss)	F_1	m_1	F_2	m_2	ν (Mc/sec)	$\delta\nu$ (Mc/sec)	Residual (Mc/sec)	Weight Factor
5271	RB85	138.877	0.070	244.059	0.102	5	-2	4	-2	358.600	0.050	0.004	400.0
5141	RB85	138.924	0.090	244.128	0.131	5	-2	4	-2	358.610	0.040	0.014	624.9
5112	RB85	139.052	0.310	244.314	0.451	5	-2	4	-2	358.625	0.075	0.028	177.4
4241	RB85	1.654	0.030	3.534	0.064	5	-2	4	-1	797.150	0.400	-0.289	6.1
4372	RB85	127.008	0.050	226.540	0.075	5	-2	4	-1	410.473	0.010	-0.001	9999.7
5231	RB85	127.024	0.060	226.564	0.090	5	-2	4	-1	410.475	0.015	0.001	4444.4
4371	RB85	127.496	0.180	227.270	0.269	5	-2	4	-1	410.480	0.010	0.001	8844.2
4061	RB85	1.592	0.030	3.402	0.064	4	4	3	3	180.050	0.300	0.171	10.4
5082	RB85	2.274	0.040	4.854	0.085	4	2	3	3	176.950	0.100	0.085	91.4
4221	RB85	16.420	0.050	34.255	0.102	1	1	2	2	173.100	0.150	-0.219	42.7
5213	RB85	17.763	0.030	36.978	0.061	1	1	2	2	172.875	0.050	0.005	399.6
5212	RB85	17.873	0.050	37.200	0.101	1	1	2	2	172.890	0.040	0.023	625.0
5201	RB85	17.911	0.060	37.277	0.121	1	1	2	2	172.975	0.100	0.108	100.0
5211	RB85	18.045	0.030	37.548	0.061	1	1	2	2	172.960	0.090	0.088	123.4
4231	RB85	18.053	0.040	37.564	0.081	1	1	2	2	172.880	0.025	0.007	1579.9

As with Y^{90}, the small value of the χ^2 reflects the conservative errors placed on the experimental resonance frequencies. Since the computer uncertainty in each parameter is the standard deviation of that parameter, there should be a 95% probability (for a normal distribution) that the true value lies within two standard deviations of the measured value. With this uncertainty, then, the measured values of the interaction constants and g_I are:

$^2D_{3/2}$ state: $a = 194.84(2)$ Mc/sec,
$b = 1466.71(12)$ Mc/sec,
$g_I = 4(6) \times 10^{-4}$;

$^2D_{5/2}$ state: $a = 147.17(1)$ Mc/sec,
$b = 1805.93(14)$ Mc/sec,
$g_I = 3(1) \times 10^{-4}$.

From these values for a and b, the zero-field hyperfine-structure separations are:

$^2D_{3/2}$ state: $\Delta\nu_{5-2} = 1919.04(24)$ Mc/sec,
$\Delta\nu_{2-4} = 102.82(18)$,
$\Delta\nu_{4-3} = 360.31(9)$;

$^2D_{5/2}$ state: $\Delta\nu_{6-5} = 1811.76(10)$ Mc/sec,
$\Delta\nu_{5-1} = 615.60(18)$,
$\Delta\nu_{1-4} = 184.74(15)$,

$$\Delta\nu_{1-2} = 36.91(11),$$

$$\Delta\nu_{2-3} = 138.98(6).$$

Figures 62 and 63 show the energy-level diagrams for both electronic states in the region 0 to 1000 gauss.

The ratios of the experimental interaction constants are

$$\frac{a'}{a''} = \frac{147.167}{194.842} = 0.7553,$$

and

$$\frac{b'}{b''} = \frac{1805.928}{1466.713} = 1.2313.$$

Theoretically, one would expect

$$\frac{a_0'}{a_0''} = \frac{3}{7}\frac{F'}{F''} = 0.4153,$$

$$\frac{b'}{b''} = \frac{10}{7}\frac{R'}{R''} = 1.2907;$$

where we have taken the effective nuclear charge as $Z_1 = 51.0$ (MUR 55). The very large deviation in the ratio of the a's again suggests a configuration-mixing effect of the type already discussed. The electronic configuration that meets the requirements for an effect of this kind is the $5d6s7s$ configuration.

As with Y^{90}, the relations that permit a calculation of the extent of this effect are

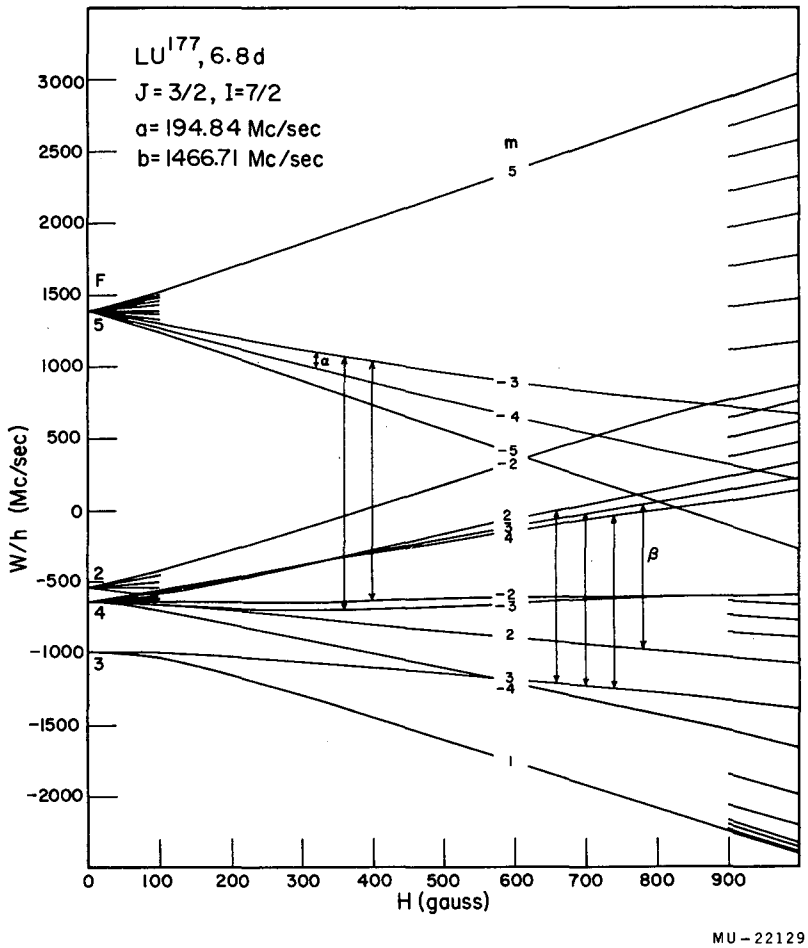

Fig. 62. Energy level diagram of the hyperfine structure in the $^2D_{3/2}$ electronic state of Lu^{177}.

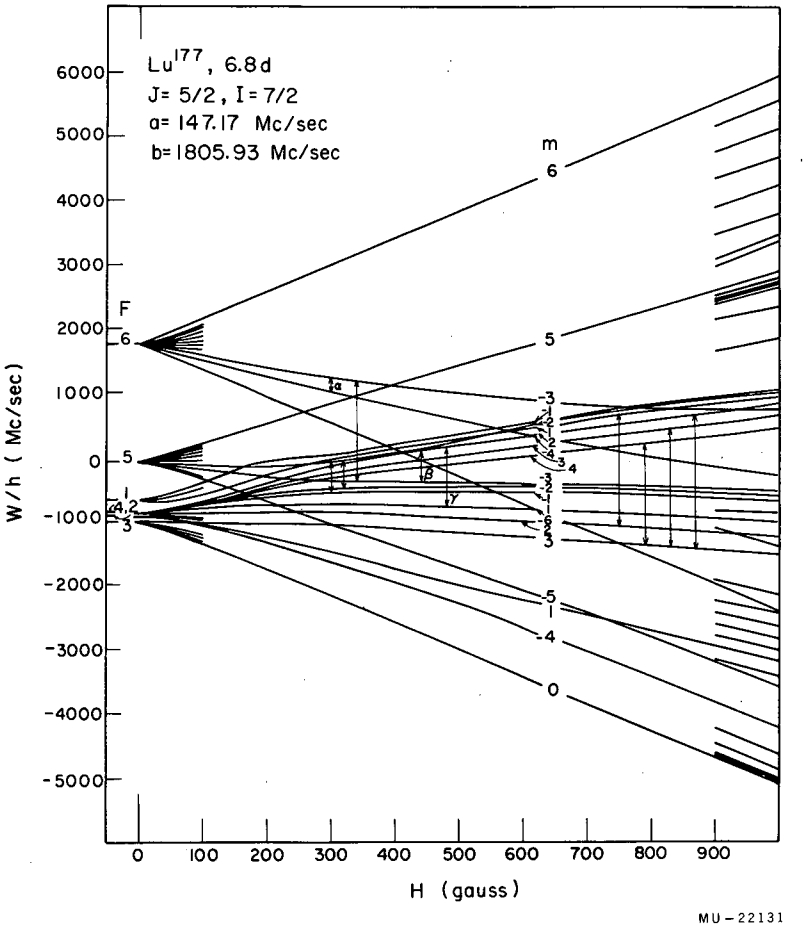

Fig. 63. Energy level diagram of the hyperfine structure in the $^2D_{5/2}$ electronic state of Lu^{177}.

$$\frac{a_0'}{a_0''} = \frac{3}{7\theta},$$

$$\delta' = -\delta'';$$

$$a' = a_0' + \delta',$$

$$a'' = a_0'' + \delta'',$$

$$\theta = \frac{F''}{F'} \left| \frac{C''}{C'} \right|^2 .$$

For lack of better information, we shall assume $|C''/C'|^2 = 1$ [(Eq.(II-72)]. Thus, $\theta = 1.0320$ and

$$a_0' = 100.354 \text{ Mc/sec},$$

$$a_0'' = 241.655 \text{ Mc/sec}.$$

From Ritter's unpublished results for Lu^{175}, we have (RIT 60)

$^2D_{3/2}$ state: a = 194.3317(4) Mc/sec,
b = 1511.4012(30) Mc/sec);

$^2D_{5/2}$ state: a = 146.7790(10) Mc/sec,
b = 1860.647(10) Mc/sec.

As with Lu^{177}, the corrected nuclear magnetic dipole interaction constants become

$$a_0' = 100.091 \text{ Mc/sec},$$

and

$$a_0'' = 241.020 \text{ Mc/sec}.$$

From Ritter's data (STE 58) and $\mu_I(Lu^{75}) = 2.0(2)$ nm we obtain, with

the aid of the Fermi Segrè formula,

$$g_I(Lu^{177}) = 3.3(3) \times 10^{-4}.$$

From Eq. (II-9a) we obtain, with Murakawa's value for the effective nuclear charge,

$$g_I(Lu^{177}) = 3.1(3) \times 10^{-4}.$$

Both these values agree within the uncertainty with the value directly measured in the $^2D_{5/2}$ electronic state,

$$g_I(Lu^{177}) = 3(1) \times 10^{-4}.$$

We shall take

$$g_I = 3.1(3) \times 10^{-4}$$

as the best value for the nuclear g factor of Lu^{177}. In units of nuclear magnetons, this quantity corresponds to

$$\mu_I(Lu^{177})^{\text{uncorr}}_{\text{expt}} = 2.0(2) \text{ nm}.$$

Since the principal uncertainty in the previous calculations could be greatly reduced if a more accurate value for the magnetic moment of Lu^{175} were known, a direct measurement of this quantity seems highly desirable.

The uncorrected nuclear electric quadrupole moment can be obtained from Eq. (II-20). For the $^2D_{3/2}$ electronic state,

$$Q(^2D_{3/2}) = 5.1(5) \text{ barns}.$$

For the $^2D_{5/2}$ electronic state,

$$Q(^2D_{5/2}) = 4.9(5) \text{ barns}.$$

These values are the same as those which one obtains by using Eq. (II-19) and Murakawa's value for Z_i. The discrepancy between the results for the two electronic states reflects that the experimental ratio of the b's is not equal to theoretical ratio. Representing this discrepancy in the uncertainty, we take the best value of the uncorrected nuclear electric quadrupole moment to be

$$Q(Lu^{177})^{uncorr}_{expt} = 5.0(6) \text{ barns.}$$

The simple single-particle shell model does not predict the spin of Lu^{177} in a straightforward manner. Consequently, we attempt to compare the experimental results with the collective model.

Mottelson and Nilsson (MOT 59) have calculated the equilibrium shape deformation parameter δ to be 0.26 for Lu^{177}. From the "Nilsson diagram" (MOT 59, p.21), the 71st proton should be in a level corresponding to I = 7/2 with even parity, in agreement with experiment. The observed β decay is also in agreement with this assignment.

If we assume that j is a good quantum number in the limit of strong coupling of the nucleon to the core, then Eq. (II-85) predicts

$$\mu_c = 1.6 \text{ nm.}$$

This value should be compared to the corrected experimental nuclear magnetic moment for Lu^{177}. From Kopfermann (KOP 58, p.450), the diamagnetic correction, κ, is 1.00827 and

$$\mu_I(Lu^{177})^{corr}_{expt} = \kappa\mu_I(Lu^{177})^{uncorr}_{expt} = 2.0(2) \text{ nm.}$$

The rather large discrepancy is of the same order of magnitude and in the same direction as the discrepancy in the case of Lu^{175} (MOT 59, p. 80).

The theoretical intrinsic quadrupole moment can be calculated from Eq. (II-87) and the estimated value for δ. Assuming $R_0 = (1.2 \times 10^{-13}) \times A^{1/3}$, we have

$$Q_0^{\text{theor}} = 7.6 \text{ barns}.$$

In the limit of strong coupling of the nucleon to the core, the measured quadrupole moment is related to the intrinsic quadrupole moment by

$$Q_I^{\text{theor}} = \frac{I}{I+1}\frac{2I-1}{2I+3} Q_0^{\text{theor}} = \frac{14}{30} Q_0^{\text{theor}}.$$

Thus, $Q_I^{\text{theor}} = 3.5$ barns. Because of the large uncertainties, the difference between theoretical and uncorrected experimental values should probably not be considered serious.

V. ACKNOWLEDGMENTS

It has been my great pleasure to be associated with a number of people who have provided invaluable assistance and inspiration in the course of my research.

In particular, my profound thanks and admiration go to Professor Howard A. Shugart, who suggested the research on the subject isotopes. His infinite patience, continual encouragement, and ever-present assistance and advice have smoothed the sometimes rocky paths that were followed in these experimental investigations. My thanks also go to Professor William A. Nierenberg, whose uncanny theoretical insight into physical problems, always expressed in a most enthusiastic manner, has gained my deepest respect.

It has been my good fortune and pleasure to be associated with Dr. W. Bruce Ewbank and Dr. Vernon J. Ehlers during the entire period of the investigations. I am deeply indebted for their experimental techniques and invaluable discussions during all phases of the research. To Dr. Lawrence L. Marino during the early part and to Miss Barbara M. Dodsworth and Mr. Y. W. Chan during the latter part of the researhc, I must accord this same deep gratitude.

My thanks also go to Dr. George J. Ritter of the National Research Council, Ottawa, Canada, who graciously provided unpublished experimental results for Lu^{175}.

The services of our technicians, Mr. Forrest S. Baker, Mr. Ray Sanchez, Mr. Ralph Stein, Mr. Mike DeVito, and Mr. Henry Battjes, have contributed materially to the success of this research. The valuable engineering advice and assistance of Mr. Douglas McDonald was also greatly appreciated.

My special thanks go to the Health Chemistry Division, which provided all the facilities for handling the radioactive isotopes. In particular, I should like to express my appreciation to Mr. John Bowen, whose services and advice--both as a health chemist and as a competent experimentalist--were especially valued. My thanks also go to Mrs. Ruth-Mary Larimer for her thoroughly competent monitoring job.

The crews of the Crocker 60-inch cyclotron and the Livermore pool-type reactor are to be commended for their skill and cooperation in the production of the various radioactive isotopes.

Finally, I am deeply indebted to my loving wife, Gloria, who has been a "graduate student's widow" these past two years, for her patient understanding and encouragement.

This work was done under the auspices of the U.S. Atomic Energy Commission.

Reprinted from THE PHYSICAL REVIEW, Vol. 116, No. 3, 734-737, November 1, 1959
Printed in U. S. A.

Nuclear Spin, Hyperfine-Structure Separation, and Magnetic Moment of 22-Hour Potassium-43*

F. RUSSELL PETERSEN, VERNON J. EHLERS, W. BRUCE EWBANK, LAWRENCE L. MARINO, AND HOWARD A. SHUGART
Department of Physics and Lawrence Radiation Laboratory, University of California, Berkeley, California

(Received June 1, 1959)

With the atomic-beam magnetic-resonance method, the nuclear spin and hyperfine-structure separation have been measured for 22-hour K^{43}. The results are $I=\frac{3}{2}$, $\Delta\nu(^2S_{\frac{1}{2}})=192.64\pm0.05$ Mc/sec. The nuclear magnetic moment calculated from these measurements is $|\mu|=0.163\pm0.002$ nuclear magneton.

I. INTRODUCTION

THE atomic-beam flop-in technique has been used to measure the nuclear spin and hyperfine-structure separation of 22-hr potassium-43 in the $^2S_{\frac{1}{2}}$ electronic state.[1] Since the apparatus and procedure employed in making measurements of these quantities with radionuclides has been described in detail elsewhere,[2] only a brief summary of the method is included here. The convenient 22-hr half-life of K^{43} and its β^- decay made beams of this isotope suitable for radioactive detection with high efficiency. The experimental results extend the evidence for a general trend in the magnetic moments of the odd-mass-number isotopes of potassium.

II. THEORY OF THE EXPERIMENT

A free atom of potassium in the $^2S_{\frac{1}{2}}$ electronic ground state may be represented in an external magnetic field $\mathbf{H}$ by the Hamiltonian,

$$\mathcal{H}=-\mu_0 g_J \mathbf{J}\cdot\mathbf{H}-\mu_0 g_I \mathbf{I}\cdot\mathbf{H}+\frac{h\Delta\nu}{I+\frac{1}{2}}\mathbf{I}\cdot\mathbf{J}, \quad (1)$$

where μ_0 is the absolute value of the Bohr magneton, $\mathbf{I}$ and $\mathbf{J}$ are the nuclear and electronic angular momenta in units of $\hbar$, g_I is the nuclear g factor $[\mu_I/(\mu_0 I)]$, g_J is the electronic g factor $[\mu_J/(\mu_0 J)]$, and $\Delta\nu$ is the zero-field hyperfine-structure separation between the $F=I+\frac{1}{2}$ and $F=I-\frac{1}{2}$ levels, in cycles per second. The energy levels of this Hamiltonian are given by the Breit-Rabi formula,[3]

$$W(F,m_F)=-\frac{h\Delta\nu}{2(2I+1)}-g_I\mu_0 H m_F \pm\frac{h\Delta\nu}{2}\left(1+\frac{4mx}{2I+1}+x^2\right)^{\frac{1}{2}}, \quad (2)$$

where

$$x=(-g_J+g_I)\frac{\mu_0 H}{h\Delta\nu}.$$

The positive sign is taken with the $F=I+\frac{1}{2}$ levels and the negative sign with the $F=I-\frac{1}{2}$ levels. The qualitative variation of the hyperfine energy levels for the case of $J=\frac{1}{2}$, $I=\frac{3}{2}$ and a positive nuclear moment is shown in Fig. 1.

In principle, the deflecting fields (A and B) of the flop-in apparatus focus on the detector only those atoms which change the signs of their effective magnetic moments while the atoms traverse the region between the A and B magnets. At high A and B fields ($x\gg0.5$ for the case in Fig. 1), the refocusing condition is satisfied for the transitions, $\Delta m_J=\pm1$. As shown in the figure, nine allowed ($\Delta m_F=\pm1, 0$) transitions are readily observable.

To second order in H, the transition labeled i has a frequency dependence of

$$\nu=\frac{(-g_J-2Ig_I)}{2I+1}\frac{\mu_0 H}{h}+2I\frac{(-g_J+g_I)^2}{(2I+1)^2}\frac{\mu_0^2 H^2}{h^2\,\Delta\nu}+\cdots. \quad (3)$$

In the "linear" Zeeman region, where the magnetic field

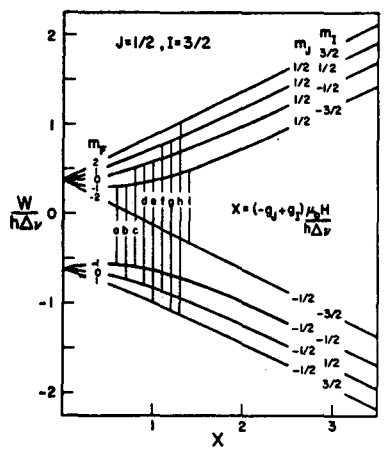

FIG. 1. The Breit-Rabi diagram for potassium-43 with an assumed positive nuclear magnetic moment.

* This research was supported in part by the U. S. Air Force Office of Scientific Research and the U. S. Atomic Energy Commission.

[1] Petersen, Ehlers, Ewbank, Marino, and Shugart, Bull. Am. Phys. Soc. Ser. II, 3, 415 (1958).

[2] Hobson, Hubbs, Nierenberg, Silsbee, and Sunderland, Phys. Rev. 104, 101 (1956).

[3] G. Breit and I. I. Rabi, Phys. Rev. 38, 2082 (1931), as extended by Millman, Rabi, and Zacharias, Phys. Rev. 53, 384 (1938).

Appendix A.

is low, the first term of this expression is dominant and the higher-order terms may be neglected. Similarly, since g_I is about 1/2000 of g_J, its effect in the equation is small. Therefore, the transition frequency is dependent essentially upon H, I, and the known constants g_J, μ_0, and h. Observation of this transition at given low fields and frequencies thus establishes the nuclear spin I.

Initial estimates of the hyperfine-structure separation $\Delta\nu$ result when transition i is followed to higher fields where the second and higher order terms in Eq. (3) contribute. For this transition, the hyperfine-structure separation may be calculated exactly from the equation

$$\Delta\nu=\left(\nu+\frac{g_I\mu_0H}{h}\right)\left(\frac{-g_J\mu_0H}{h}-\nu\right)\Big/\left(\nu+\frac{g_J\mu_0H}{(2I+1)h}+\frac{2I}{2I+1}\frac{g_I\mu_0H}{h}\right), \quad (4)$$

where ν is the resonant frequency of transition i and other symbols have been defined previously. In this equation, g_I is an unknown but may be estimated with the aid of the Fermi-Segrè formula,[4]

$$\frac{\Delta\nu}{\Delta\nu'}\cong\left|\frac{g_I}{g_{I'}}\right|\left(\frac{2I+1}{2I'+1}\right), \quad (5)$$

where the primed and unprimed quantities refer to two isotopes of the same element. Equations (4) and (5) may be solved simultaneously for $\Delta\nu$ and g_I by assuming first a positive and then a negative sign for g_I. Although the Fermi-Segrè formula involves certain simplifying assumptions, moments calculated from it are normally in error by less than 1%.

As seen in Fig. 1, eight of the observable transition frequencies approach $\Delta\nu$ as the external field approaches zero. The field dependence of these transitions may be computed from the Breit-Rabi equation. With the apparatus used in this work, the transitions *b* and *c*, as well as *e* and *f*, form unresolved doublets. The transition *d* exhibits only small-field dependence at low fields. The resulting resonance is narrow and therefore provides the best measurements of the zero-field hyperfine-structure separation.

III. ISOTOPE PRODUCTION AND IDENTIFICATION

K^{43} was produced on the Berkeley 60-inch Crocker cyclotron by the reaction $A^{40}(\alpha,p)K^{43}$. The natural argon gas at 2 atmos absolute pressure was contained in a water-cooled aluminum cylinder of cross section $1\frac{1}{2}\times5$ inches and of length 19 inches. One end of this container was provided with a "window assembly" to admit the bombarding particles. After a bombardment, potassium atoms were recovered from the walls of the target container by solution in distilled water containing about 30 mg of potassium chloride carrier. Three washings, each approximately 200 ml in volume, were adequate to remove the major portion of the activity. Then the solution was reduced in volume, pipetted into the atomic-beam oven, and evaporated to dryness. An excess of finely divided calcium metal was added to cause reduction of the potassium ions when the oven was later heated in the atomic-beam apparatus.

Since K^{42} (12.5-hr) is also produced by the reaction $A^{40}(\alpha,pn)K^{42}$ during a bombardment, this isotope forms an unwanted background in these experiments. For bombardments with 40-Mev alpha particles, continuous-flow proportional counters showed the initial activity of K^{42} to be 60 times that of K^{43}. As a result, an experiment was conducted to determine roughly the relative yield of K^{43} to K^{42} as a function of the beam energy. At about 20 Mev, the activity ratio K^{42}/K^{43} was reduced to 4. Subsequently, the preferential decay of K^{42} further decreased this ratio before use of the sample. At 20 Mev, 100 to 140 microampere-hours of bombardment produced adequate K^{43} activity for 15 hours of running time, with resonance signals of 3 to 30 counts per minute (10-minute collecting time) above a 2-count/min counter background.

Samples of the transmitted potassium beam were collected on sulfur surfaces and counted in continuous-flow proportional counters. Because the samples were inserted directly into the sensitive volume of the counters, radiation into 2π steradians of solid angle was counted. Each resonance exposure was decayed for 3 or 4 days to verify the presence of 22-hour K^{43}. The half-life and identity of this isotope have been well established by previous investigators.[5–7]

IV. EXPERIMENTAL PROCEDURE

For the work on K^{43}, the resistance-heated oven was inserted into the atomic-beam apparatus by means of an oven-loader assembly. This assembly, containing electrical, thermocouple, and water-cooling connections, could be introduced into the apparatus without disturbing the high vacuum within.

The easily detected potassium carrier, which was added during the chemistry, facilitated initial alignment of the oven. Also, observation of the low-field flop-in resonance ($F, m_F=2, -1\leftrightarrow 2, -2$) of stable potassium before and after each radioactive exposure served to calibrate the transition magnetic field (C field) and to indicate the beam intensity for normalization.

Radiofrequencies for the $\Delta F=0$ transitions were generated by a Tektronix Type 190 oscillator. For the $\Delta F=\pm1$ transitions, a Hewlett-Packard Model 608 A oscillator and two Instruments For Industries wide-band amplifiers were used. All frequencies were monitored with a Hewlett-Packard Model 524B frequency counter, whose 100-kc/sec internal-reference frequency

[4] E. Fermi and E. Segrè, Z. Physik **82**, 729 (1933).

[5] Overstreet, Jacobson, and Stout, Phys. Rev. **75**, 231 (1949).

[6] G. Anderson, Phil. Mag. **45**, 621 (1954).

[7] T. Lindqvist and A. C. G. Mitchell, Phys. Rev. **95**, 444 (1954).

TABLE I. Values of $\Delta\nu$ predicted from low-frequency resonances.

K^{39} (Mc/sec)	K^{41} (Mc/sec)	Hfs separation (for either positive or negative magnetic moment) (Mc/sec)
10.89±0.05	12.15±0.50	177±41
15.36±0.05	17.70±0.75	184±33
24.30±0.05	29.90±0.50	186±9
39.25±0.30	52.60±0.50	188±6

was compared weekly with an Atomichron.

V. RESULTS

From Eq. (3), the spins and frequencies of two detectable low-frequency resonances at a given field are related approximately by

$$\nu_1=\left(\frac{2I_2+1}{2I_1+1}\right)\nu_2,$$

where the subscripts 1 and 2 may refer to radioactive K^{43} and stable K^{39}, respectively. When a search was made at frequencies corresponding to spins of $\frac{5}{2}$, 2, $\frac{3}{2}$, and $\frac{1}{2}$, the buttons corresponding to $I=2$ and $I=\frac{3}{2}$ gave definite indications of resonances. Subsequent decay of the activity collected on the $I=2$ button confirmed its identity as K^{42}, which has a known spin of two.[8] Similarly, the decay of the $I=\frac{3}{2}$ sample showed an enrichment of K^{43} over the normal composition of the beam. Because these resonances were quite broad, a portion of the tail of the spin-2 resonance contributed to the $I=\frac{3}{2}$ signal. However, decay analysis distinguished the contribution of each isotope to the resonance.

On a subsequent run, four resonances of K^{43} were resolved at progressively higher values of the C field. These confirmed the spin ($I=\frac{3}{2}$) and roughly determined the hyperfine-structure separation, $\Delta\nu$, of K^{43}. A summary of these results appears in Table I. The relatively large uncertainties in the frequencies of these resonances resulted from broad-resonance lines. It should be noted that the usual consistency argument[9] for determining the sign of the moment cannot be used for K^{43} in this experiment. Owing to a small magnetic moment, the hyperfine-structure separations calculated for a positive magnetic moment and for a negative magnetic moment, respectively, lie well within the errors of the measurements. As a result, the data presented here cannot determine the sign of the moment.

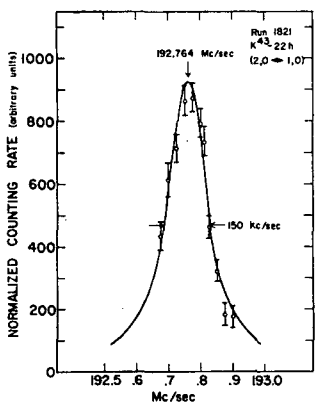

FIG. 2. A bell-shaped curve fitted to a field-independent resonance by a least-squares procedure.

After the wide line width was reduced by changing the radio-frequency hairpin and by repositioning it in the C field, a search for the direct transitions ($\Delta F=\pm1$) was begun. Table II summarizes the results. The field-independent line (F, $m_F=2$, $0\leftrightarrow1$, 0, transition d in Fig. 1) was observed seven times in fields from ~2.3 to ~8 gauss. Proper dependence of this line upon the magnetic field established its identity. The two unresolved doublet frequencies which occur above and below that of the field-independent line were also measured.

For each resonance, all data were corrected for counter background, for fluctuations in beam intensity, and for radioactive decay. Each resonance-peak button was also decayed to establish the enrichment of K^{43}. Next, a bell-shaped curve was fitted to the data of each resonance by a least-squares procedure. An example of a fitted curve of one of the field-independent resonances is shown in Fig. 2. From the curve-fitting procedure, the peak frequency, the width at half-maximum, and the uncertainty in peak frequency due to the uncertainties of input points were obtained. The uncertainty of the peak frequency was taken as a combination of one-eight of the full width at half-maximum and of the uncertainty of the peak due to the statistical uncertainty of input data points. The uncertainty in the calibration frequency was estimated from consideration of the reproducibility of the calibration resonance.

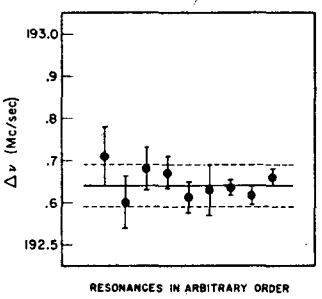

FIG. 3. A plot of the calculated hyperfine-structure separations obtained from $\Delta F=\pm1$ resonances. The heavy line indicates the weighted average of all observations, while the dashed lines indicate the quoted uncertainty in the final value.

The final value of $\Delta\nu$ is taken as the weighted average of all hyperfine-structure separation measurements listed in Table II. The measurements are plotted in Fig. 3, which also shows the weighted average and

[8] E. H. Bellamy and K. F. Smith, Phil. Mag. **44**, 33 (1953).

[9] J. R. Zacharias, Phys. Rev. **61**, 270 (1942).

TABLE II. Results of $\Delta F=\pm 1$ transitions. $\Delta\nu^+$ and $\Delta\nu^-$ are hyperfine-structure separations predicted by the Breit-Rabi equation by assuming a positive and a negative magnetic moment, respectively.

$F,m_F \leftrightarrow F',m_{F'}$	ν_{cal} (Mc/sec)	ν_{res} (Mc/sec)	$\Delta\nu^+$ and $\Delta\nu^-$ (Mc/sec)
$2,0 \leftrightarrow 1,0$	5.845±0.020	193.995±0.049	192.681±0.050
$2,0 \leftrightarrow 1,0$	4.650±0.020	193.515±0.038	192.670±0.038
$2,0 \leftrightarrow 1,0$	4.290±0.020	193.335±0.036	192.613±0.037
$2,0 \leftrightarrow 1,0$	3.515±0.020	193.120±0.059	192.630±0.060
$2,0 \leftrightarrow 1,0$	2.550±0.020	192.897±0.018	192.636±0.018
$2,0 \leftrightarrow 1,0$	2.040±0.020	192.787±0.020	192.618±0.021
$2,0 \leftrightarrow 1,0$	1.595±0.020	192.764±0.020	192.661±0.020
Unresolved doublet $\{2,0 \leftrightarrow 1,-1$; $2,-1 \leftrightarrow 1,0\}$	2.580±0.020	190.407±0.068	192.709±0.070
Unresolved doublet $\{2,0 \leftrightarrow 1,1$; $2,1 \leftrightarrow 1,0\}$	2.575±0.020	195.364±0.057	192.600±0.062
		Weighted average with estimated uncertainty	192.64±0.05.

stated uncertainty by the full and dashed lines, respectively. The best value of $\Delta\nu$, with estimated uncertainty, is therefore

$$\Delta\nu=192.64\pm0.05 \text{ Mc/sec.}$$

In conjunction with the known constants of K^{39} or K^{41}, the Fermi-Sergè formula was used to obtain the absolute value of the nuclear magnetic dipole moment of K^{43} to within about 1%. The result is

$$|\mu|=0.163\pm0.002 \text{ nuclear magneton.}$$

Some of the ground-state properties of three odd isotopes of potassium are now known (K^{39}, K^{41}, and K^{43}). The nuclear spins of all are $I=\frac{3}{2}$ which, on the basis of the simple shell model, arises from one missing proton in the $d_{\frac{3}{2}}$ shell. The nuclear magnetic moments of this series show a monotonic decrease, with values of +0.391 nm for K^{39}, +0.215 nm for K^{41}, and ±0.163 nm for K^{43}. Although the resolution in this experiment was insufficient to establish the sign of K^{43}, it should be noted that the positive-sign choice would make the measurement lie within the lower Schmidt limit of +0.124 nm.

ACKNOWLEDGMENTS

The authors wish to thank Professor W. A. Nierenberg and Professor H. B. Silsbee for their interest in this research.

APPENDIX B

Fundamental and Atomic Constants

These fundamental constants (COH 57) have been used in the calculations in the text and are collected here for reference:

$a_o = 5.29172(2) \times 10^{-9}$ cm,

$c = 2.997930(3) \times 10^{10}$ cm/sec,

$e = 4.80286(9) \times 10^{-10}$ esu,

$h = 6.62517(23) \times 10^{-27}$ erg-sec,

$M/m = 1836.12(2)$,

$\mu_o = 0.92731(2) \times 10^{-20}$ erg/gauss.

Atomic constatns that have been useful for magnetic field measurements, moment calculations, and other purposed are listed below. The values of all moments are uncorrected for dielectric and Sternheimer effects.

K^{39}

$I = 3/2$,	(MIL 34; MIL 35)
$\Delta\nu = 461.719690(30)$ Mc/sec	(BLO 60)
$\mu_I = 0.390873(13)$ nm,	(BRU 54)
$g_J = -2.00228(2)$;	(RAM 56)

K^{41}

$I = 3/2$,	(MAN 36)
$\Delta\nu = 254.013870(35)$ Mc/sec,	(BLO 60)
$\mu_I = 0.21453(3)$ nm,	(BRU 54)
$g_J = -2.00228(2)$;	(RAM 56)

Rb^{85}

$I = 5/2$, (KOP 33a; KOP 33b)

$\Delta\nu = 3035.735(2)$ Mc/sec, (HED 52)

$\mu_I = 1.34819(3)$ nm, (YAS 51)

$g_J = -2.00238(4)$; (RAM 56)

Rb^{87}

$I = 3/2$, (KOP 33a; KOP 33b)

$\Delta\nu = 6834.685(2)$ Mc/sec, (DAL 53)

$\mu_I = 2.74140(5)$ nm, (YAS 51)

$g_J = -2.00238(4)$; (RAM 56)

Y^{89}

$I = 1/2$, (CRA 49; KUH 50)

$a(^2D_{3/2}) = -57.217(15)$Mc/sec, (FRI 59)

$a(^2D_{5/2}) = -28.749(30)$Mc/sec, "

$\mu_I = -0.136825(4)$ nm, (BRU 54)

$g_J(^2D_{3/2}) = -0.79927(11)$, (PEN 59)

$g_J(^2D_{5/2}) = -1.20028(19)$; "

La^{139}

$I = 7/2$, (AND 34)

$a(^2D_{3/2}) = 141.1959(16)$Mc/sec (TIN 57)

$b(^2D_{3/2}) = 44.781(14)$Mc/sec, "

$c(^2D_{3/2}) = 0.15(44)$ kc/sec, "

$a(^2D_{5/2}) = 182.1706(6)$ Mc/sec, "

$b(^2D_{5/2}) = 54.213(14)$ Mc/sec, "

$c(^2D_{5/2}) = -0.6(1.0)$ kc/sec, "

μ_I = 2.7614(2) nm, (SHE 51)

Q = 0.230(10) barns, (TIN 57)

$g_J(^2D_{3/2})$ = -0.7988(5), "

$g_J(^2D_{5/2})$ = -1.201(2); "

Lu^{175}

I = 7/2, (SCH 35)

$a(^2D_{3/2})$ = 194.3317(4) Mc/sec, (RIT 60)

$b(^2D_{3/2})$ = 1511.4012(30)Mc/sec, "

$a(^2D_{5/2})$ = 146.7790(10) Mc/sec, "

$b(^2D_{5/2})$ = 1860.647(10) Mc/sec, "

μ_I = 2.0(2) nm, (STE 57; STE 58)

Q = 5.6(5) barns, " "

$g_J(^2D_{3/2})$ = -0.79911(10), (RIT 60)

$g_J(^2D_{5/2})$ = -1.20035(20). "

REFERENCES

AND 34 O. E. Anderson, Phys. Rev. 45, 685 (1934).

BAK 60 Forrest R. Baker, Graphs and Tables of Zero-Field Hyperfine-Structure Level Ordering in Free Atoms, UCRL-9364, Aug. 1960.

BED 52 B. Bederson and V. Jaccarino, Phys. Rev. 87, 228 (1952).

BEN 59 N. Benczer-Koller, A. Schwarzschild, and C. S. Wu, Phys. Rev. 115, 108 (1959).

BET 58 R. H. Betts, O. F. Dahlinger, and D. M. Munro, Can. J. Phys. 36, 73 (1958).

BLI 57 R. J. Blin-Stoyle, Theories of Nuclear Moments (Oxford University Press, London, 1957).

BLO 60 Arnold L. Bloom and John B. Carr, Phys. Rev. 119, 1946 (1960).

BOH 50 A. Bohr and V. F. Weisskopf, Phys. Rev. 77, 94 (150).

BOH 51 A. Bohr, Phys. Rev. 81, 331 (1951).

BRE 60 M. H. Brennan and A. M. Bernstein, Phys. Rev. 120, 927 (1960).

BRU 54 E. Brun, J. Oeser, H. H. Staub, and C. G. Telschow, Phys. Rev. 93, 172 (1954).

CAS 36 H. B. G. Casimer, On the Interaction Between Atomic Nuclei and Electrons (Tyler's Tweede Genootschap, Haarlem, 1936).

COH 57 E. R. Cohen, K. M. Crowe, and J. W. M. DuMond, Fundamental Constants of Physics (Interscience Publishers, Inc., New York, 1957).

CON 57 E. U. Condon and G. H. Shortley, The Theory of Atomic Spectra (Cambridge University Press, Cambridge, England, 1957).

CRA 49a M. F. Crawford and A. L. Schawlow, Phys. Rev. 76, 1310 (1949).

CRA 49b M. F. Crawford and N. Olson, Phys. Rev. 76, 1528 (1949).

DAL 53 R. T. Daly, Jr., and J. R. Zacharias, Phys. Rev. 91A, 476 (1953).

EHL 60 Vernon J. Ehlers, The Nuclear Spins and Moments of Several Radioactive Gallium Isotopes (thesis), UCRL-9123, March, 1960.

FRI 59 G. Fricke, H. Kopfermann, and S. Penselin, Z. Physik 154, 218 (1959).

GAL 58 C. J. Gallagher, Jr., and S. A. Moszkowski, Phys. Rev. 111, 1282 (1958).

HEV 36 G. Hevesy and Hilde Levi, Kgl. Danske Videnskab. Selskab Mat.-fys. Medd. 14, No. 5 (1936).

ION 60 N. J. Ionesco-Pallas, Phys. Rev. 117, 505 (1960).

KIR 54 H. W. Kirby and M. L. Salutsky, Phys. Rev. 93, 1051 (1954).

KOP 33a H. Kopfermann, Naturwissen. 21, 24 (1933).

KOP 33b Hans Kopfermann, Z. Physik 83, 417 (1933).

KOP 58 Hans Kopfermann, Nuclear Moments, English translation by E. E. Schneider (Academic Press, Inc., New York, 1958).

KOS 52 G. F. Koster, Phys. Rev. 86, 148 (1952).

KUH 50 H. Kuhn and G. K. Woodgate, Proc. Phys. Soc. (London) A63, 830 (1950).

LAN 60 L. M. Langer and D. R. Smith, Phys. Rev. 119, 1308 (1960).

MAN 36 J. H. Manley, Phys. Rev. 49, 921 (1936).

MAR 59 Lawrence L. Marino, Some Nuclear Properties of Bi^{206}, Tl^{200}, Th^{201}, Th^{202}, In^{109}, In^{110m}, and In^{111} (thesis), UCRL-8721, April, 1959.

MAR 35 J. K. Marsh and S. Sugden, Nature 136, 102 (1935).

MAY 55 Maria Goeppert Mayer and J. Hans D. Jensen, Elementary Theory of Nuclear Shell Structure (John Wiley and Sons, Inc., New York, 1955).

MEG 29 William F. Meggers and Bourdon F. Scribner, Bur. Standards J. Research 5, 73 (1930).

MEG 32 W. F. Meggers, Bur. Standards J. Research 9, 239 (1932).

MIL 34 Sidney Millman, Marvin Fox, and I. I. Rabi, Phys. Rev. 46, 320 (1934).

MIL 35 S. Millman, Phys. Rev. 47, 739 (1935).

MOT 59 Ben R. Mottelson and Sven Gosta Nilsson, Kgl. Danske Videnskab. Selskab Mat.-fys. Skrifter 1, No. 8 (1959).

MUR 55 K. Murakawa, Phys. Rev. 98, 1285 (1955).

NIE 57 William A. Nierenberg, A Method for Minimizing a Function of n Variables, UCRL-3816, June, 1957.

NOR 51 L. A. Nordheim, Revs. Modern Phys. 23, 322 (1951).

PEN 59 Siegfried Penselin, Z. Physik 154, 231 (1959).

PET 58 F. Russell Petersen, Vernon J. Ehlers, W. Bruce Ewbank, Lawrence L. Marino, and Howard A. Shugart, Bull. Am. Phys. Soc., Ser. II, 3, 415 (1958).

PET 59a F. Russell Petersen, Vernon J. Ehlers, W. Bruce Ewbank, Lawrence L. Marino, and Howard A. Shugart, Phys. Rev. 116, 734 (1959).

PET 59b F. R. Petersen and H. A. Shugart, Bull. Am. Phys. Soc., Ser. II, 4, 452 (1959).

PET 60a F. R. Petersen and H. A. Shugart, Bull. Am. Phys. Soc., Ser. II, 5, 273 (1960).

PET 60b F. R. Petersen and H. A. Shugart, Bull. Am. Phys. Soc., Ser. II, 5, 343 (1960).

RAC 42 G. Racah, Phys. Rev. 62, 438 (1942).

RAI 51 L. J. Rainwater, Phys. Rev. 79, 432 (1951).

RAM 53 Norman F. Ramsey, Nuclear Moments (John Wiley and Sons, Inc., New York, 1953).

RAM 56 Norman F. Ramsey, Molecular Beams (Oxford University Press, London, 1956).

RIT 60 George J. Ritter (National Research Council, Ottawa, Canada) private communication, 1960.

ROS 32 J. E. Rosenthal and G. Breit, Phys. Rev. 41, 459 (1932).

SCH 35 H. Schüler and T. Schmidt, Z. Physik 95, 265 (1935).

SCH 37 T. Schmidt, Z. Physik 106, 358 (1937).

SCH 55 Charles Schwartz, Phys. Rev. 97, 380 (1955).

SHE 51 Robert E. Sheriff and Dudley Williams, Phys. Rev. 82, 651 (1951).

STE 57 Andreas Steudel, Naturwiss. 44, 371 (1957).

STE 58 Andreas Steudel, Z. Physik 152, 599 (1958).

STR 58 D. Strominger, J. M. Hollander, and G. T. Seaborg, Revs. Modern Phys. 30, 585 (1958).

SUN 56 Robert J. Sunderland, The Nuclear Spins of Rb^{82}, Rb^{83}, and Rb^{84} (thesis), University of California, Berkeley, 1956.

TIN 57 Yu Ting, Phys. Rev. 108, 295 (1957).

VOL 55 Herbert L. Volchok and J. Lawrence Kulp, Phys. Rev. 97, 102 (1955).

YAS 51 E. Yasaitis and B. Smuller, Phys. Rev. 82, 750 (1951).

ZUR 60 Donald H. Zurlinden (Lawrence Radiation Laboratory) private communication, 1960.